

GEORGIA INSTITUTE OF TECHNOLOGY
OFFICE OF CONTRACT ADMINISTRATION
SPONSORED PROJECT INITIATION

Date: 15 October 1979

Project Title: Misers Bluff II Data Reduction

Project No: A-2465

Project Director: Mr. E.E. Martin

Sponsor: Stanford Research Institute International; Menlo Park, Ca 94025

Agreement Period: From 8/1/79 Until 12/31/79

Type Agreement: Subcontract No. C-10137 (under Prime No. DNA001-79-C-0181)

Amount: \$55,407

Reports Required: Final Technical Report

Sponsor Contact Person (s):

Technical Matters

Alan A. Burns
Project Technical Monitor

Contractual Matters
(thru OCA)

H.G. Nielsen
Subcontract Administrator

Stanford Research Institute International
333 Ravenswood Avenue
Menlo Park, CA 94025
415/326-6200
TWX: 910/373-1246

Defense Priority Rating: None

Assigned to: RAIL/RED (School/Laboratory)

COPIES TO:

Project Director
Division Chief (EES)
School/Laboratory Director
Dean/Director-EES
Accounting Office
Procurement Office
Security Coordinator (OCA)
Reports Coordinator (OCA)

Library, Technical Reports Section
EES Information Office
EES Reports & Procedures
Project File (OCA)
Project Code (GTRI)
Other _____

GEORGIA INSTITUTE OF TECHNOLOGY
OFFICE OF CONTRACT ADMINISTRATION

SPONSORED PROJECT TERMINATION

REVISED - MOD. NO. 2

Date: 1/27/81

Project Title: Misers Bluff II Data Reduction

Project No: A-2465

Project Director: Mr. E. E. Martin

Sponsor: Stanford Research Institute International; Menlo Park, CA 94025

Effective Termination Date: 12/31/80

Clearance of Accounting Charges: _____

Grant/Contract Closeout Actions Remaining:

- Final Invoice and Closing Documents
- Final Fiscal Report
- Final Report of Inventions
- Govt. Property Inventory & Related Certificate
- Classified Material Certificate
- Other _____

Assigned to: RAIL/RED (XXXX)
(School/Laboratory)

COPIES TO:

Project Director
Division Chief (EES)
School/Laboratory Director
Dean/Director-EES
Accounting Office
Procurement Office
Security Coordinator (OCA)
~~Reports Coordinator (OCA)~~

Library, Technical Reports Section
EES Information Office
Project File (OCA)
Project Code (GTRI)
Other _____

A-2465

Final Technical Report
Georgia Tech Project A-2465

**RADAR PROPOGATION THROUGH DUST CLOUDS
LOFTED BY HIGH EXPLOSIVE TESTS
MISERS BLUFF PHASE II**

by
E. E. Martin

October 1980

Prepared for
SRI International
Menlo Park, California

GEORGIA INSTITUTE OF TECHNOLOGY

**Engineering Experiment Station
Atlanta, Georgia 30332**



Final Technical Report
Georgia Tech Project A-2465

Radar Propagation through Dust Clouds
Lofted by High Explosive Test
- MISERS BLUFF PHASE II -

by
E. E. Martin

Prepared for:

SRI International
Menlo Park, California

GEORGIA INSTITUTE OF TECHNOLOGY
Engineering Experiment Station
Atlanta, Georgia 30332

October 1980

ABSTRACT

Measurements of the radar reflectivity and attenuation characteristics of the dust clouds lofted by the two Events of the MISERS BLUFF Phase II Test Series were accomplished during the summer of 1978. The data collected during the field operation were reduced and analyzed. Results of the analysis show that for the 120 ton event, peak radar cross sections of $2.8 \times 10^{-6} \text{ m}^2/\text{m}^3$ and $3.5 \times 10^{-5} \text{ m}^2/\text{m}^3$ were recorded at 9.4 GHz and 35 GHz, respectively. No attenuation was measured for this event at 9.4 GHz and only minimal attenuation was measured at 35 GHz. The actual attenuation measurement was subject to large errors due to the limited number of points and high variations in the data; however, the attenuation associated with the event is expected to be less than 3 dB at 35 GHz. Much larger radar cross sections and significant attenuation were measured during the 720-ton event. The measured peak radar cross sections for this event were $1.2 \times 10^{-4} \text{ m}^2/\text{m}^3$ and $7.0 \times 10^{-4} \text{ m}^2/\text{m}^3$ at 9.4 GHz and 35 GHz, respectively. The maximum attenuation occurred approximately 2 seconds after detonation and reached magnitudes of 6.3 dB and 10.2 dB at 9.4 GHz and 35 GHz, respectively.

TABLE OF CONTENTS

<u>Section</u>		<u>Page</u>
1	INTRODUCTION.....	1
2	EXPERIMENTAL AND ANALYTICAL PROCEDURES.....	4
	2.1 CALIBRATION PROCEDURES.....	4
	2.2 CALIBRATION ERRORS.....	5
	2.3 EXPECTED MEASUREMENT ACCURACY.....	6
	2.4 DATA CALIBRATION AND REDUCTION.....	7
3	EXPERIMENTAL RESULTS.....	8
	3.1 RADAR BACKSCATTER CROSS SECTION.....	8
	3.1.1 EARLY AND INTERMEDIATE TIME PERIOD....	9
	3.1.2 LATE TIME PERIOD.....	21
	3.2 ATTENUATION COEFFICIENT.....	31
	3.2.1 METHOD OF ANALYSIS.....	31
	3.2.2 VERIFICATION OF ANALYSIS PROCEDURE....	35
	3.3 FREQUENCY DEPENDENCY.....	37
4	CONCLUSIONS	53
	4.1 OVERVIEW.....	53
	4.2 EVENT 1 MEASUREMENTS SUMMARY.....	53
	4.3 EVENT 2 MEASUREMENTS SUMMARY.....	54
	REFERENCES	55
Appendix A		
	RADAR CROSS SECTION VERSUS RANGE.....	56

LIST OF ILLUSTRATIONS

<u>FIGURE</u>		<u>PAGE</u>
1	9.4 GHz radar cross section vs. range; Event 2, $T_0 + 1$ second.....	10
2	35 GHz radar cross section vs. range; Event 2, $T_0 + 1$ second.....	11
3	Waterfall plot showing the 9.4 GHz radar signal for the first 10 seconds of Event 1.....	12
4	Waterfall plot showing the 35 GHz radar signal for the first 10 seconds of Event 1.....	13
5	Waterfall plot showing the 9.4 GHz radar signal for the first 10 seconds of Event 2.....	15
6	Waterfall plot showing the 35 GHz radar signal for the first 10 seconds of Event 2.....	16
7	Radar cross section vs. time; 9.4 GHz, Event 1.....	17
8	Radar cross section vs. time; 35 GHz, Event 1.....	18
9	Radar cross section vs. time; 9.4 GHz, Event 2.....	19
10	Radar cross section vs. time; 35 GHz, Event 2.....	20
11	Waterfall plot showing the 9.4 GHz radar signal during the vertical scan of the cloud for Event 2 beginning at 11:00:52.....	22
12	Waterfall plot showing the 35 GHz radar signal during the vertical scan of the cloud for Event 2 beginning at 11:00:52 hours.....	23
13	Antenna track for Event 2 data beginning at 11:00:51.....	24
14	Waterfall plot showing the 9.4 GHz radar signal during the vertical scan of the dust cloud beginning at 11:02:36.....	25
15	Waterfall plot shown in the 9.4 GHz radar signal during the vertical scan of the dust cloud beginning at 11:02:36.....	26

LIST OF ILLUSTRATIONS (continued)

<u>FIGURE</u>		<u>PAGE</u>
16	Antenna track for Event 2 data beginning at 11:02:36.....	27
17	Waterfall plot showing the 9.4 GHz radar signal during one scan of the dust cloud beginning at 11:01:50.....	28
18	Waterfall plot showing the 35 GHz radar signal during one scan of the dust cloud beginning at 11:01:50.....	29
19	Antenna track for Event 2 data beginning at 11:01:52.....	30
20	Waterfall plot showing the 9.4 GHz radar signal during a scan of the dust cloud for Event 2 beginning at 11:05:00.....	32
21	Waterfall plot showing the 35 GHz radar signal during a scan of the dust cloud for Event 2 beginning at 11:05:00.....	33
22	Antenna track for Event 2 data beginning at 11:05:00.....	34
23	Frequency dependence vs. range for 1 to 1.8 seconds after detonation of Event 1.....	39
24	Frequency dependence vs. range for 2 to 2.8 seconds after detonation of Event 1.....	40
25	Frequency dependence vs. range for 7 to 7.8 seconds after detonation of Event 1.....	41
26	Frequency dependence vs. range for 19.4 to 19.8 seconds after detonation of Event 1.....	42
27	Frequency dependence vs. range for 1 to 1.8 seconds after detonation of Event 2.....	44
28	Frequency dependence vs. range for 5 to 5.8 seconds after detonation of Event 2.....	45
29	Frequency dependence vs. range for 12 to 12.8 seconds after detonation of Event 2.....	46

LIST OF ILLUSTRATIONS (continued)

<u>FIGURE</u>		<u>PAGE</u>
30	Frequency dependence vs. range for 19 to 19.8 seconds after detonation of Event 2.....	47
31	Comparison of the value of N before (dashed) and after (solid) being corrected for attenuation; Event 2 data at 11:00:02.1.....	48
32	Frequency exponent (N) vs. time for the single range cell of peak radar cross section. Event 1....	49
33	Frequency exponent (N) vs. time for the single range cell of peak radar cross section. Event 2....	50
34	Average frequency dependency exponent (N) for late time period; Event 2.....	52

LIST OF TABLES

<u>TABLE</u>		<u>PAGE</u>
1	EXPECTED MEASUREMENT ACCURACY.....	7
2	AVERAGE ATTENUATION AT 9.4 GHz AND 35 GHz FOR EVENT 2.....	36
3	COMPARISON OF THE TWO METHODS FOR DETERMINING THE DIFFERENCE IN ATTENUATION.....	38

SECTION 1
INTRODUCTION

The Defense Nuclear Agency conducted a series of high explosive test during the Summer of 1978 at the Planet Ranch Test Site located near Lake Havasu City, Arizona. These tests were designed to supply data needed in support of the MX program. A number of add-on experiments, independent of the MX program, were conducted to take advantage of the various phenomena resulting from these high explosive detonations. This series of tests was designated MISERS BLUFF II and consisted of two events. The first event was the detonation of a single 120-ton domed cylinder of ammonium nitrate and fuel oil (ANFO). The second event consisted of the simultaneous detonation of six 120-ton domed cylinders of ANFO. The six cylinders were equally spaced around a 200-meter diameter circle.

An experiment was designed by SRI International to measure the electromagnetic scattering and attenuation properties of the dust clouds lofted by these explosions. The fundamental goal of the experiment was to supply information needed to evaluate the performance of millimeter wave radar systems in the presence of extensive dust clouds lofted by surface or near-surface nuclear detonations. Tests such as the MISERS BLUFF II test series are currently the only means by which basic data on the low-altitude atmospheric effects of high energy detonations can be obtained. The results must then be scaled to the much larger nuclear environment by appropriate theoretical or empirical means. The Georgia Institute of Technology Engineering Experiment Station (GIT/EES) furnished four radars operating at frequencies of 9.375 GHz, 35 GHz, 69.9 GHz, and 95 GHz for collecting the radar backscatter data. SRI International furnished a modified AN/MPQ 18 antenna pedestal, a 10-foot X-band antenna, and the data acquisition and recording system. A description of the test site, radars, and experimental procedures use in collecting the data,

and selected preliminary data were included in a previous report.^[1] This current report covers the work accomplished during a follow-on data reduction program under subcontract P.O. No. 10137.

The data from the 70 GHz and 95 GHz radars were carefully reviewed. Data from the 70 GHz radar showed no evidence of a signal originating from the dust cloud at any time during the first twenty seconds. Data from the 95 GHz radar showed that one range cell contained a signal only about 2 dB above the noise level. This signal was present for approximately 8 seconds before falling below the noise level. The signal at 95 GHz was not of sufficient quality to justify further analysis. Loss of the data at 70 GHz and 95 GHz is due primarily to two factors: (1) Insufficient receiver sensitivity, and (2) Waveguide and component losses within the radar systems. A third reason for lack of performance at these two frequencies is the limited power available from transmitter sources operating at millimeter wavelengths. The electromagnetic scattering properties at these two frequencies may, however, be estimated by theoretically projecting the results obtained at 9.4 GHz and 35 GHz to these shorter wavelengths.

The results of this current analysis indicate that the measured radar cross sections for the two events were smaller than had been predicted by the original mathematical model. A refined model which takes into account the dielectric properties of the material gives closer agreement with the measured results.^[2] For Event 1, the peak volumetric radar cross sections at 9.4 GHz and 35 GHz were $2.8 \times 10^{-6} \text{ m}^2/\text{m}^3$ and $3.4 \times 10^{-5} \text{ m}^2/\text{m}^3$, respectively. The corresponding values for Event 2 were $1.2 \times 10^{-4} \text{ m}^2/\text{m}^3$ and $7.0 \times 10^{-4} \text{ m}^2/\text{m}^3$.

The attenuation properties of the dust cloud lofted during Event 1 were investigated; however, the results were not conclusive due to the variability of the data. It is estimated that little or no measurable attenuation was experienced at 9.4 GHz and that less than 3 dB attenuation was present at 35 GHz. In

light of the small measured radar cross section for Event 1, this estimate appears to be consistent with the values measured for Event 2.

Significant attenuation was measured at both 9.4 GHz and 35 GHz during the first few seconds of Event 2. For both events, the attenuation measurement was based on the reduction in the average radar signal return from the bluff behind ground zero. The maximum measured attenuation was 6.3 dB at 9.4 GHz and 10.2 dB at 35 GHz.

SECTION 2
EXPERIMENTAL AND ANALYTICAL PROCEDURES

2.1 CALIBRATION PROCEDURE

The calibration procedures used during the field operation were designed to give an absolute radar cross section reference level for comparison to a stepped IF receiver transfer characteristic. The procedure used was to first generate a stepped receiver transfer characteristic by inputting an arbitrary signal from a signal generator into the IF section of the receiver. This level was then reduced in 10 dB steps over the full dynamic range of the receiver as the receiver outputs were digitized and recorded. The radars were then turned on and pointed towards corner reflectors of known radar cross section. Signals were recorded from three corner reflectors used as calibration references. The primary reference was a 24.3 cm x 8.2 cm dihedral corner reflector designed to produce a 1° vertical plane beamwidth and to have a 30 dBsm cross section at 95 GHz. The dihedral corner reflector was rotated 22.5° from vertical, mounted on a stand 8 feet high, and located in the Bill Williams river bed 1275 meters from the radars. The other two calibration references were trihedral corner reflectors having radar cross sections of 55 dBsm and 60 dBsm at 95 GHz; they were located on the bluff behind ground zero and near the top of Black Mesa.

The calibration results were within 4 dB of the calculated performance at 70 GHz and 95 GHz, but were inconsistent with the calculated theoretical performance of the two lower frequency radars. At 9.4 GHz and 35 GHz, the calibration results deviated from the calculated results by up to 18 dB. Multipath effects are the most probable cause for such a large deviation from the expected return. Effects of multipath propagation on returns from the two trihedral corner reflectors were anticipated because of their location relative to the radars, however, the dihedral corner reflector was thought to be positioned so that

the local terrain would act as a "radar fence" and minimize multipath effects. Apparently, sufficient forward scattering from the ground surface existed to invalidate system calibration using the dihedral corner reflector.

The 9.4 GHz and 35 GHz radars were recalibrated in the laboratory at Georgia Tech after they were returned from the field. This calibration was achieved by inserting a known RF signal into the waveguide at the dual mode couplers. This absolute power calibration was then used as the basis for comparison with the IF calibration recorded in the field. The RF power calibration actually allowed a better definition of the low level signals since the lower 15 dB segment of dynamic range was divided into 3 dB, rather than 10 dB, steps.

2.2 CALIBRATION ERRORS

The radar calibration required that two sets of calibration data be recorded. The first set of data was recorded in the field as set of digital numbers corresponding to each 10 dB step of the IF attenuator. The second set of data was recorded in the laboratory as voltage levels corresponding to a known input power. The two sets of calibrations were plotted on appropriate scales and overlaid to facilitate conversion from input power level (in dBm) to digital numbers. These converted data were entered into the computer for conversion of the raw data into volumetric radar cross section.

Inaccuracies in overlaying the RF power calibration curve and the IF calibration curve resulted in errors of +3.0 dB at 9.4 GHz and -0.4 dB at 35 GHz in the preliminary data presented in the original report.^[1] The absolute error in the calibration is expected to be no more than ± 1.5 dB for levels greater than 10^{-8} m^2/m^3 at 9.4 GHz and 10^{-6} m^2/m^3 at 35 GHz. The last 15 dB of the calibration curves, i.e., levels below 10^{-8} m^2/m^3 and 10^{-6} m^2/m^3 , are more sensitive to signal level because of the near flat shape of the receiver transfer characteristics and could cause errors as great as 3.5 dB.

Other errors in the calibration procedure are attributable to inaccuracies in the power measuring equipment used to measure the transmitter and the signal generator power and to antenna gain errors used in the radar equation. The power meter used in the field prior to the test was an HP432B with appropriate thermistor mounts. Manufacturing specifications state an accuracy of $\pm 2\%$ for this meter. The same meter was used in measuring the power output of the signal generator used to inject the calibration signal into the waveguides. The remaining errors in the backscatter measurement are associated with the antennas.

There were no gain measurements made on either the 9.4 GHz or 35 GHz antennas. The 35 GHz antenna was manufactured by TRG Inc., and beam patterns were made prior to delivery of the antenna to Georgia Tech. Based on a 50% efficiency and the measured E & H plane beamwidths, a gain of 48 dB was calculated for this antenna. The accuracy of the gain calculation is expected to be within ± 1 dB.

The 9.4 GHz antenna gain calculation was based on the frequency of operation and its diameter using a 50% efficiency. No gain or pattern measurements were available for this antenna. Calculated values normally give good results for primary feed parabolic dish antennas, and the calculated gain of 47 dB is expected to be accurate to within ± 1 dB.

2.3 EXPECTED MEASUREMENT ACCURACY

The overall error in the radar measurement system is dependent on the amplitude of the return signal because of the shape of the calibration curve. This error is important in interpreting measurement data for times greater than 30 seconds after detonation since most of these late time signals were near or below the "knee" of the calibration curve. Table 1 shows the estimated accuracy for the measurement as a function of the measured cross section.

TABLE 1. EXPECTED MEASUREMENT ACCURACY

Signal Level m^2/m^3	Radar	Expected Accuracy
1.3×10^{-8}	9.4 GHz	3.1 dB
1.3×10^{-8}	9.4 GHz	5.1 dB
1.2×10^{-6}	35 GHz	3.1 dB
1.2×10^{-6}	35 GHz	5.1 dB

2.4 DATA CALIBRATION AND REDUCTION

The data collected in the field were recorded as binary numbers corresponding to the integrated video voltage. Similar data for receiver voltage transfer characteristics in 10 dB steps over the dynamic range of the systems were also recorded. These voltage transfer characteristics formed the basis for a "look-up table" used to compute the volumetric radar cross section of each recorded data sample. An additional data point computed from a least square fit over the last 20 dB of the calibration curve was inserted in the "look-up" table to increase resolution in the region of transition from a linear to a logarithmic receiver characteristic. A linear interpolation between points in the look-up table was used to determine intermediate cross section values. A calibration of input power versus output voltage was used to determine the value of the zero dB level of the look-up table. This zero dB value of received power was converted to radar cross section by substituting the known radar parameters into the range equation and solving for cross section.

A CDC Cyber computer was used to access, demultiplex, and calibrate the data. A computational routine was included in the computer program to calculate the frequency dependent exponent (N) and to correct for attenuation. Print and plot routines were used to generate tabulation and plots of the calibrated radar cross section data.

SECTION 3
EXPERIMENTAL RESULTS

3.1 RADAR BACKSCATTER CROSS SECTION

The power received by the radar is related to the cross section of the ensemble of scatterers within that volume of resolution defined by the radar beamwidth and pulse length. When the radar signal propagates through an attenuating medium, the received power is reduced; hence, appropriate corrections must be made before the true backscatter cross section can be determined. A significant amount of attenuation was present during the first few seconds of Event 2. Little or no attenuation was measured during Event 1.

The material lofted by the explosions was not uniformly distributed throughout the dust cloud; therefore, an attenuation factor was calculated and applied separately to each range bin. The attenuation for a given range bin was determined by apportioning the total attenuation according to the ratio of the cross section of that cell to the sum of the cross section of all cells over the extent of the dust cloud. Equation (1) describes the relationship used to calculate the individual attenuation constants

$$\alpha_k = \frac{\eta_k}{\sum_{i=1}^m \eta_i} \alpha_T \quad (1)$$

where α_k is the attenuation associated with the kth cell, η_k is the backscatter cross section of the kth cell, η_i is the backscatter cross section of the ith cell, m is the number of cells associated with the dust cloud, and α_T is the total measured attenuation. The summation is taken over the total extent of the dust cloud.

A computer routine was written to calculate the individual attenuation constants and to compute the true cross section according to

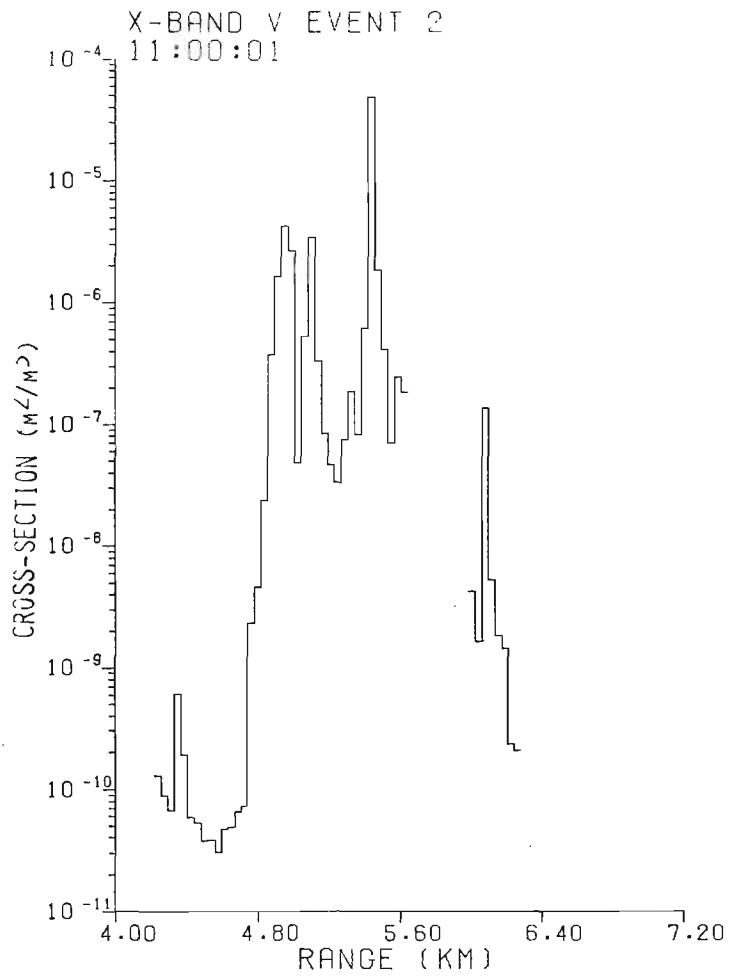
$$\eta_k = \eta_k^* 10^{\sum_{i=1}^{k-1} \alpha_i + 0.5\alpha_k} \quad (2)$$

where η_k and η_k^* are the true and measured values of the backscatter cross section, respectively. This correction was applied to the first 10 seconds of the Event 2 data. The values of α_T were derived from the attenuation constants computed from the reduction in the radar cross section of the bluff behind ground zero.

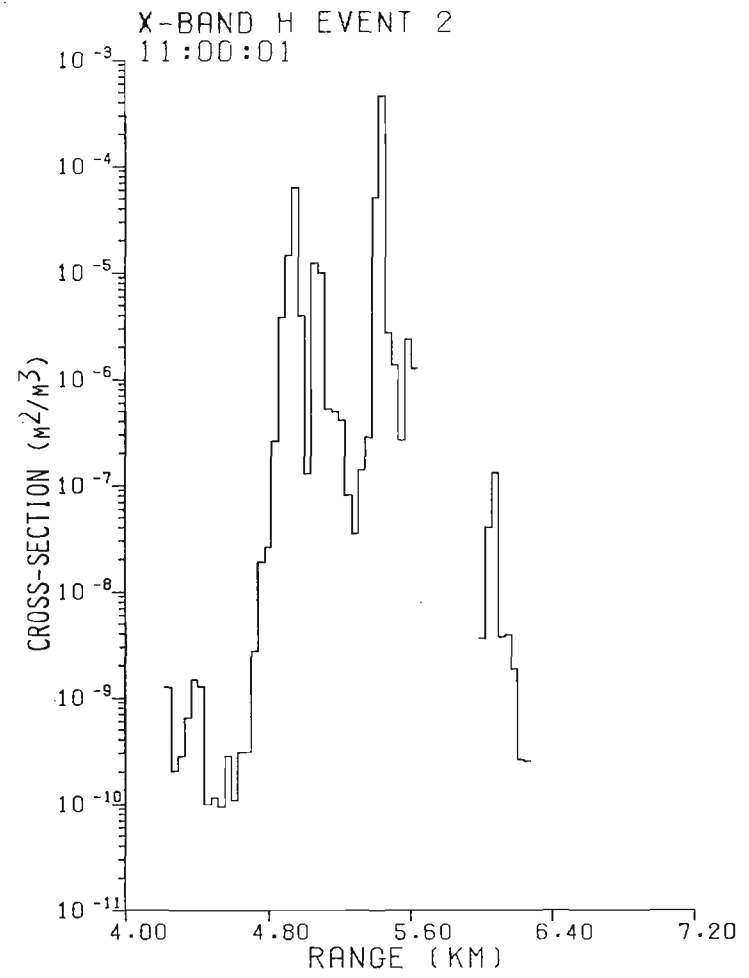
3.1.1 EARLY AND INTERMEDIATE TIME PERIOD

Figures 1 and 2 show the volumetric radar cross section (η) versus range for 9.4 GHz and 35 GHz one second after detonation of Event 2. These data were corrected for the effect of attenuation according to Equations (1) and (2). Both the parallel polarized (horizontal) and the cross polarized (vertical) backscatter cross section are shown. Signals occurring at ranges between 4.2 and 4.4 km are the returns from the ridge in front of ground zero. Signals occurring at ranges between 5.2 and 5.6 km are the returns from the bluff behind ground zero. Those signals occurring between the ridge and the bluff are due entirely to the dust and debris lofted by the explosion. The last 10 data samples (range bins 41 through 50) were offset in range to sample the signals from the corner reflector located at the top of Black Mesa. Additional plots of the calibrated data taken at 2 second intervals for the first 12 seconds of Event 1 and for the first 20 seconds of Event 2 are shown in the Appendix A.

Large amounts of data can be presented in a compact form by using a waterfall plot format. These plots are useful for showing gross changes in the structural features and in the growth of the cloud as a function of time. Figures 3 and 4 are waterfall plots of the data taken during the first 10 seconds

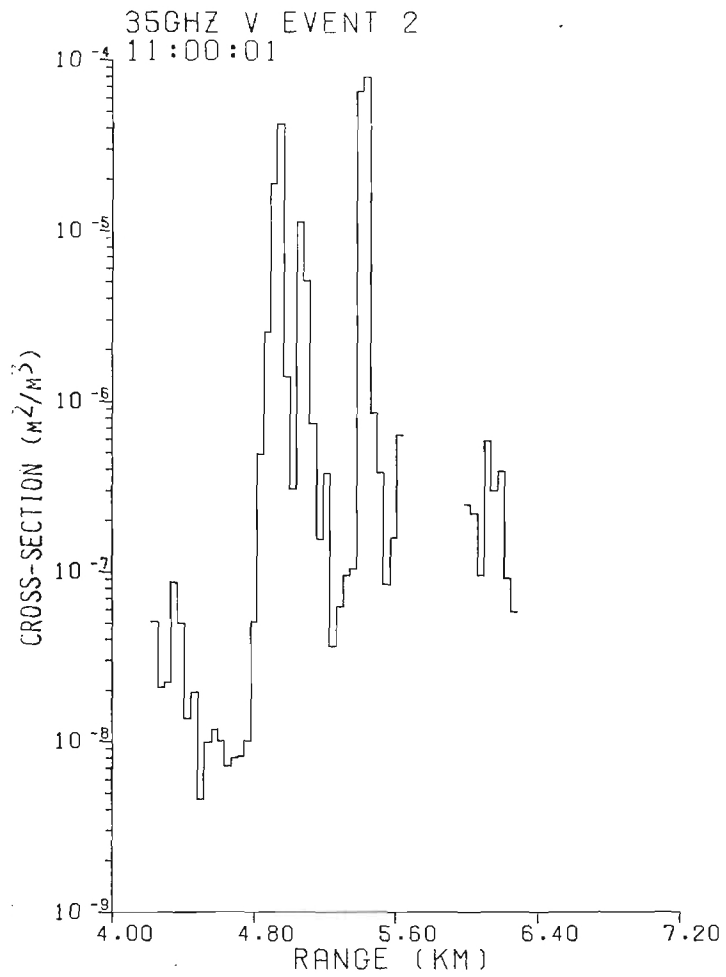


a. HV Polarization

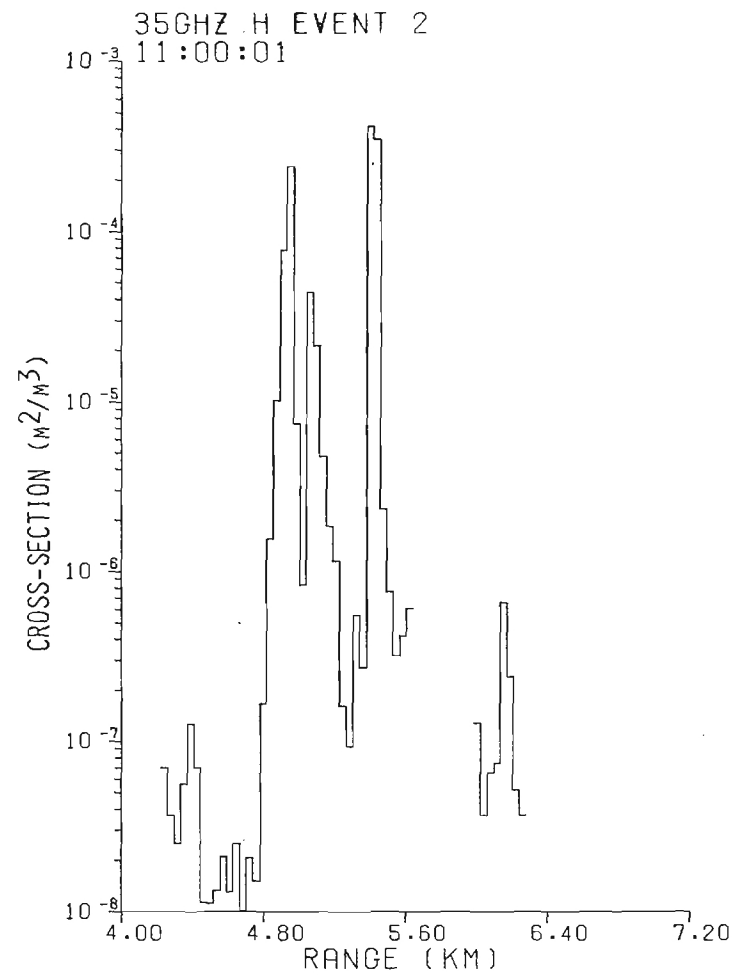


b. HH Polarization

Figure 1. 9.4 GHz radar cross section vs. range; Event 2, $T_0 + 1$ second.



a. HV Polarization



b. HH Polarization

Figure 2. 35 GHz radar cross section vs. range; Event 2, $T_0 + 1$ second.

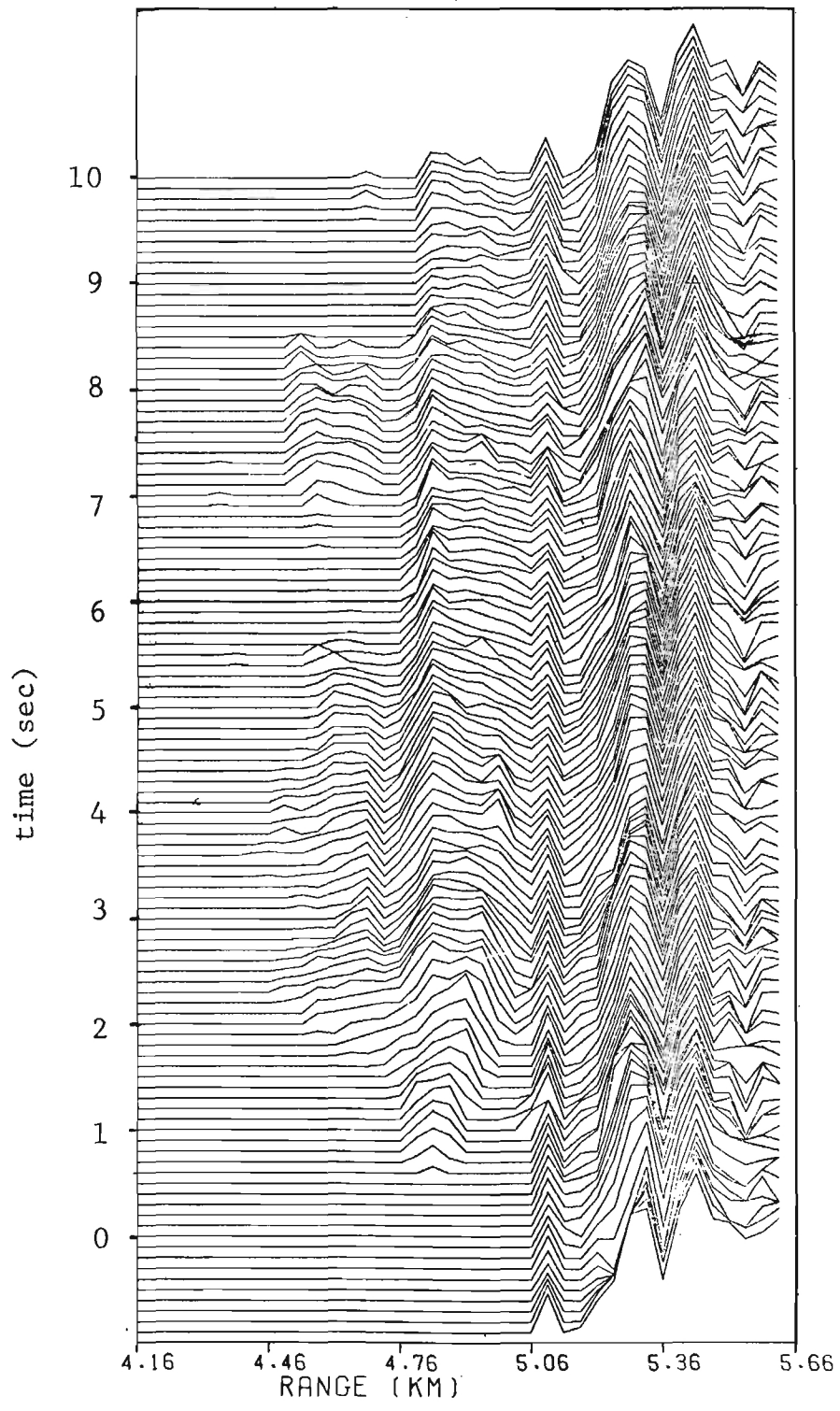


Figure 3. Waterfall plot showing the 9.4 GHz radar signal for the first 10 seconds of Event 1.

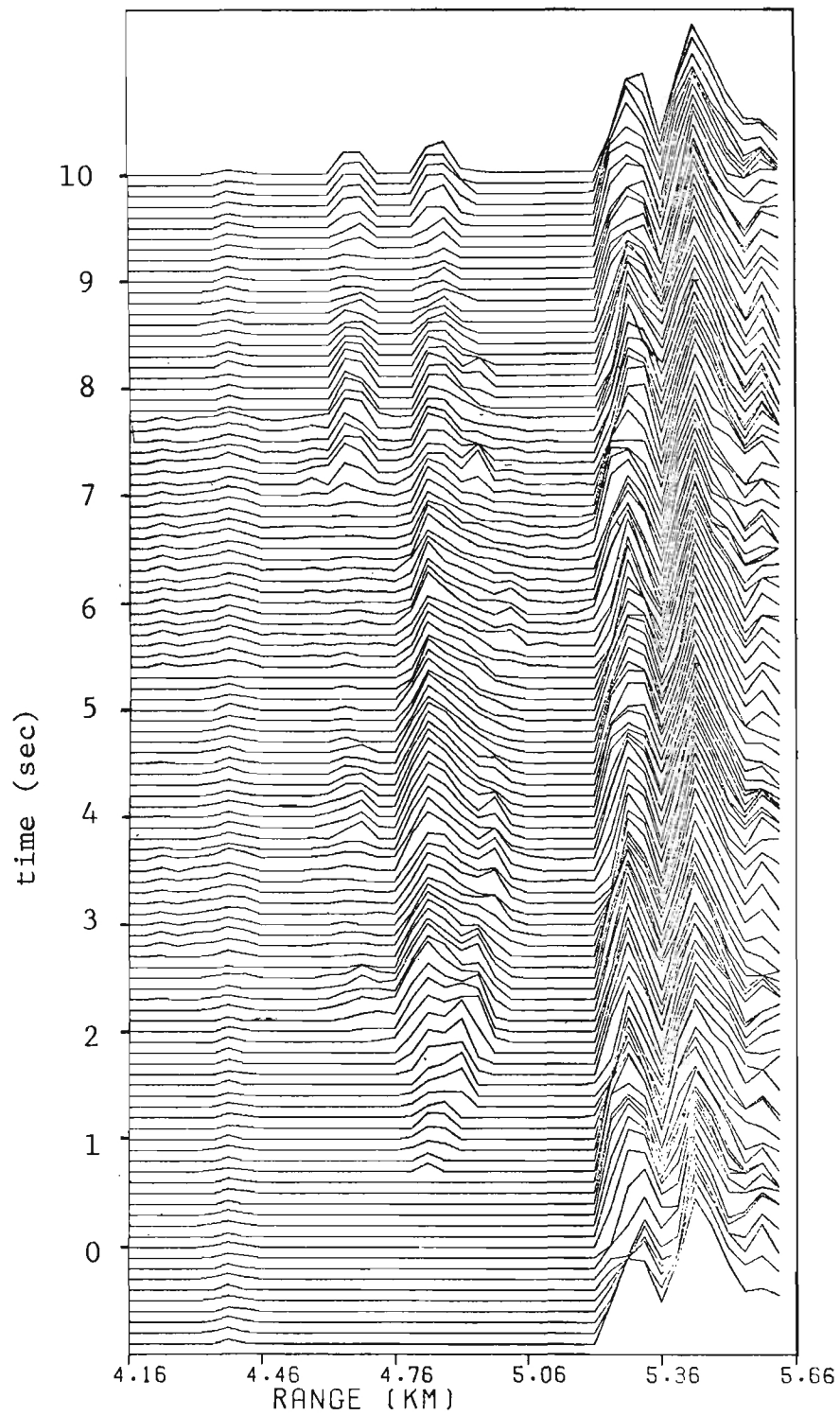


Figure 4. Waterfall plot showing the 35 GHz radar signal for the first 10 seconds of Event 1.

after detonation for Event 1. Similar plots for Event 2 data are shown in Figures 5 and 6. During Event 1, the maximum radar cross section initially occurred at a range of 4.83 km and, except for short periods, remained at this range during the first 10 seconds. During Event 2, the maximum cross section occurred at a range of 4.95 km over the first two seconds and then progressed out in range to 5.02 km at approximately 7 seconds.

The maximum radar cross section for the first 20 seconds is shown in Figures 7 and 8 for Event 1 and in Figures 9 and 10 for Event 2. The radar cross section reached a maximum at approximately 2 seconds after detonation for both events. The maximum radar cross section for Event 2 was approximately 15.9 dB greater at 10 GHz and 12.9 dB greater at 35 GHz than the maximum for Event 1. The Event 1 data appear more variable than the Event 2 data. Antenna motion was considered as a possible cause of the greater variability during Event 1; however, the maximum pointing variation for either event did not exceed one half beamwidth from the mean position during the first 10 seconds.

Between 2 and 14 seconds after the Event 2 detonation, the radar cross section fell off at a rate which may be approximated to within 3 dB by a linear regression line. For the data shown in Figures 9 and 10, the radar cross section is approximately given by:

$$\sigma(9.4) = 10^{-(3.41 + 0.263t)} \quad (\text{for } 2 < t < 14) \quad (3)$$

and

$$\sigma(35) = 10^{-(2.79 + 0.192t)} \quad (\text{for } 2 < t < 14) \quad (4)$$

For Event 2, a distinct change in the slope of the data occurs at approximately 14 seconds. At this time, the radar cross section had fallen by nearly 31 dB at 9.4 GHz and 24 dB at 35 GHz.

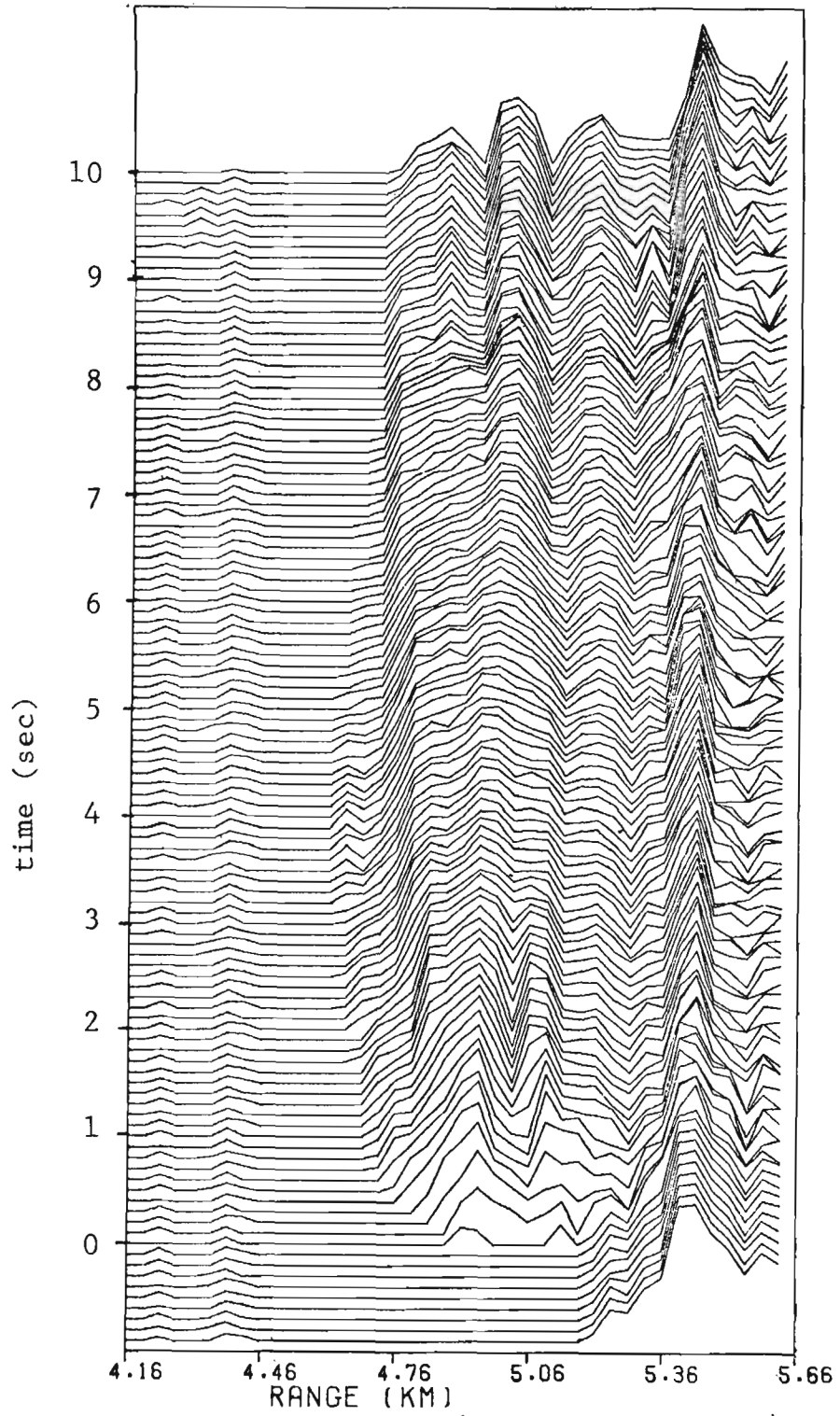


Figure 5. Waterfall plot showing the 9.4 GHz radar signal for the first 10 seconds of Event 2.

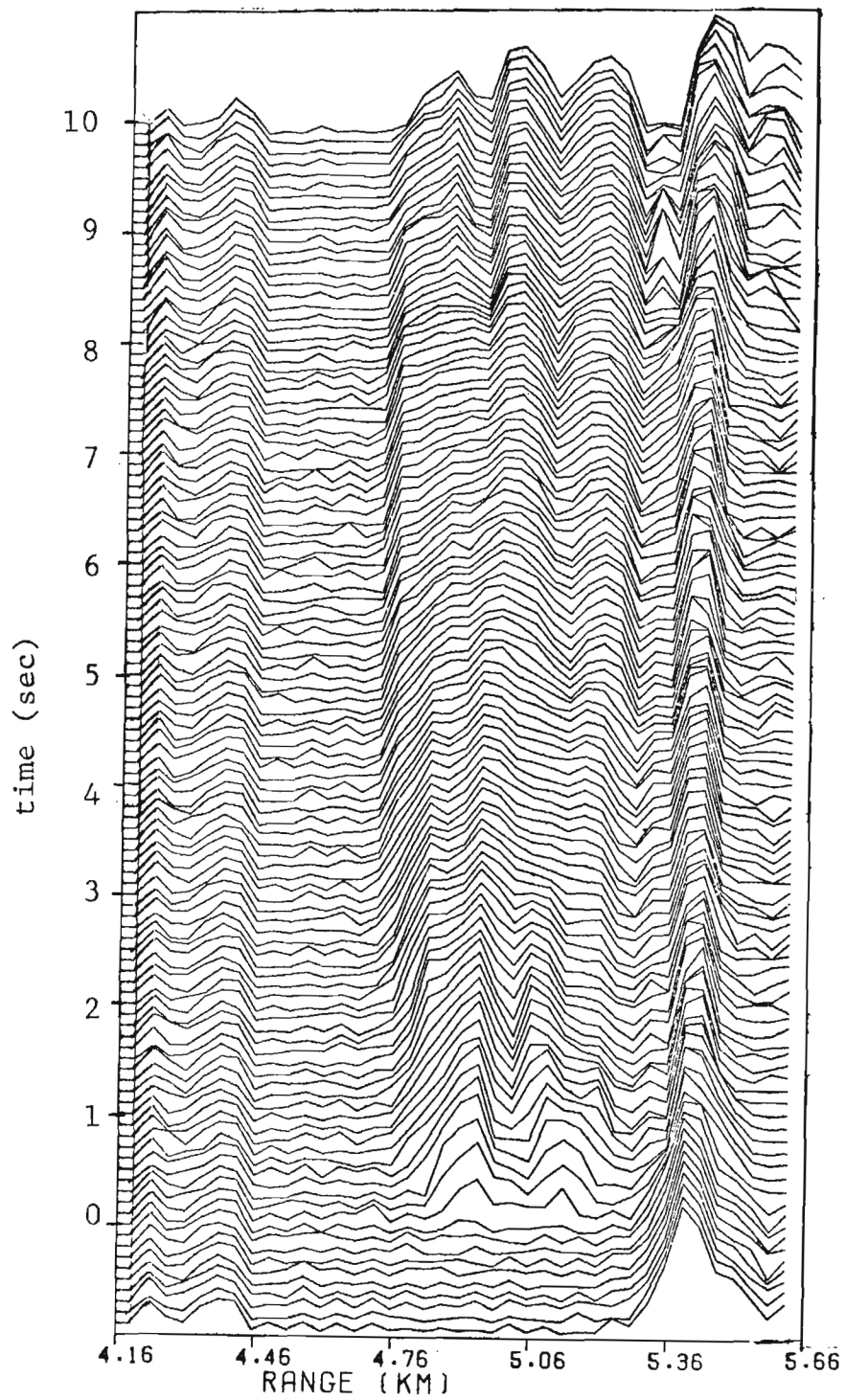


Figure 6. Waterfall plot showing the 35 GHz radar signal for the first 10 seconds of Event 2.

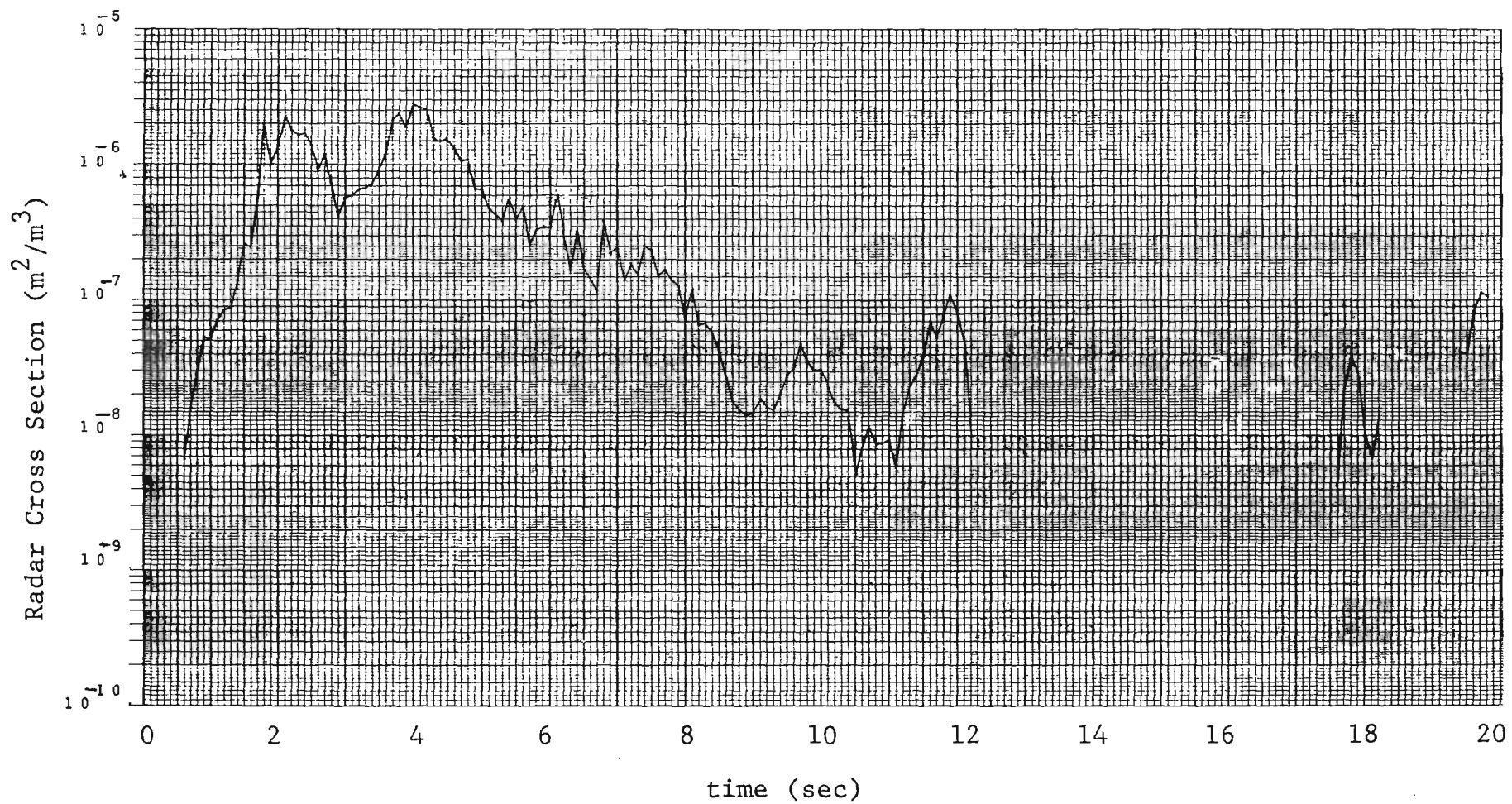


Figure 7. Radar cross section vs. time; 9.4 GHz, Event 1.

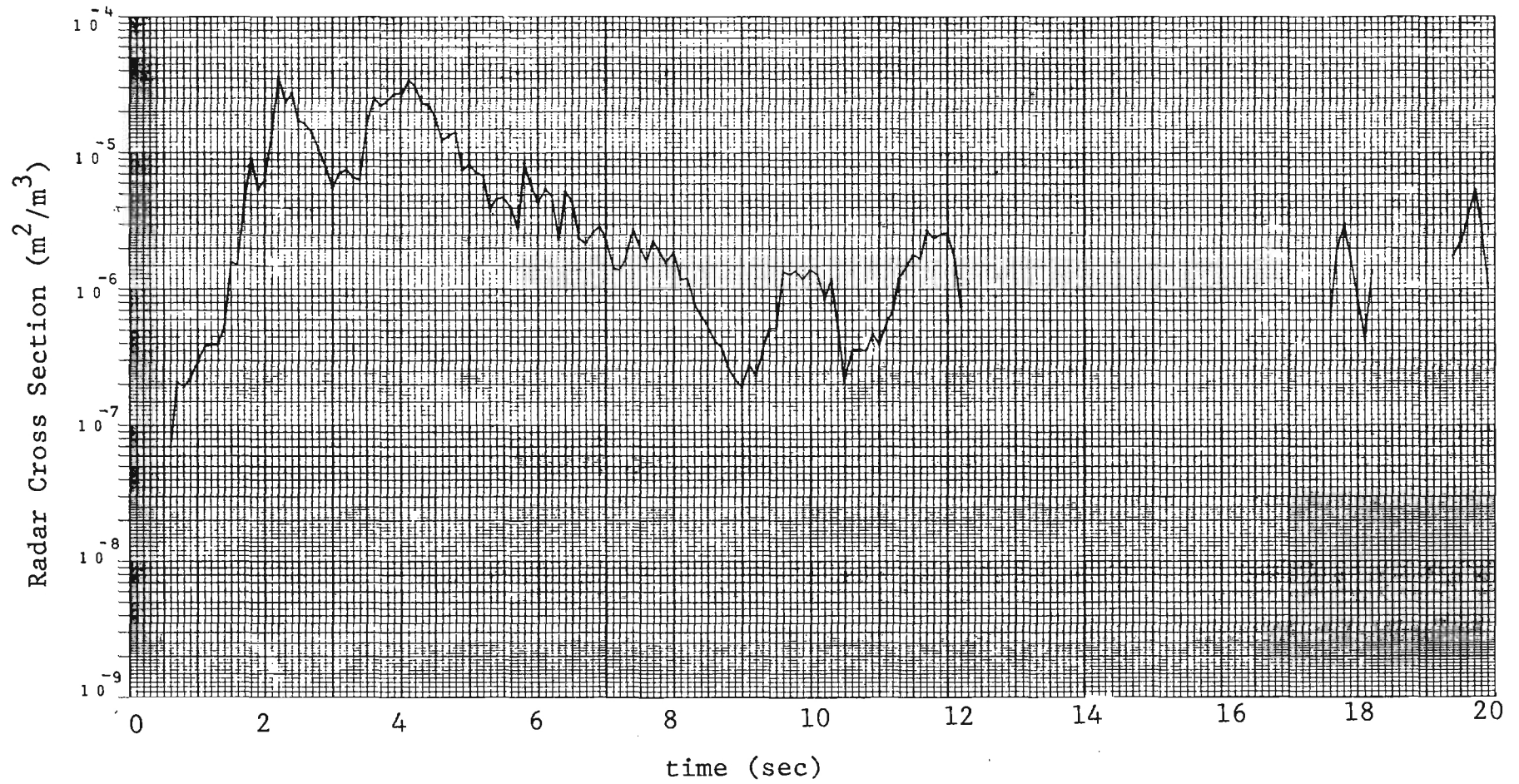


Figure 8. Radar cross section vs. time; 35 GHz, Event 1

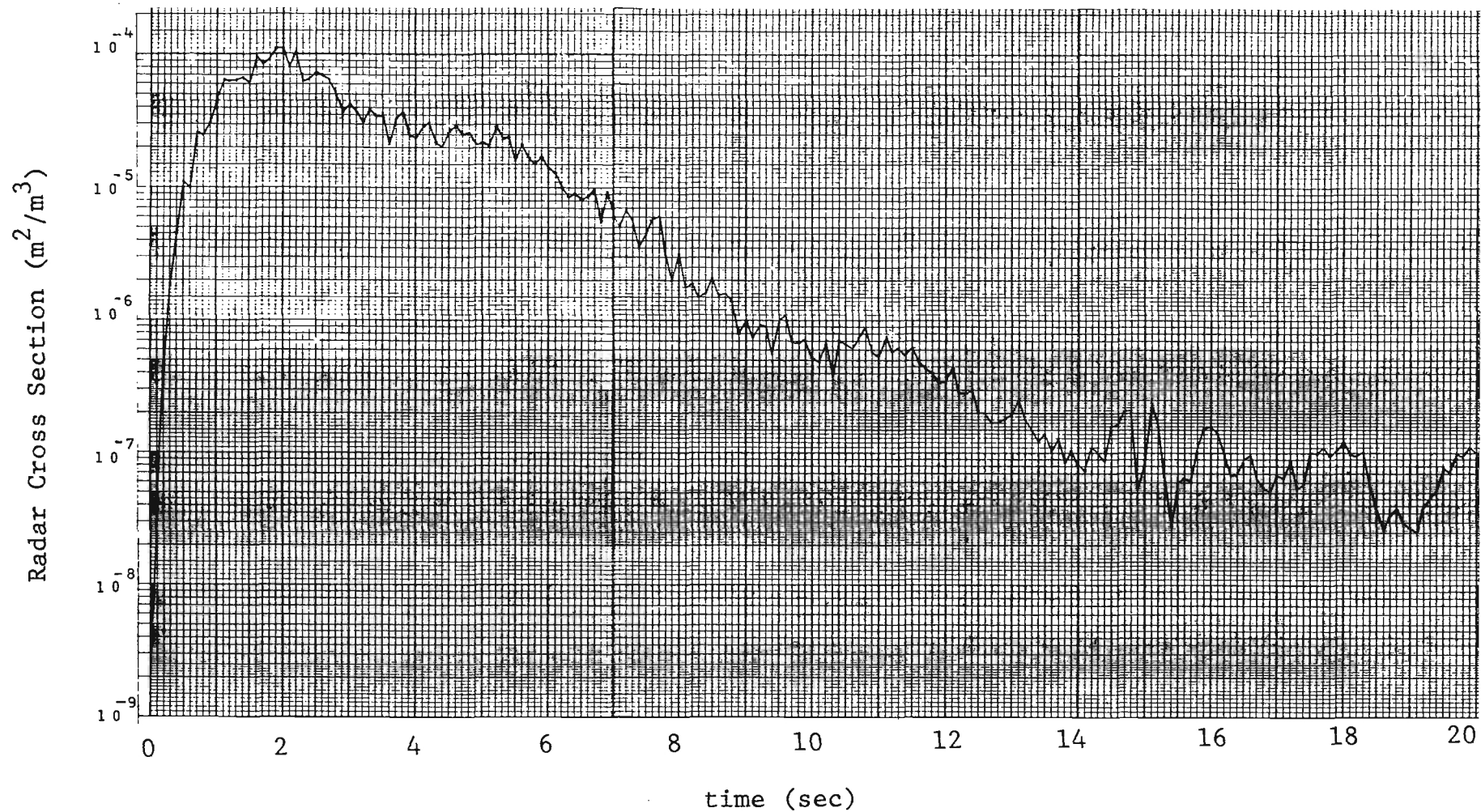


Figure 9. Radar cross section vs. time; 9.4 GHz, Event 2.

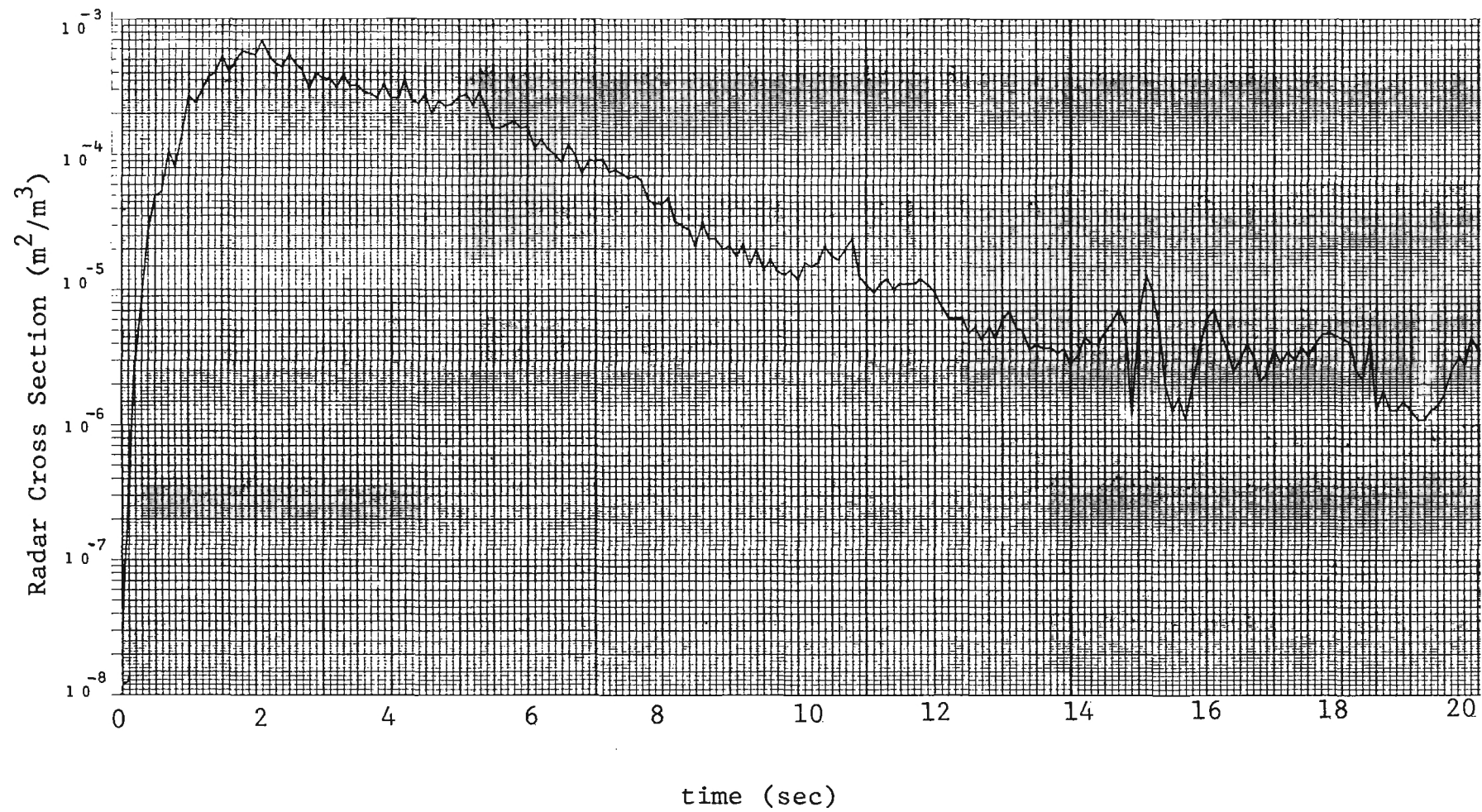


Figure 10. Radar cross section vs. time; 35 GHz, Event 2.

3.1.2 LATE TIME PERIOD

Waterfall plots of the data for first 60 seconds of Event 1 show that only a small amount of data was received after 12.3 seconds. Data were present for several short intervals over the first minute, but only the data occurring during the first 20 seconds were included in the analysis. The Event 2 dust cloud was significantly larger than that for Event 1, and signals occurring as late as 5 minutes after Event 2 detonation have been recovered.

Approximately 27 seconds after Event 2 detonation, the radars began a raster scan of the dust cloud and remained in that mode, except for short periods. Two manual vertical scans of the cloud were made: one at 11:00:52 hours, and one at 11:02:36 hours. Waterfall plots of the 9.4 GHz and 35 GHz radar signals received between 52 and 58 seconds are shown in Figures 11 and 12. Figure 13 is a photograph of the TV display showing the antenna track during this time period. The maximum radar cross sections recorded during the scan were $2.7 \times 10^{-8} \text{ m}^2/\text{m}^3$ at 9.4 GHz and $1.7 \times 10^{-6} \text{ m}^2/\text{m}^3$ at 35 GHz and occurred at a range of 4987 meters.

Waterfall plots of the signals received during the second vertical scan are shown in Figures 14 and 15. Figure 16 is a photograph of the TV display showing the antenna track during this scan. The maximum radar cross sections recorded during this scan were $1.1 \times 10^{-8} \text{ m}^2/\text{m}^3$ at 9.4 GHz and $4.4 \times 10^{-7} \text{ m}^2/\text{m}^3$ at 35 GHz. The maximum occurred at a range of 4987 meters and was in the lower part of the stem.

Waterfall plots of the data from one scan of the cloud at 11:01:50 hours are shown in Figures 17 and 18. Figure 19 is a photograph of the TV display showing the antenna track for this scan. The peak cross radar sections were $6.6 \times 10^{-9} \text{ m}^2/\text{m}^3$ at 9.4 GHz and $3.7 \times 10^{-7} \text{ m}^2/\text{m}^3$ at 35 GHz. Plots of the data received from 11:05:00 through 11:05:03 hours are shown in Figures 20 and 21. A photograph of the display showing the antenna track for

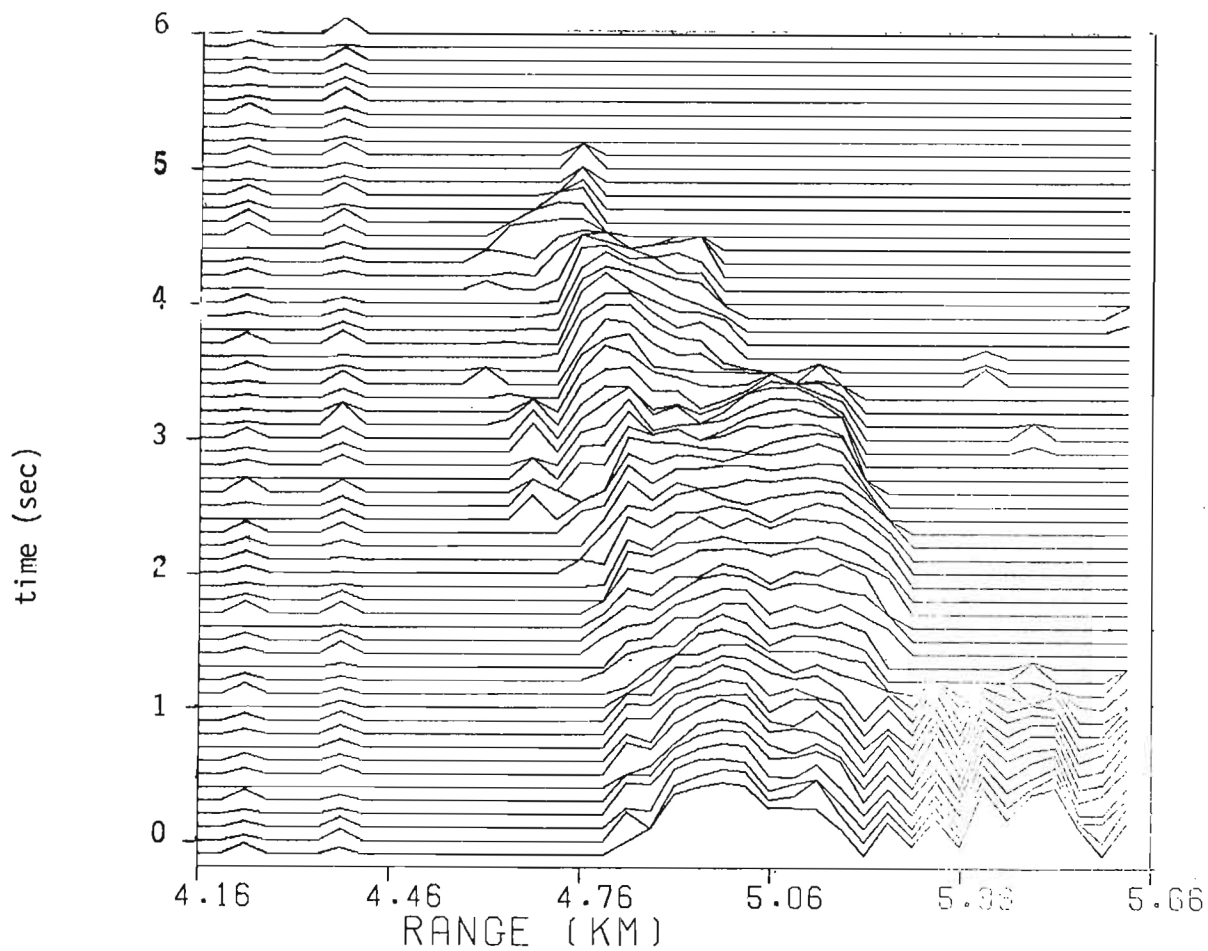


Figure 11. Waterfall plot showing the 9.4 GHz radar signal during the vertical scan of the cloud for Event 2 beginning at 11:00:52.

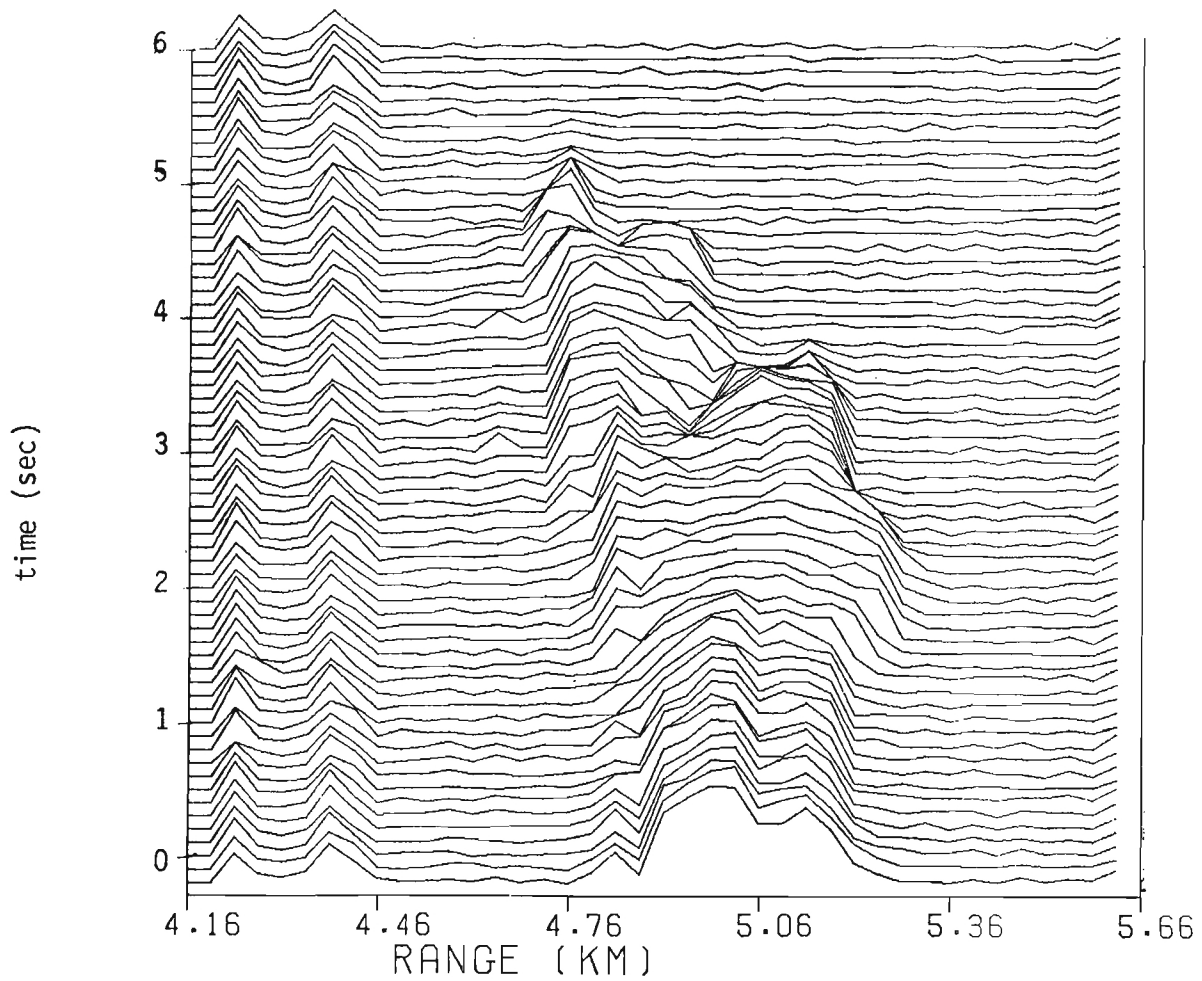


Figure 12. Waterfall plot showing the 35 GHz radar signal during the vertical scan of the cloud for Event 2 beginning at 11:00:52 hours.

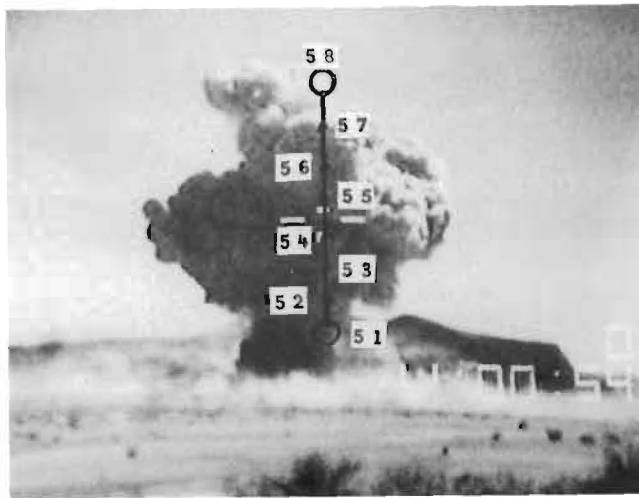


Figure 13. Antenna track for Event 2 data beginning at 11:00:51.

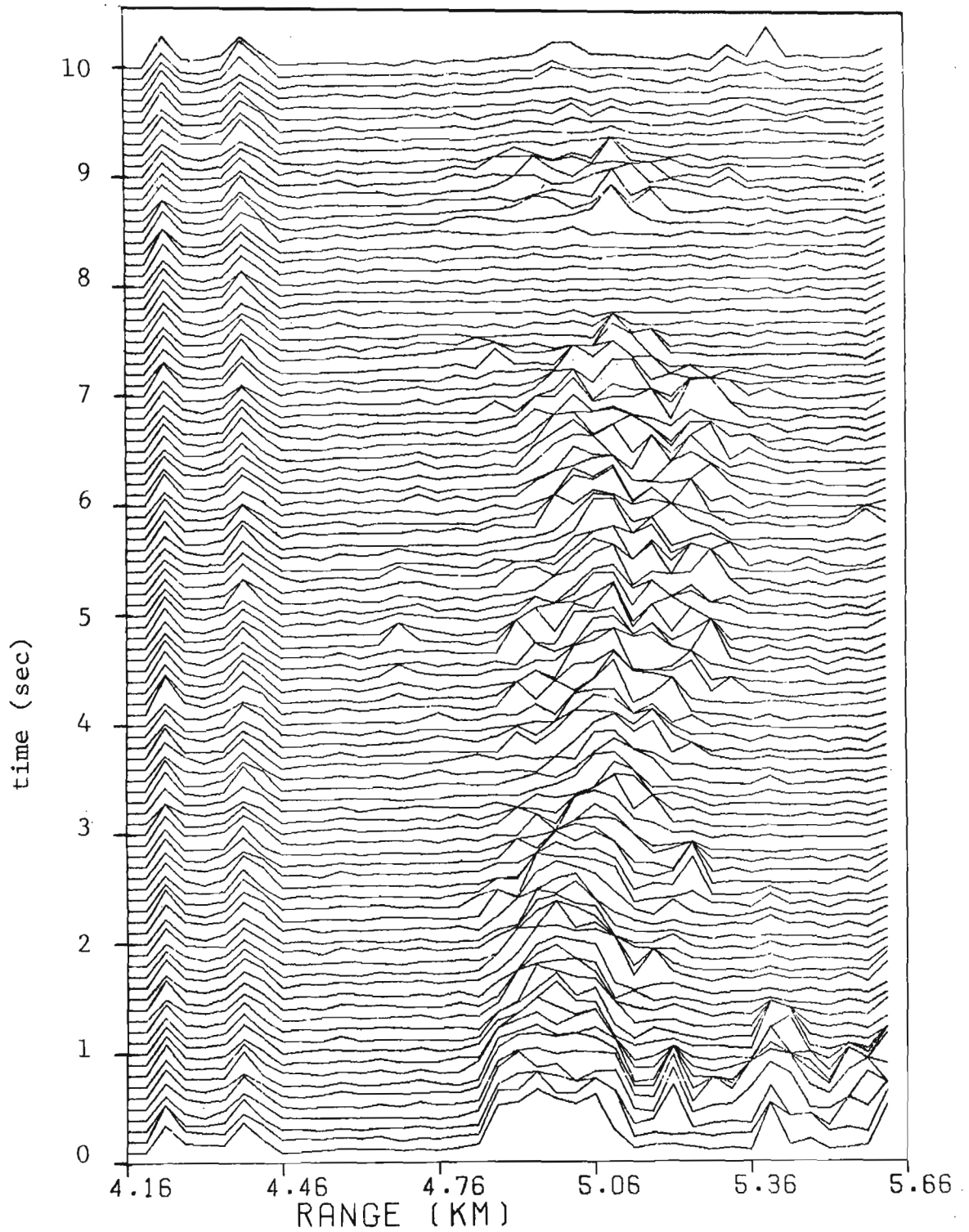


Figure 14. Waterfall plot showing the 9.4 GHz radar signal during the vertical scan of the dust cloud beginning at 11:02:36.

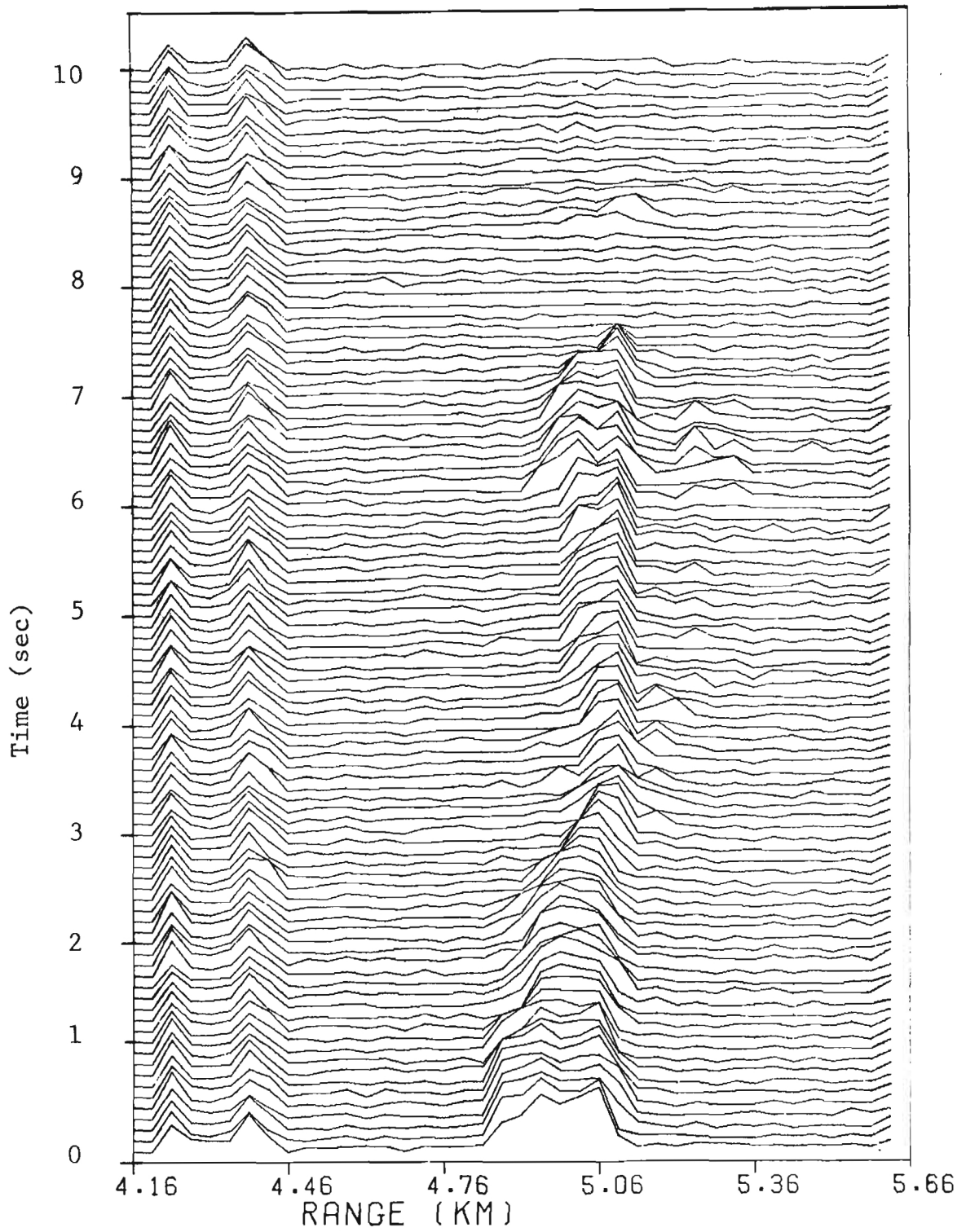


Figure 15. Waterfall plot shown in the 9.4 GHz radar signal during the vertical scan of the dust cloud beginning at 11:02:36.

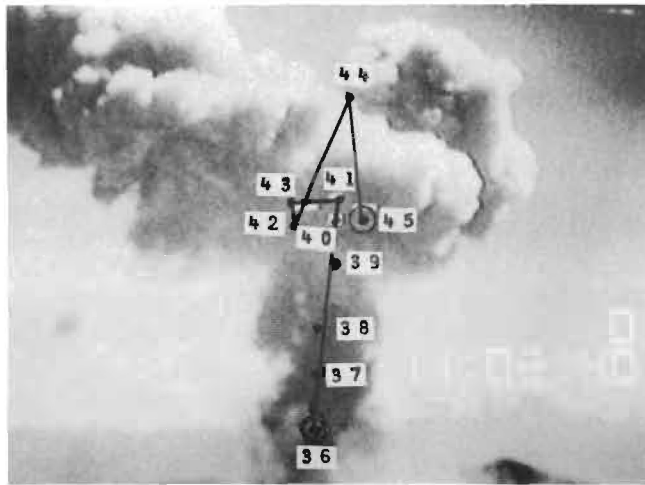


Figure 16. Antenna track for Event 2 data beginning at 11:02:36.

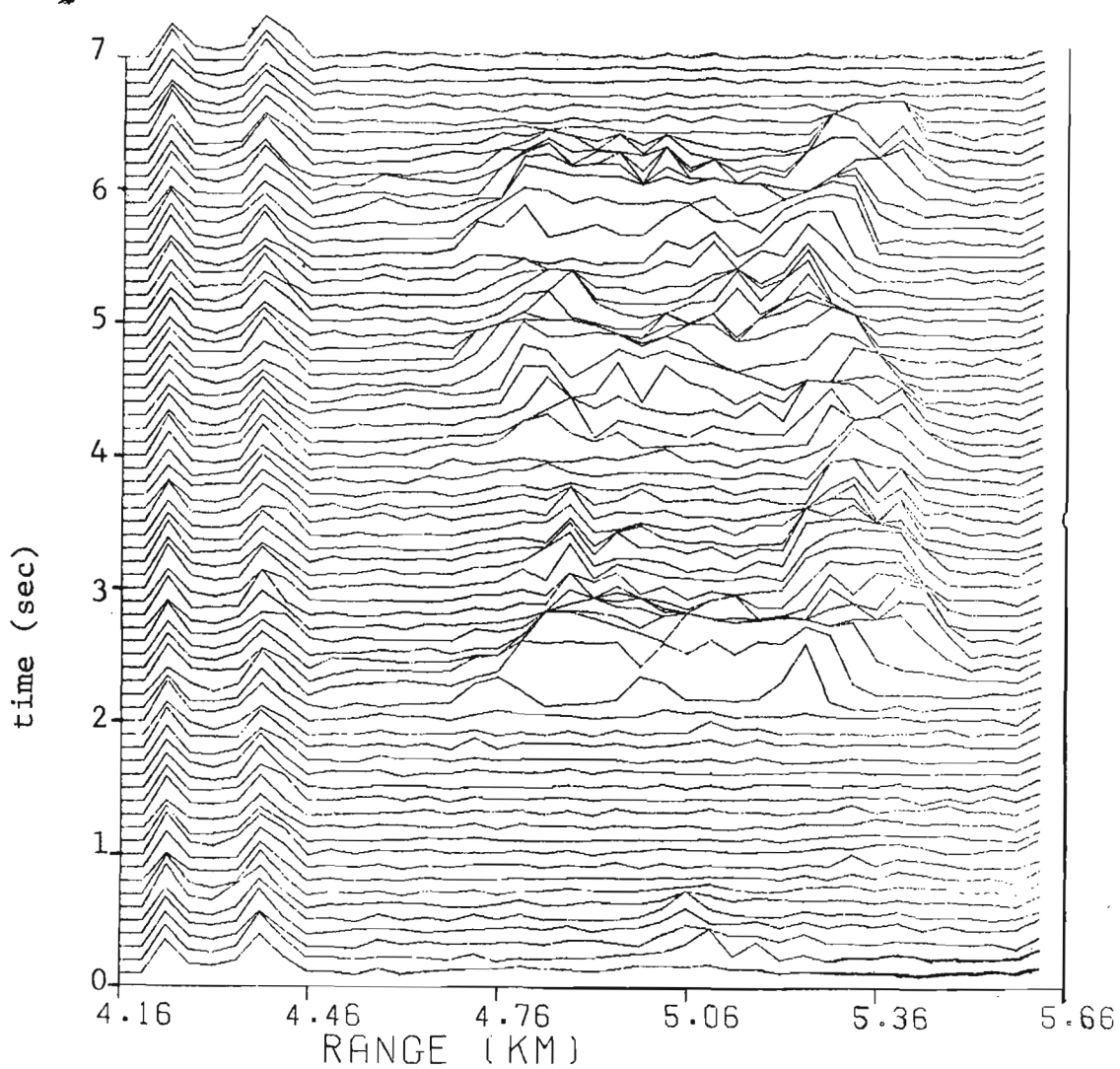


Figure 17. Waterfall plot showing the 9.4 GHz radar signal during one scan of the dust cloud beginning at 11:01:50.

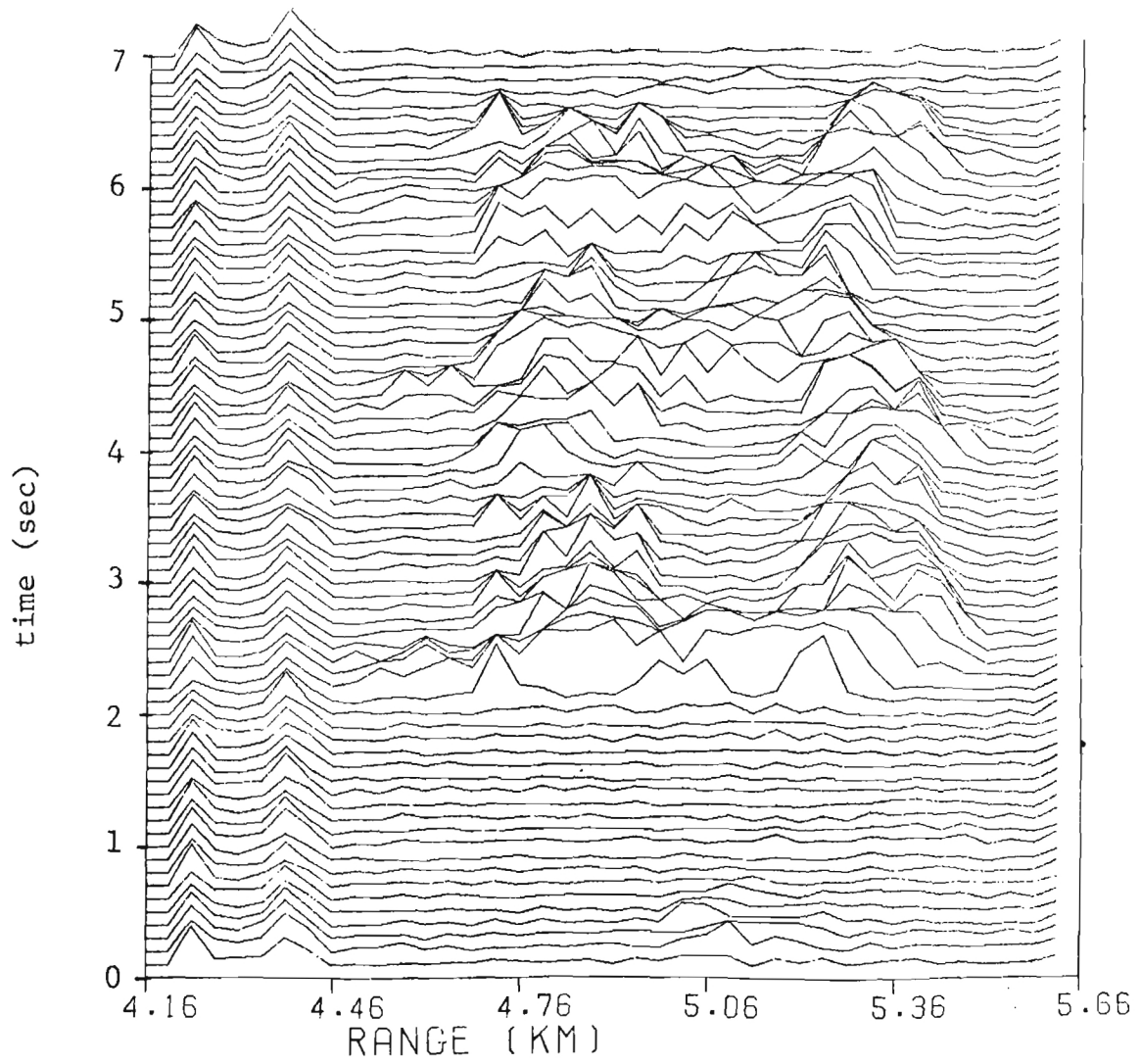


Figure 18. Waterfall plot showing the 35 GHz radar signal during one scan of the dust cloud beginning at 11:01:50

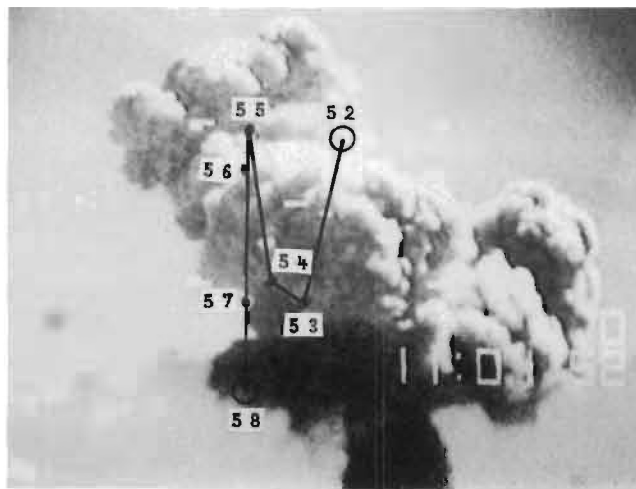


Figure 19. Antenna track for Event 2 data beginning at 11:01:52.

this time period is shown in Figure 22. The peak radar cross sections recorded during this period were 1.4×10^{-9} at 9.4 GHz and 4.7×10^{-8} at 35 GHz. These peaks occurred at 11:05:02.6 hours and a range of 4875 meters.

3.2 ATTENUATION COEFFICIENT

Both scattering losses and absorption losses act on radar signals propagating through the dust cloud. The sum of the scattering and absorption losses is the extinction loss. The experiment was designed so that the extinction loss could be measured directly by observing the reduction in the return from a corner reflector located on the bluff behind ground zero. This experiment as designed was not successful during Event 1 because the wind carried the dust cloud out of the line-of-sight between the radar and the corner reflector. During Event 2, the shock wave dislodged the corner reflector from its anchor so that it could not be used to provide extinction data. Thus in both events, the primary reference for determining the extinction coefficient was lost.

Since the bluff behind ground zero reflected part of the incident signal, the radar return from the bluff was used to investigate the attenuation properties of the dust cloud. Since the bluff is an extended target, the results of the loss measurement are influenced by whatever integrating effect this extended reference target has on the scattering losses.

3.2.1 METHOD OF ANALYSIS

The time variation in the radar returns from the irregular rocky surface of the bluff were investigated to determine if these signals were sufficiently stable to use as a reference for the attenuation measurements. Four separate range cells and 5 one-second time intervals were used in the investigation for Event 2. For Event 2, the peak variations in the signal from the bluff were within ± 1 dB of the mean value in 32 of the 40 samples. The variation for Event 2 was greater than ± 3 dB in

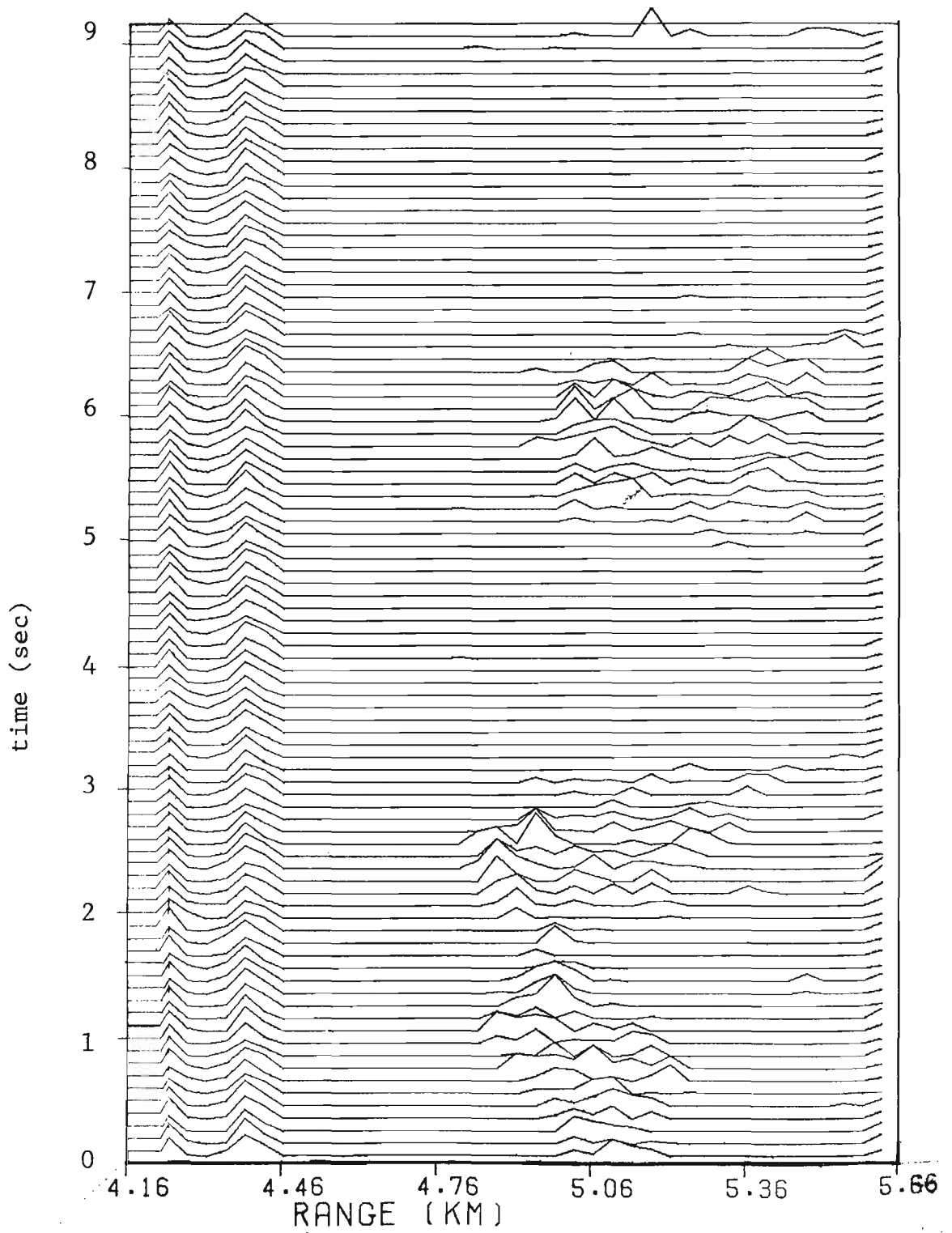


Figure 20. Waterfall plot showing the 9.4 GHz radar signal during a scan of the dust cloud for Event 2 beginning at 11:05:00.

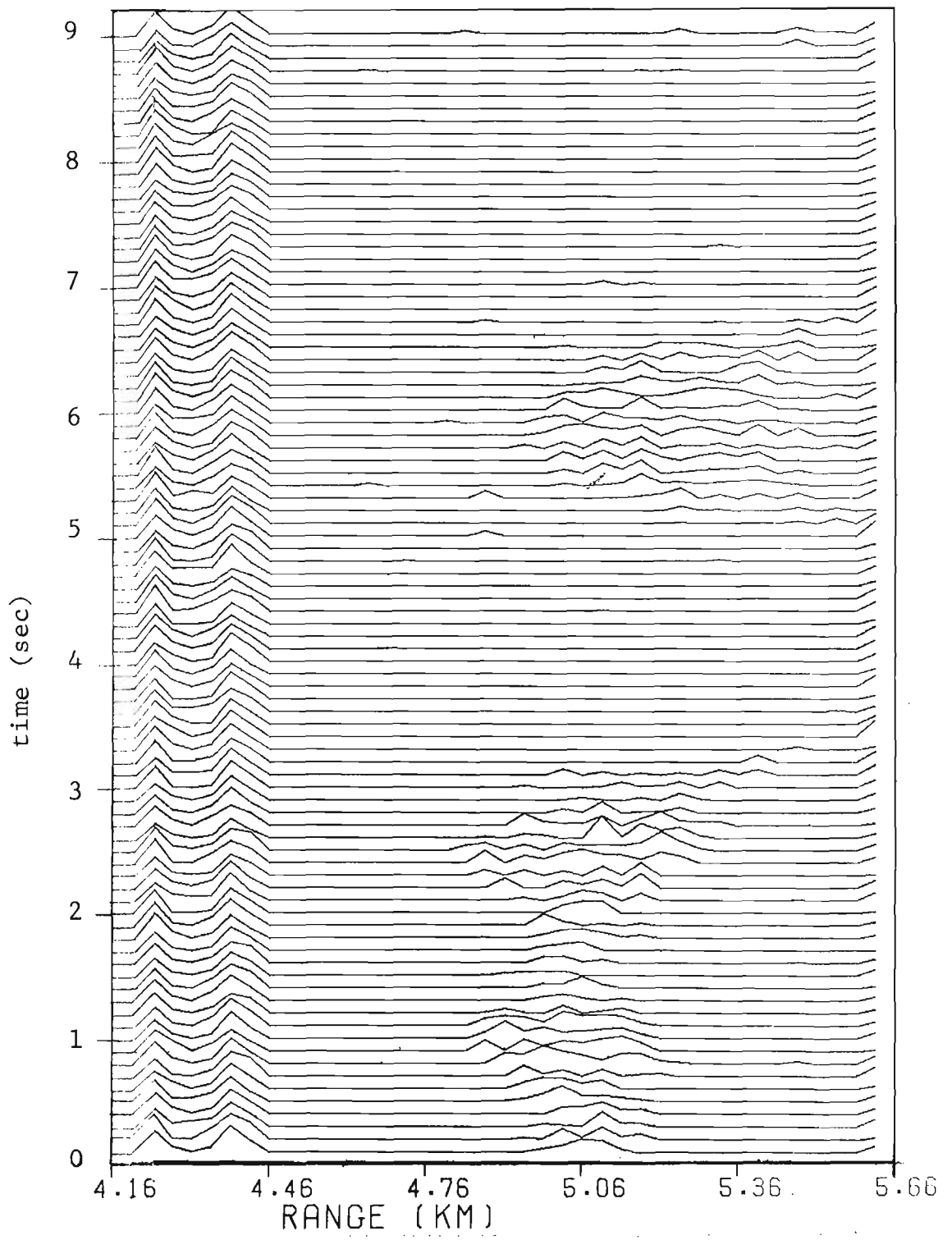


Figure 21. Waterfall plot showing the 35 GHz radar signal during a scan of the dust cloud for Event 2 beginning at 11:05:00.

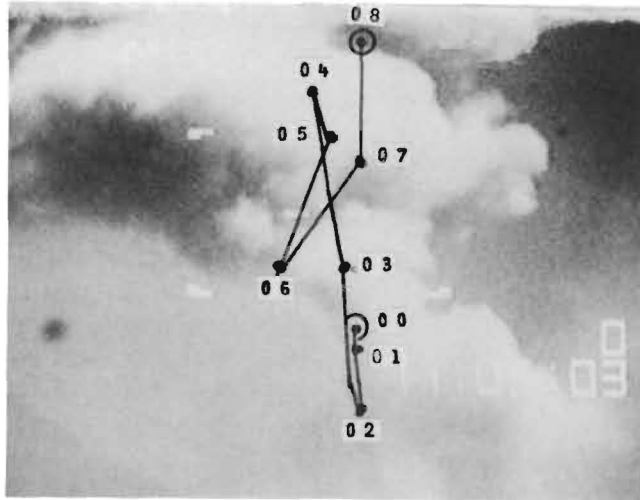


Figure 22. Antenna track for Event 2 data beginning at 11:05:00.

only two samples; these two samples had 6 to 21 dB deviations and were not included in computing the predetonation mean values. The predetonation reference for Event 1 was established in the same manner as for Event 2, but only 10 data samples were included. The peak variation of any of the 10 samples for Event 1 was 3.1 dB below the mean value.

The post detonation values of the reflectivity of the bluff were compared to the values established prior to detonation to determine the attenuation. In each case, a one second average for each range cell was used. For Event 2, four range cells were averaged to give the final attenuation. The attenuation for Event 1 was calculated only for the range cell containing the dominant return; the value was highly variable with time and averaged to only 0.2 dB at 9.4 GHz and 2.1 dB at 35 GHz for the first 4 seconds. The much smaller size of the Event 1 explosion and the approximately 16 dB lower radar cross section indicate that the average attenuation, even at the early (1-4 seconds) time, is small and can be neglected without introducing a serious error.

The measured values of attenuation for the first seven seconds of Event 2 are listed in Table 2. Only the data for the first 7 seconds were considered in this analysis because the antenna position shifted between 7 and 8 seconds and the predetonation reference was no longer valid for the new position.

3.2.2 VERIFICATION OF ANALYSIS PROCEDURE

The radar cross section is exponentially related to frequency by

$$\sigma \approx (f)^N \quad (5)$$

In the presence of attenuation, the true value of the radar cross section is related to the measured value by

$$\sigma = \sigma^* e^{\alpha} \quad (6)$$

TABLE 2. AVERAGE ATTENUATION AT 9.4 GHz AND 35 GHz FOR EVENT 2

Time Interval (Seconds)	9.4 GHz α (dB)	35 GHz α (dB)
0-1	0.61	2.81
1-2	6.28	10.22
2-3	4.45	9.65
3-4	2.56	8.27
4-5	4.39	9.73
5-6	4.71	7.13
6-7	3.03	6.09

where σ^* is the measured value and α is the attenuation constant. These two relationships (Equations 5 and 6) can be used to derive an expression relating the difference between the attenuation at two frequencies to the measured values of the radar cross section at the two frequencies. This relationship is given by forming the ratio

$$\frac{\sigma_1^* e^{\alpha_1}}{\sigma_2^* e^{\alpha_2}} = \left(\frac{f_1}{f_2}\right)^N \quad (7)$$

and solving for N.

$$N = \frac{\ln \left(\frac{\sigma_1^*}{\sigma_2^*} \right)}{\ln \left(\frac{f_1}{f_2} \right)} + \frac{\alpha_1 - \alpha_2}{\ln \left(\frac{f_1}{f_2} \right)} \quad (8)$$

If the first term on the right in Equation (8) is called N^* , the measured frequency dependency component, then Equation (8) can be written as

$$(\alpha_1 - \alpha_2) = (N - N^*) \left(10 \log \frac{f_1}{f_2}\right) \quad (9)$$

where α_1 and α_2 are the attenuation in dB at the respective frequencies.

If a symmetrical distribution of material throughout the dust cloud is assumed, the difference in attenuation ($\alpha_1 - \alpha_2$) can be calculated by using the value of N for the closest range cell and the value of N^* calculated for the furthest range cell. The radar cross section data indicated that the necessary symmetry from the first to the last range cell did not exist; but that a large percentage of the mass of the dust cloud is located in several central range cells. The difference in attenuation ($\alpha_1 - \alpha_2$) for the high mass region was computed by assuming that this region was symmetrical. The value used for N was the average of the 3 cells leading the central 3 cells, and the value used for N^* was the average of the 3 cells trailing the central 3 cells. Since the majority of the mass of the cloud contributing to the attenuation was located in the 3 central cells, the value of N was not significantly affected by attenuation, and the maximum effect of the attenuation is reflected in the value of N^* . Table 3 is a comparison of the values of ($\alpha_1 - \alpha_2$) derived from the bluff reflectivity data to the values calculated from Equation (9). Good agreement exists between these independent methods of arriving at the difference in attenuation at the two frequencies; thus tending to validate the use of the bluff as an attenuation reference.

3.3 FREQUENCY DEPENDENCY

The General relationship between frequency and backscatter cross section was given in Equation (5). The frequency exponent, N , is related to the distribution of particle sizes within the dust cloud and is, therefore, an important parameter for developing mathematical models describing the backscatter and attenuation from debris lofted by nuclear explosions. Values of

N were calculated for both events of the MISERS BLUFF II explosions.

TABLE 3. COMPARISON OF THE TWO METHODS FOR DETERMINING THE DIFFERENCE IN ATTENUATION

Time (Seconds)	Bluff Data $\alpha(9.4) - \alpha(35)$ (db)	$K(N-N^*)$ $\alpha(9.4) - \alpha(35)$ (dB)
0-1	2.2	1.9
1-2	3.9	3.8
2-3	5.2	6.1
3-4	5.7	5.2
4-5	5.3	2.6
5-6	2.4	2.8
6-7	3.1	1.3

The variation of N as a function of range at 0.2 second intervals is shown in Figure 23. This plot covers the early growth period from 1.0 to 1.8 seconds after Event 1 detonation. The criteria for determining the validity of a point was that the received signal in both radars had to be at least 2 dB greater than the lowest noise level recorded in a given data record. Using this criteria, only three values for N are shown in the first plot in Figure 23. This indicates that material of sufficient radar cross section to reflect a detectable signal back to the radar existed only over three range cells, or approximately 112 meters. Within 0.8 seconds, the cloud had expanded to cover 8 cells, or approximately 300 meters. The range cell containing the maximum radar cross section at 9.4 GHz is indicated with an asterisk on each plot. Additional plots of N versus range are shown in Figures 24 through 26 for one second time intervals beginning 2, 7, and 19 seconds after Event 1 detonation. These plots show that the variation in the value of N is a function of both range and time. The minimum N of 0.5 occurred 2.6 seconds

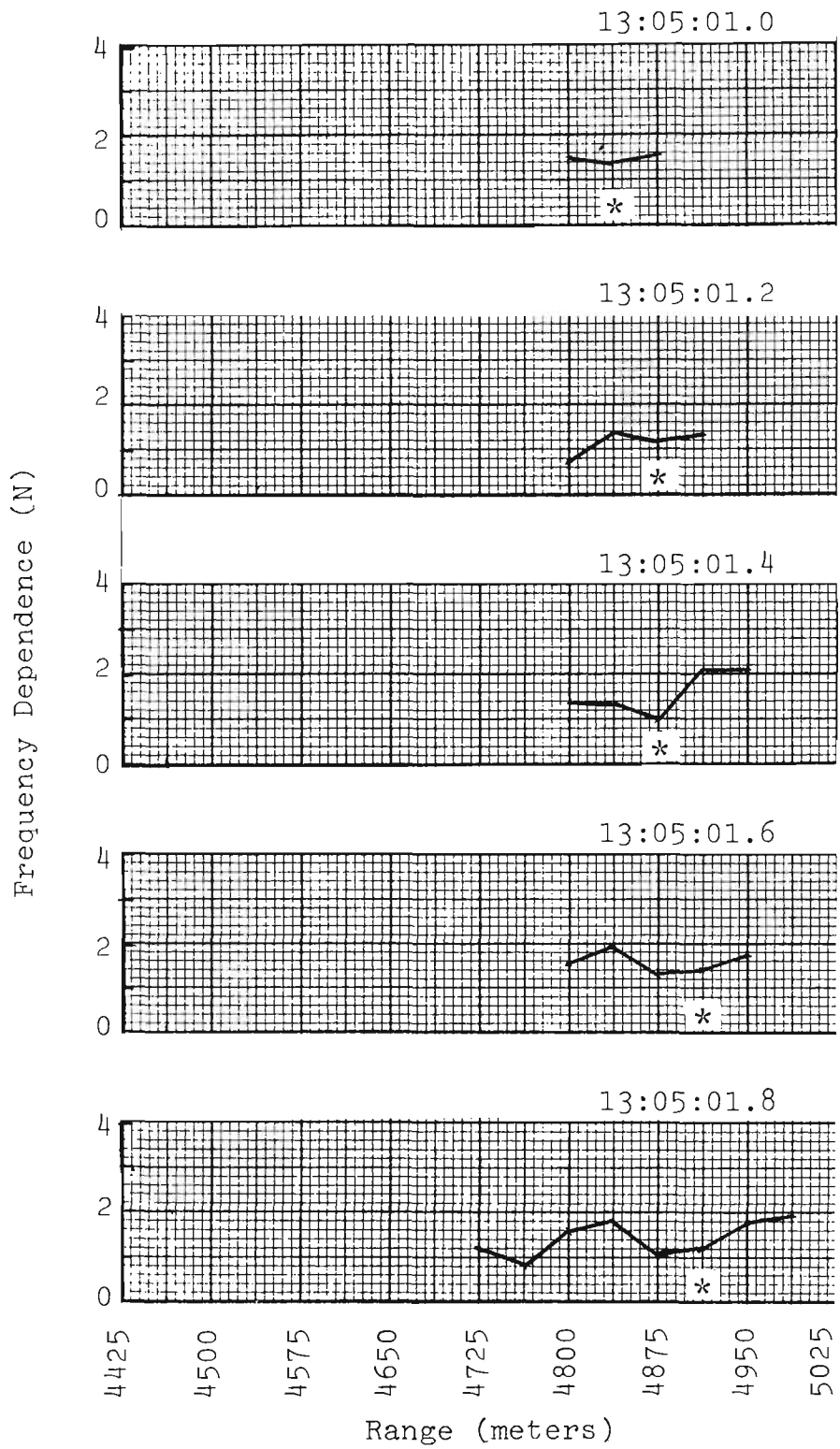


Figure 23. Frequency dependence vs. range for 1 to 1.8 seconds after detonation of Event 1.

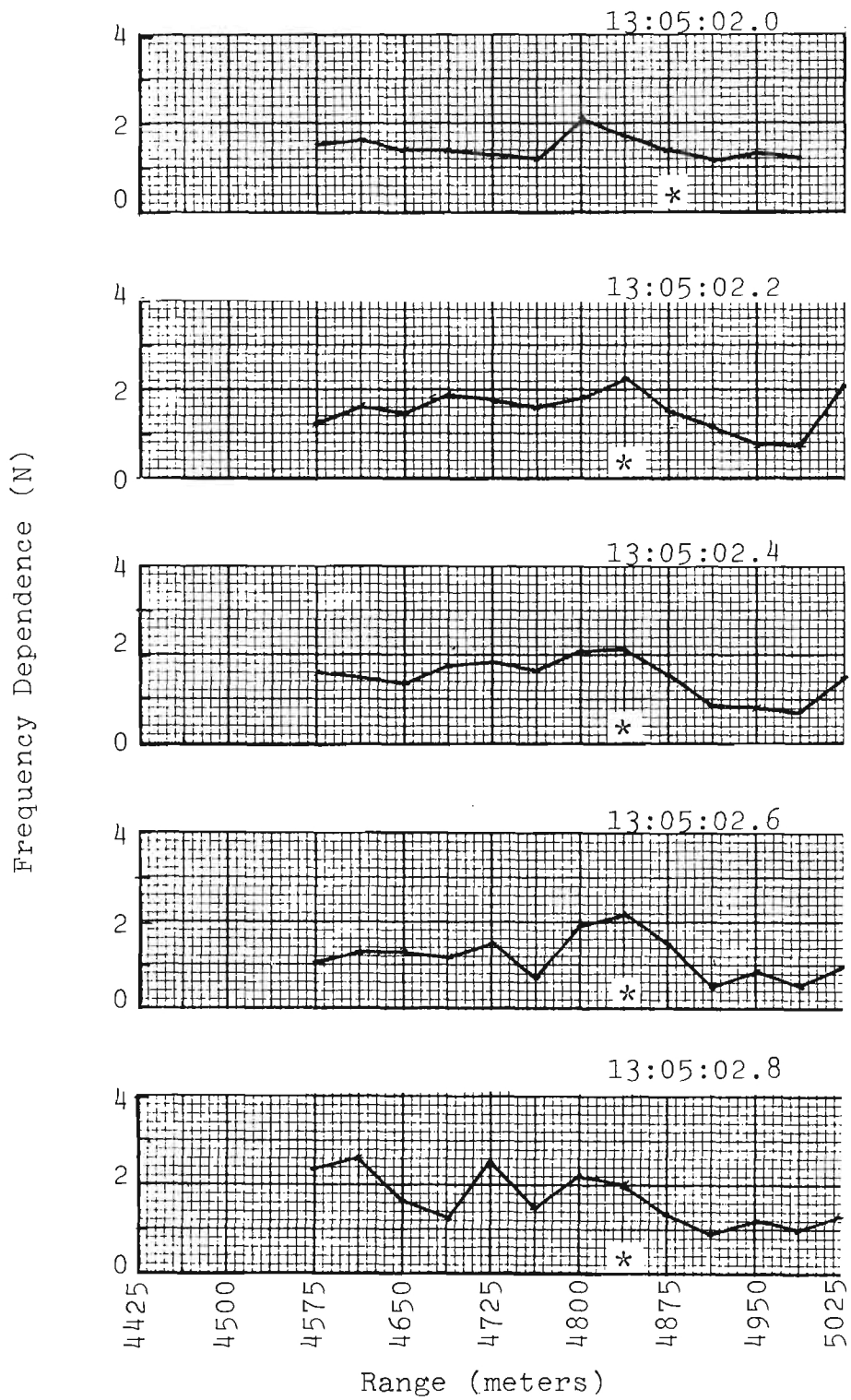


Figure 24. Frequency dependence vs. range for 2 to 2.8 seconds after detonation of Event 1.

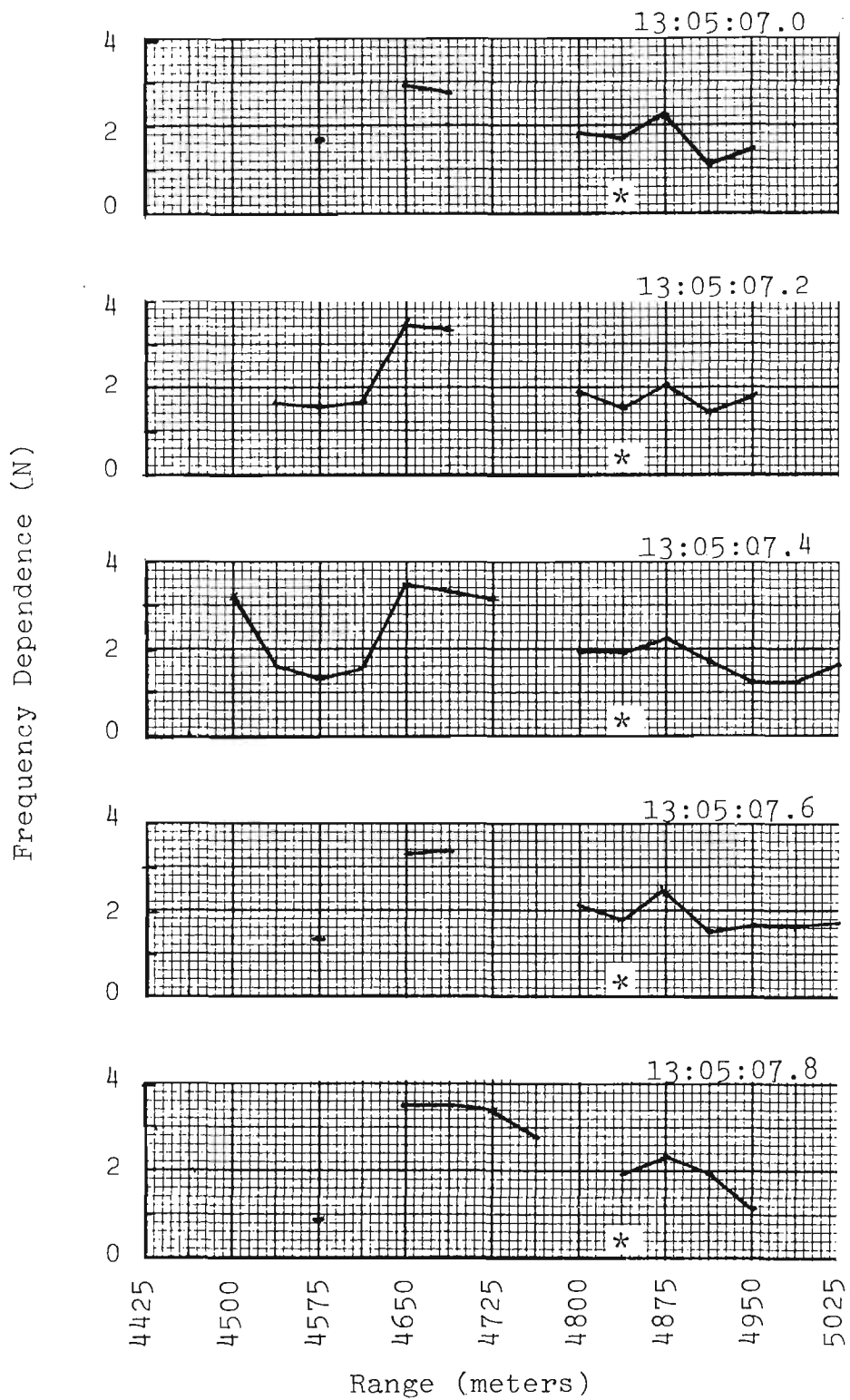


Figure 25. Frequency dependence vs. range for 7 to 7.8 seconds after detonation of Event 1.

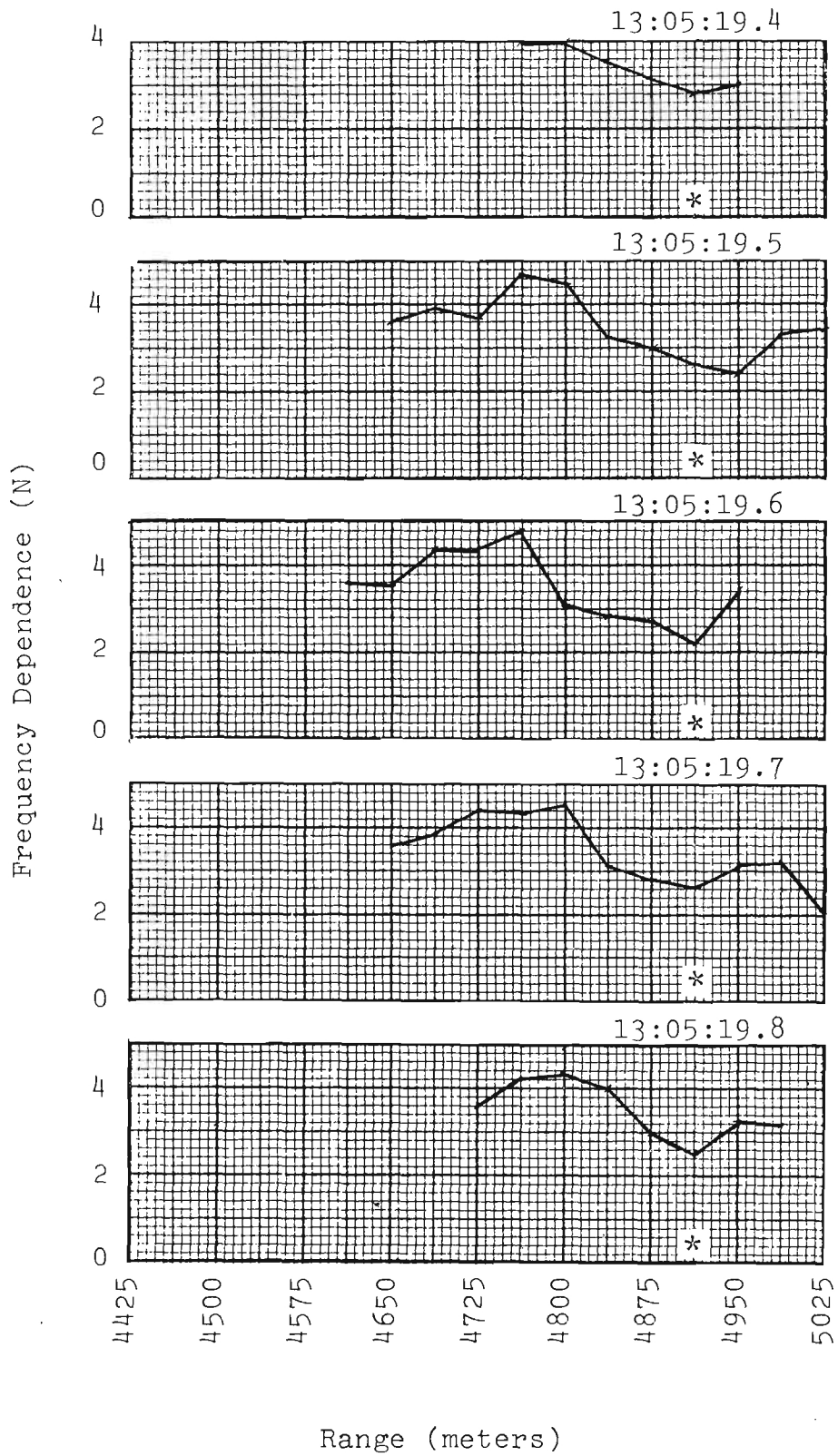


Figure 26. Frequency dependence vs. range for 19.4 to 19.8 seconds after detonation of Event 1.

after detonation at a range of 4912 meters. These data also show that the maximum radar cross section does not necessarily occur at the same range as the minimum N.

Plots of N versus range from the Event 2 data are shown in Figures 27 through 30 for the time periods of 1, 5, 12, and 19 seconds after detonation. Much lower values of N (near 0) were recorded during the first two seconds after detonation of this event. Generally, the same variability with range was observed for both events. Nineteen seconds after detonation, the measured values of N had exceeded 4 for Event 1 and was approaching 4 for Event 2. An example of the effect of attenuation on the values of N is shown in Figure 31, where the corrected (solid) and uncorrected (dashed) plots of N are given for the data collected at 2.1 seconds after detonation.

The long term trend in the value of N is needed for developing models that can predict the duration of significant attenuation and reflectivity due to nuclear explosion. The single most representative measure of N during the earlier time period was thought to be associated with the range cell of maximum radar cross section. Figure 32 is a plot of N versus time for the first 20 seconds of Event 1. The values of N were calculated from the data shown in Figures 7 and 8 and do not show a trend towards increasing values until after 6 seconds. Figure 33 shows the values of N versus time for the Event 2 data shown in Figures 9 and 10. These data show a very definite trend towards increasing values of N over the 2 to 14 second time period. The solid line shown in Figure 33 is a plot of the equation

$$N = 1.08 + 0.124t \quad (\text{for } 2 < t < 14) \quad (10)$$

which was derived from Equations (3) and (4).

Primary emphasis was placed on reducing the early (first 20 seconds) data from these experiments, but some data were reduced for Event 2 time periods as late as 5 minutes after detonation. Most of the data during the late time period was very low in

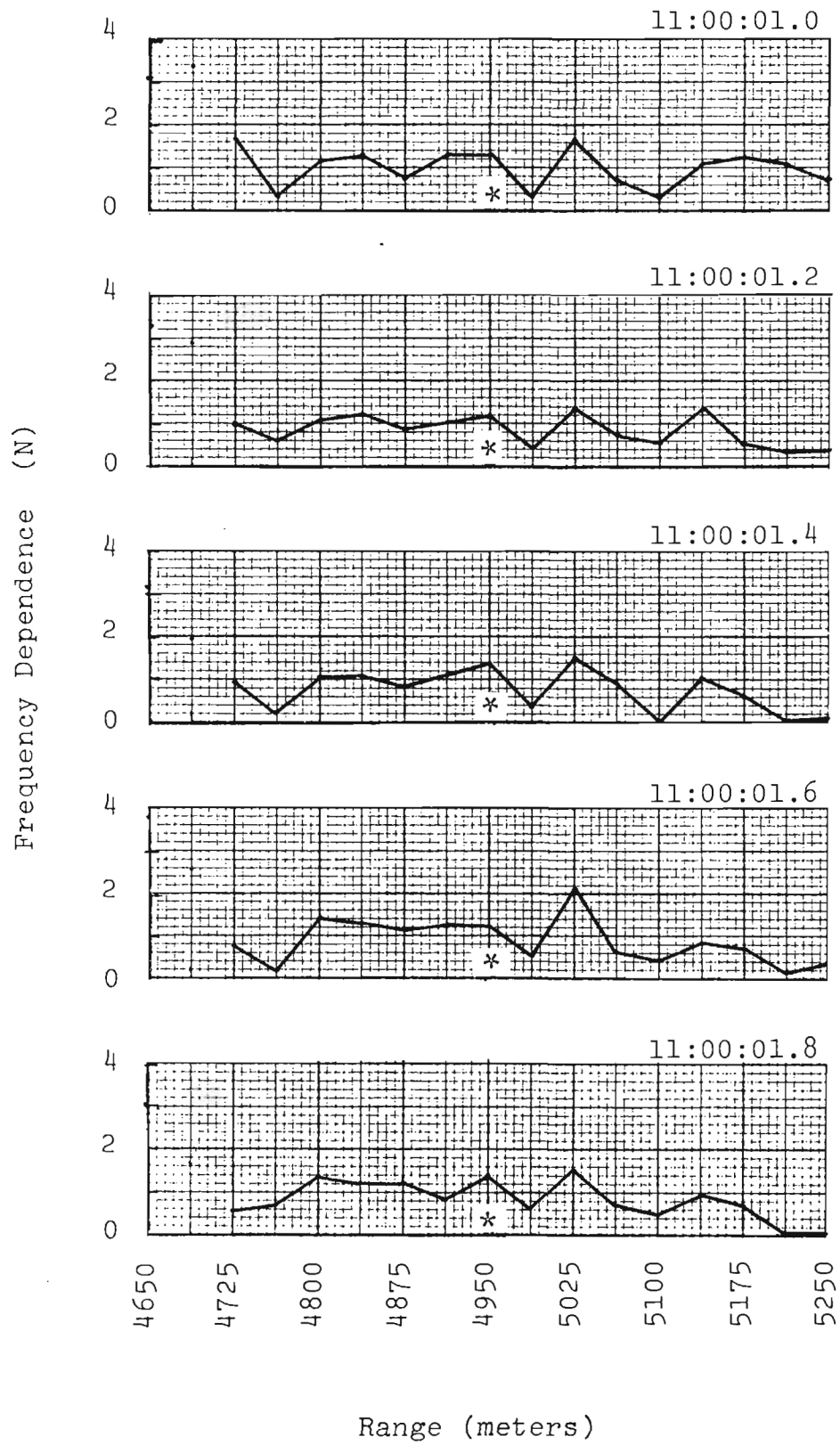


Figure 27. Frequency dependence vs. range for 1 to 1.8 seconds after detonation of Event 2.

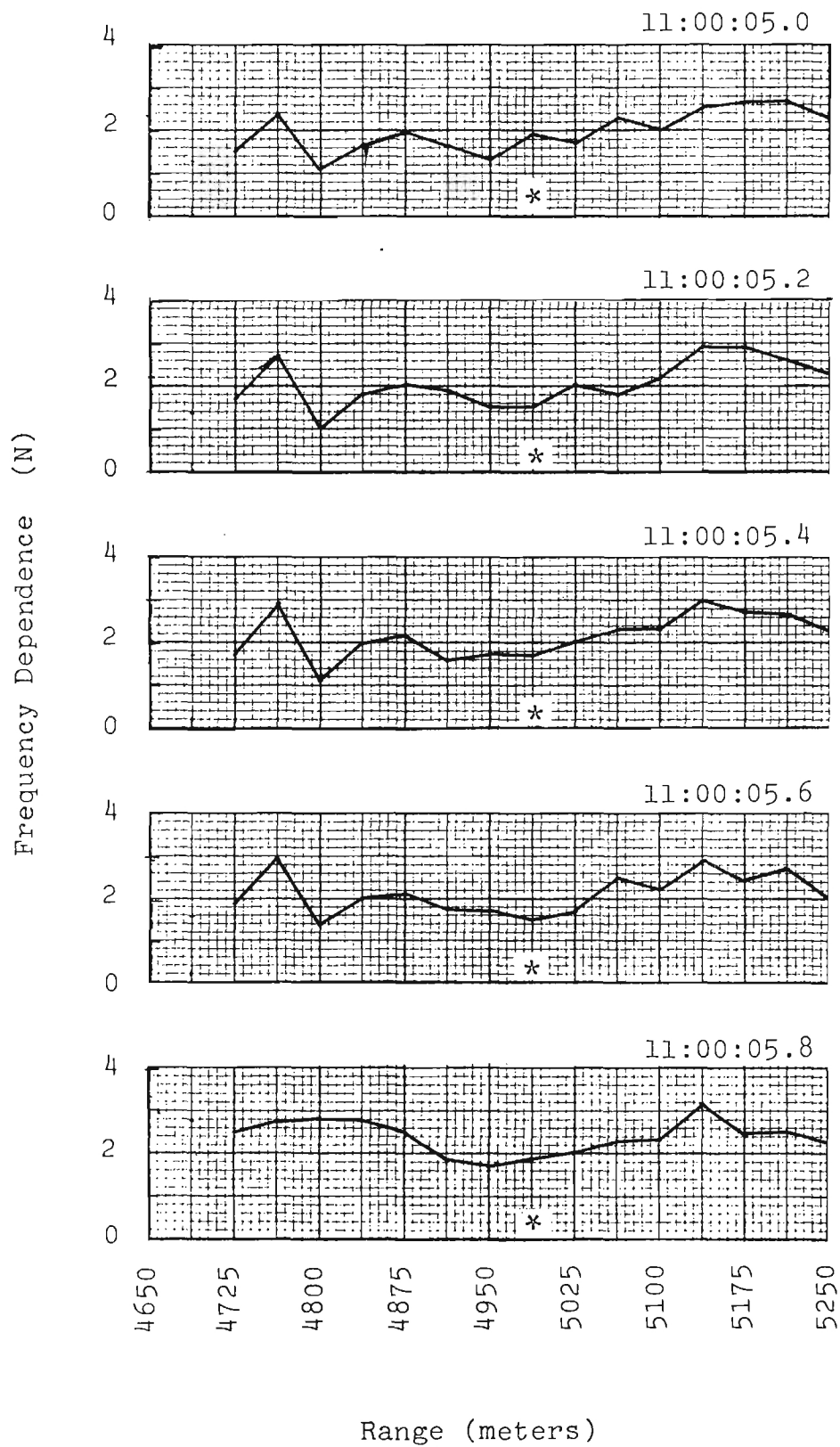


Figure 28. Frequency dependence vs. range for 5 to 5.8 seconds after detonation of Event 2.

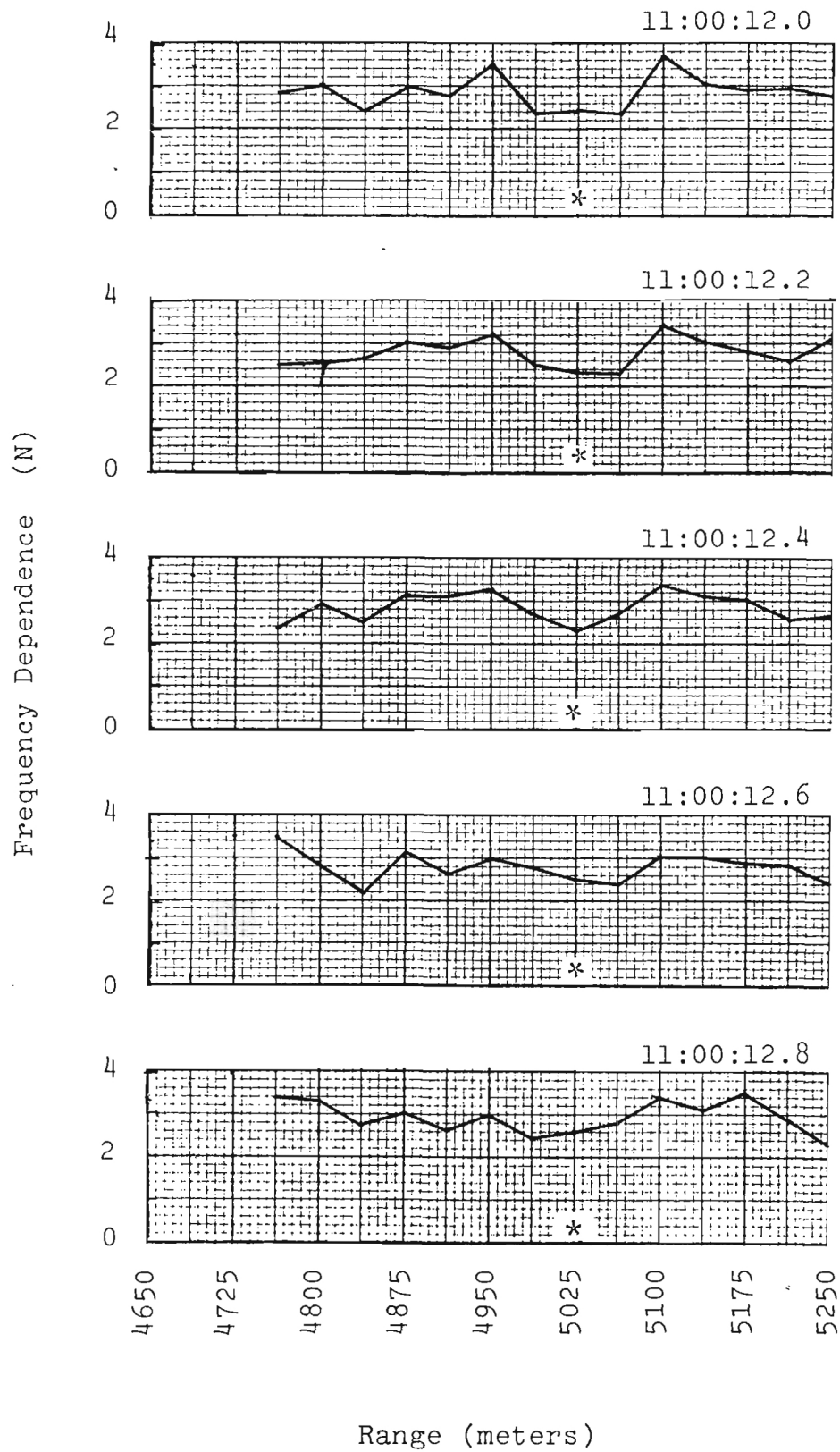


Figure 29. Frequency dependence vs. range for 12 to 12.8 seconds after detonation of Event 2.

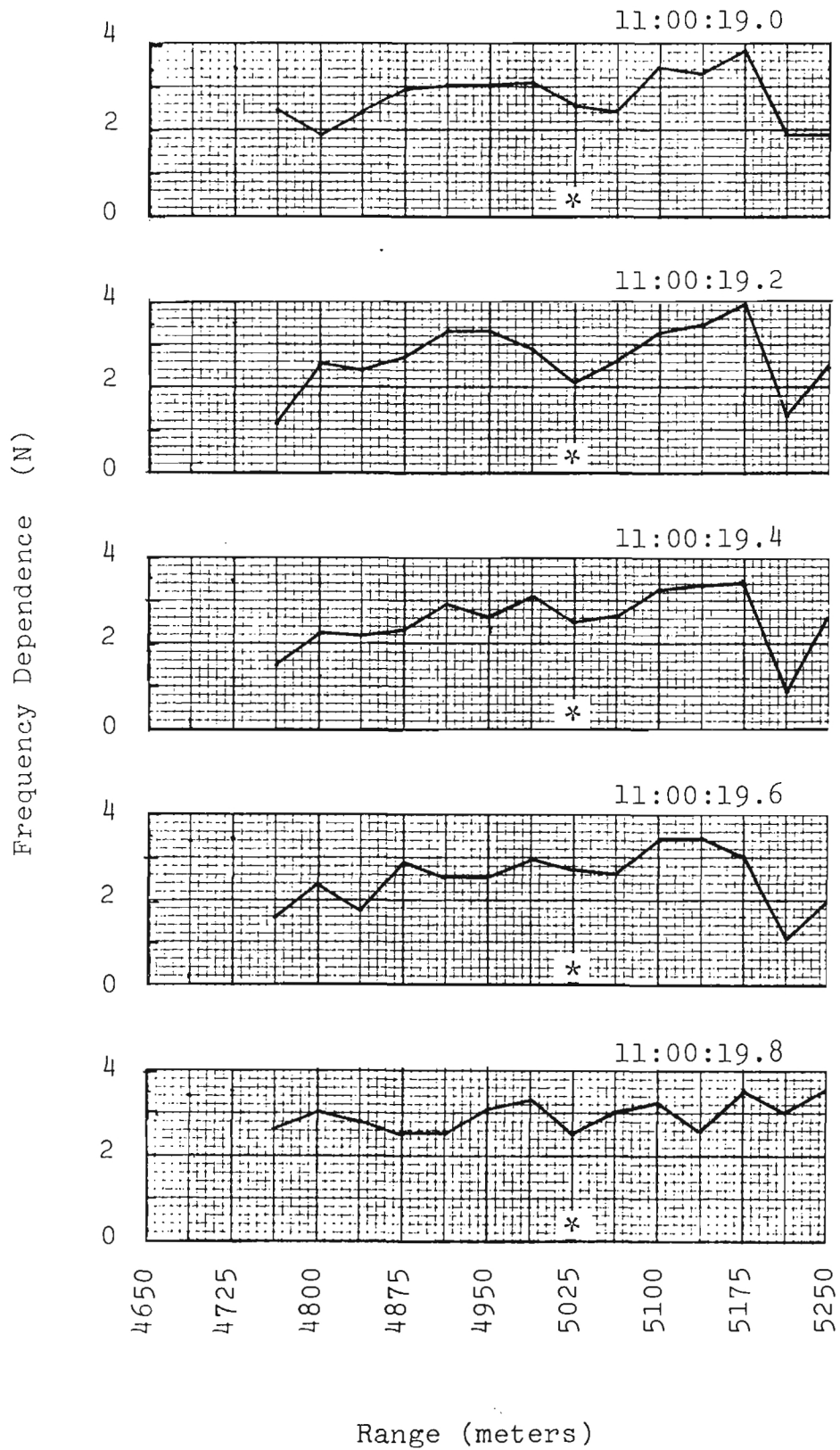


Figure 30. Frequency dependence vs. range for 19 to 19.8 seconds after detonation of Event 2.

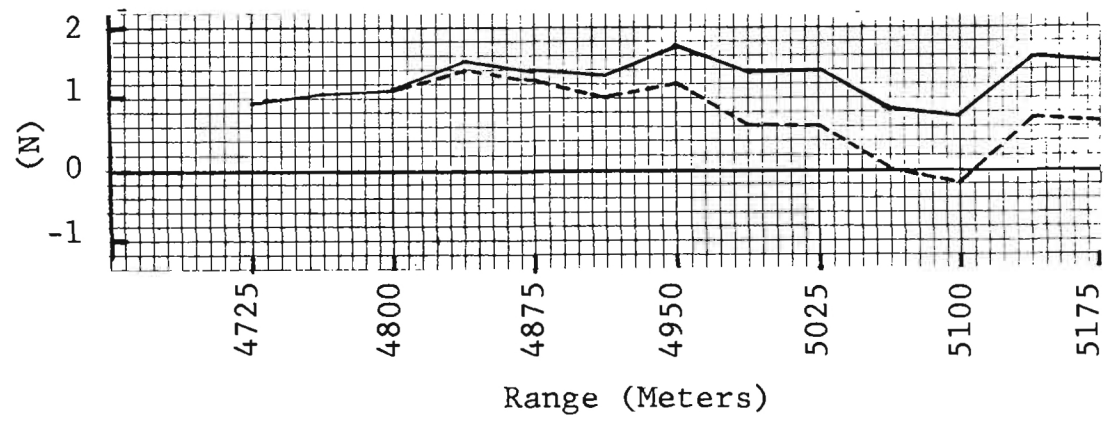


Figure 31. Comparison of the value of N before (dashed) and after (solid) being corrected for attenuation; Event 2 data at 11:00:02.1.

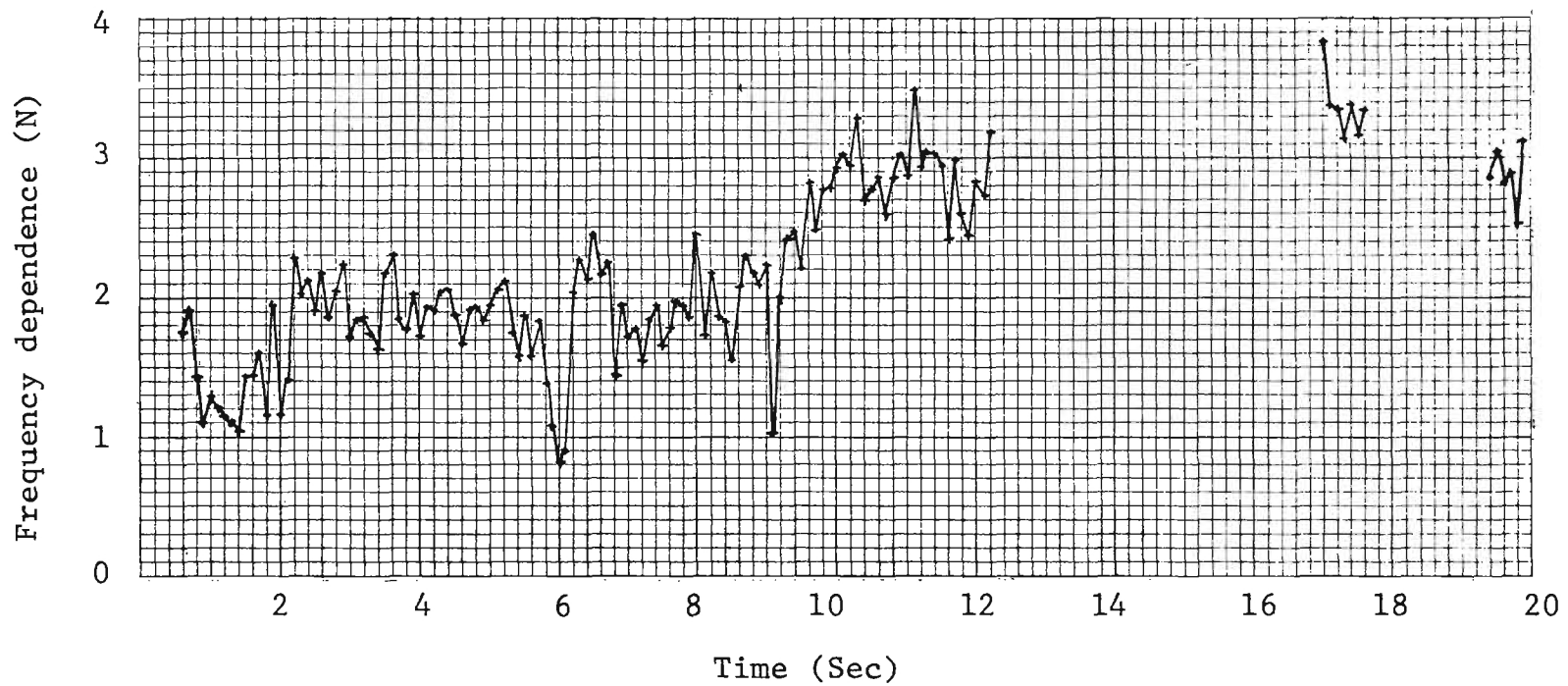


Figure 32. Frequency exponent (N) vs. time for the single range cell of peak radar cross section. Event 1

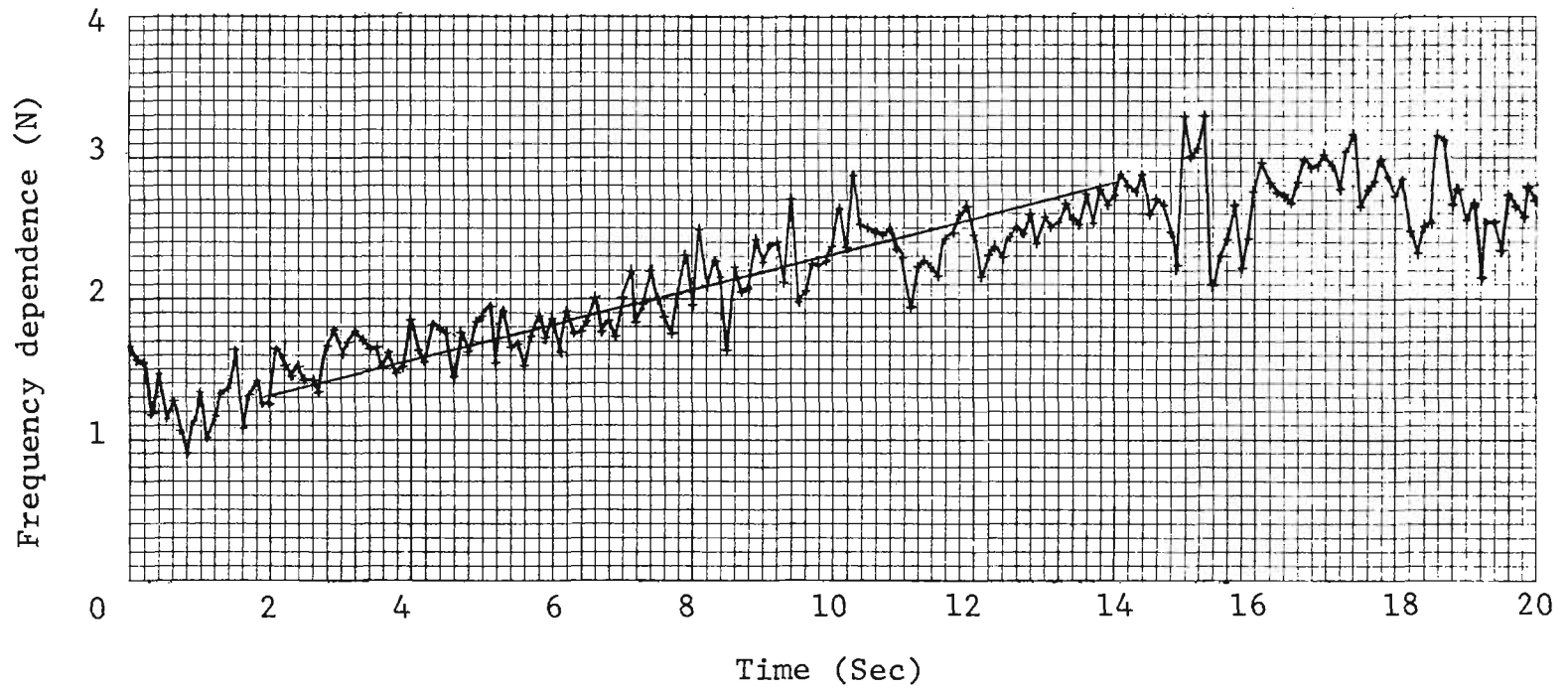


Figure 33. Frequency exponent (N) vs. time for the single range cell of peak radar cross section. Event 2.

amplitude and did not cover a wide dynamic range. In addition, the antenna was usually in a scanning mode and, therefore, the data were received from different positions in space. For these reasons, selection of the range cell of maximum cross section to evaluate the N versus time relationship resulted in a wide distribution of data points in which no real trend was observable. A better criteria for showing this relationship was to average the values of N from all range cells for a 1-second period. These averages for Event 2 are plotted in Figure 34. Trend analysis used to evaluate the N versus time relationship for the late time period indicated that these averaged data can be approximated by

$$N = \frac{\log t + 2.28}{1.3} \quad (11)$$

Equation (11) shows a logarithmic increase for N during the late time period. This is in contrast to Equation (10) which shows that N increases linearly with time during the early time period.

The value of N, based on Rayleigh scattering, should approach 4 during the late time period. Figure 34 shows that the value of N continued to increase between the last two points which have values of 3.45 at 240 seconds and 3.52 at 341 seconds. During the associated aircraft sampling experiment, particles as large as one half centimeter were reported to have hit the aircraft windshield. Since the first aircraft sampling was done 4 minutes after detonation, a value of 3.5 is not unreasonable for this late time period, although there is no estimate for the density of large particles at this later time period.

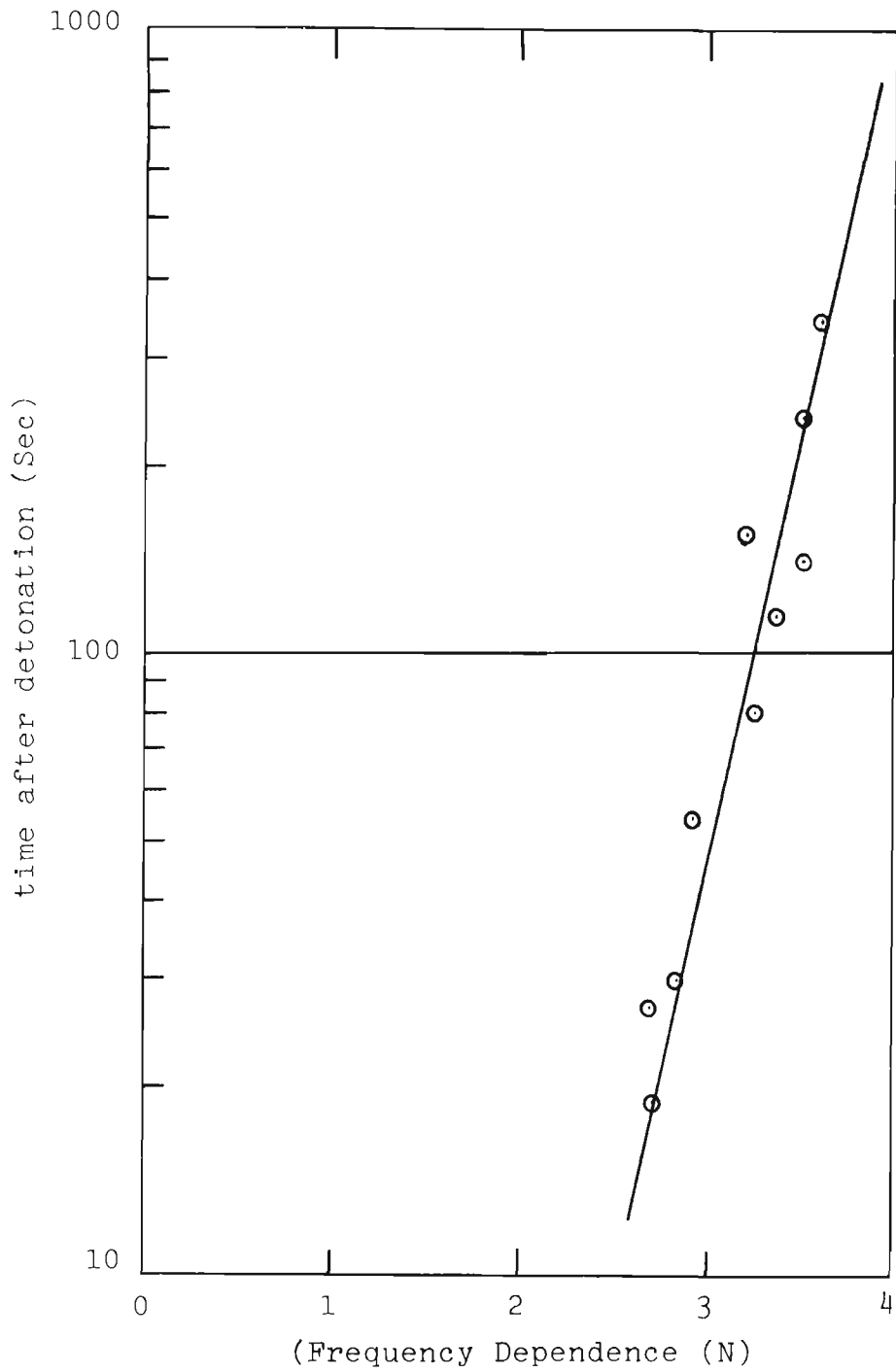


Figure 34. Average frequency dependency exponent (N) for late time period; Event 2.

SECTION 4 CONCLUSIONS

4.1 OVERVIEW

The goal of the radar experiments was to measure the back-scatter cross section and attenuation properties of the dust cloud lofted by the MISERS BLUFF - Phase II Test. These measurements were to be made at four frequencies ranging from 9.4 GHz to 95 GHz. The goals were completely met at the two lower frequencies. Loss of data at the two higher frequencies is significant since the millimeter wave region of the electromagnetic spectrum is of particular interest to defense agencies for both communication and radar applications.

The experiment should be repeated using a modified version of the 95 GHz radar at the earliest opportunity. This radar should be a bistatic system (i.e., separate transmitter and receiver antennas) since this configuration would allow approximately 10 dB better performance by reducing signal loss due to system components. In addition, significant improvement could be realized by using currently available balanced mixer preamplifiers. The overall improvement in system performance could be as much as 20 to 25 dB.

4.2 EVENT 1 MEASUREMENTS SUMMARY

Event 1 of this test series consisted of the detonation of a single 120-ton stack of ANFO. The maximum volumetric radar cross sections measured for this event at 9.4 GHz and 35 GHz were $2.8 \times 10^{-6} \text{ m}^2/\text{m}^3$ and $3.4 \times 10^{-5} \text{ m}^2/\text{m}^3$, respectively. The variations in the measured radar cross-sections were large; changes were as great as 10 dB within a one second time period. These variations occurred at both frequencies and appear to be entirely due to changes occurring inside the dust cloud.

The radar returns from the bluff behind ground zero were examined before and after the explosion in an effort to assess

the attenuation of the dust cloud. The result of the computed attenuation showed large variations with both positive and negative values. The attenuation was small at both frequencies and can be neglected without seriously affecting the radar cross section values or the computed frequency dependency exponent.

The values of the frequency dependency exponent ranged from 0.5 at 2 seconds after detonation to occasional values greater than 4 as early as 19 seconds after detonation.

4.3 EVENT 2 MEASUREMENTS SUMMARY

Event 2 consisted of the detonation of six 120-ton stacks of ANFO. The radar cross sections measured for this event were significantly higher than for Event 1. Radar cross sections of $1.2 \times 10^{-4} \text{ m}^2/\text{m}^3$ and $7.0 \times 10^{-4} \text{ m}^2/\text{m}^3$ were measured at 9.4 GHz and 35 GHz, respectively. Short term variations in the cross sections were not as great as those observed for Event 1.

The attenuation computed for this event was significant at both frequencies during the first 10 seconds. The maximum attenuation occurred 2 seconds after detonation, and was 6.3 dB at 9.4 GHz and 10.2 dB at 35 GHz. The attenuation was computed only over the first 7 seconds because the antenna position was changed at that time. The attenuation was projected out to 10 seconds based on the predicted difference in attenuation due to the range effect on the frequency dependency exponent.

The frequency dependency exponent values ranged from near zero during the early 1 to 2 second time period to values greater than 4 at late times. A linear regression was computed from the early peak radar cross-section data. These regression equations were used to drive an equation approximating the frequency dependency exponent over the period of 2 to 14 seconds.

REFERENCES

1. E. E. Martin, "Radar Reflectivity of Dust Cloud Lofted By Misers Bluff II High Explosive Test," Final Technical Report, Georgia Tech Project A-2104, March 1979.
2. A. Burns Private Correspondence dated 22 January 1980, SRI International.

APPENDIX A

RADAR CROSS SECTION VERSUS RANGE

LIST OF ILLUSTRATIONS

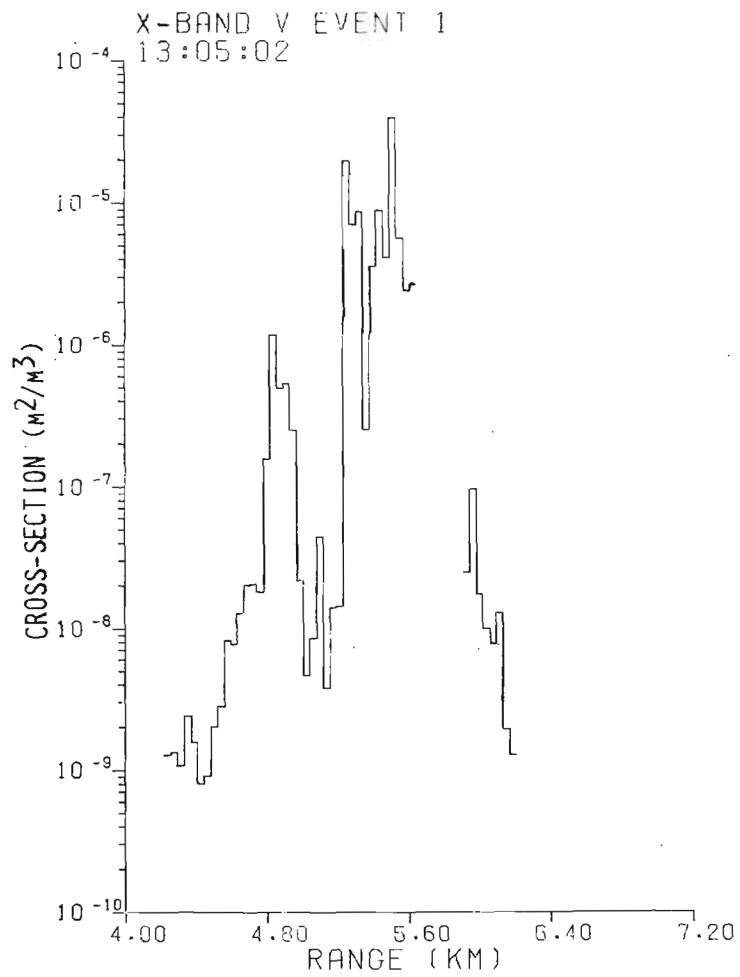
<u>FIGURE</u>		<u>PAGE</u>
A-1	9.4 GHz radar cross section vs. range; Event 1, $T_O + 2$ seconds.....	60
A-2	35 GHz radar cross section vs. range; Event 1, $T_O + 2$ seconds.....	61
A-3	9.4 GHz radar cross section vs. range; Event 1, $T_O + 4$ seconds.....	62
A-4	35 GHz radar cross section vs. range; Event 1, $T_O + 4$ seconds.....	63
A-5	9.4 GHz radar cross section vs. range; Event 1, $T_O + 6$ seconds.....	64
A-6	35 GHz radar cross section vs. range; Event 1, $T_O + 6$ seconds.....	65
A-7	9.4 GHz radar cross section vs. range; Event 1, $T_O + 8$ seconds.....	66
A-8	35 GHz radar cross section vs. range; Event 1, $T_O + 8$ seconds.....	67
A-9	9.4 GHz radar cross section vs. range; Event 1, $T_O + 10$ seconds.....	68
A-10	35 GHz radar cross section vs. range; Event 1, $T_O + 10$ seconds.....	69
A-11	9.4 GHz radar cross section vs. range; Event 1, $T_O + 12$ seconds.....	70
A-12	35 GHz radar cross section vs. range; Event 1, $T_O + 12$ seconds.....	71
A-13	9.4 GHz radar cross section vs. range; Event 2, $T_O + 2$ seconds.....	72
A-14	35 GHz radar cross section vs. range; Event 2, $T_O + 2$ seconds.....	73
A-15	9.4 GHz radar cross section vs. range; Event 2, $T_O + 4$ seconds.....	74

LIST OF ILLUSTRATIONS (continued)

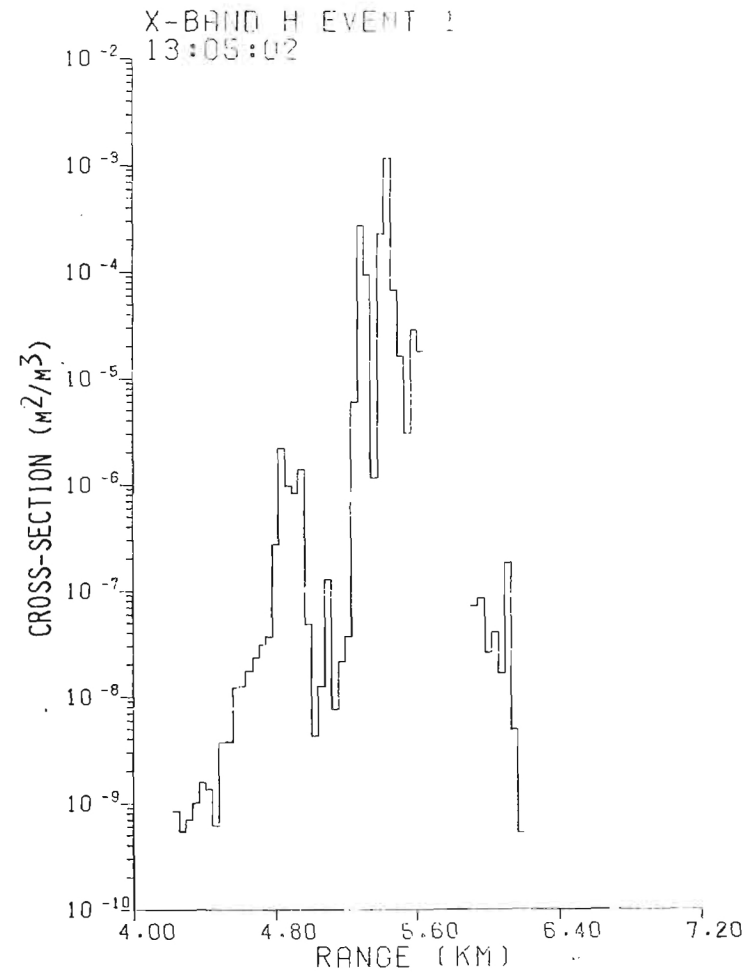
<u>FIGURE</u>		<u>PAGE</u>
A-16	35 GHz radar cross section vs. range; Event 2, $T_0 + 4$ seconds.....	75
A-17	9.4 GHz radar cross section vs. range; Event 2, $T_0 + 6$ seconds.....	76
A-18	35 GHz radar cross section vs. range; Event 2, $T_0 + 6$ seconds.....	77
A-19	9.4 GHz radar cross section vs. range; Event 2, $T_0 + 8$ seconds.....	78
A-20	35 GHz radar cross section vs. range; Event 2, $T_0 + 8$ seconds.....	79
A-21	9.4 GHz radar cross section vs. range; Event 2, $T_0 + 10$ seconds.....	80
A-22	35 GHz radar cross section vs. range; Event 2, $T_0 + 10$ seconds.....	81
A-23	9.4 GHz radar cross section vs. range; Event 2, $T_0 + 12$ seconds.....	82
A-24	35 GHz radar cross section vs. range; Event 2, $T_0 + 12$ seconds.....	83
A-25	9.4 GHz radar cross section vs. range; Event 2, $T_0 + 14$ seconds.....	84
A-26	35 GHz radar cross section vs. range; Event 2, $T_0 + 14$ seconds.....	85
A-27	9.4 GHz radar cross section vs. range; Event 2, $T_0 + 16$ seconds.....	86
A-28	35 GHz radar cross section vs. range; Event 2, $T_0 + 16$ seconds.....	87
A-29	9.4 GHz radar cross section vs. range; Event 2, $T_0 + 18$ seconds.....	88
A-30	35 GHz radar cross section vs. range; Event 2, $T_0 + 18$ seconds.....	89

LIST OF ILLUSTRATIONS (continued)

<u>FIGURE</u>		<u>PAGE</u>
A-31	9.4 GHz radar cross section vs. range; Event 2, $T_0 + 20$ seconds.....	90
A-32	35 GHz radar cross section vs. range; Event 2, $T_0 + 20$ seconds.....	91

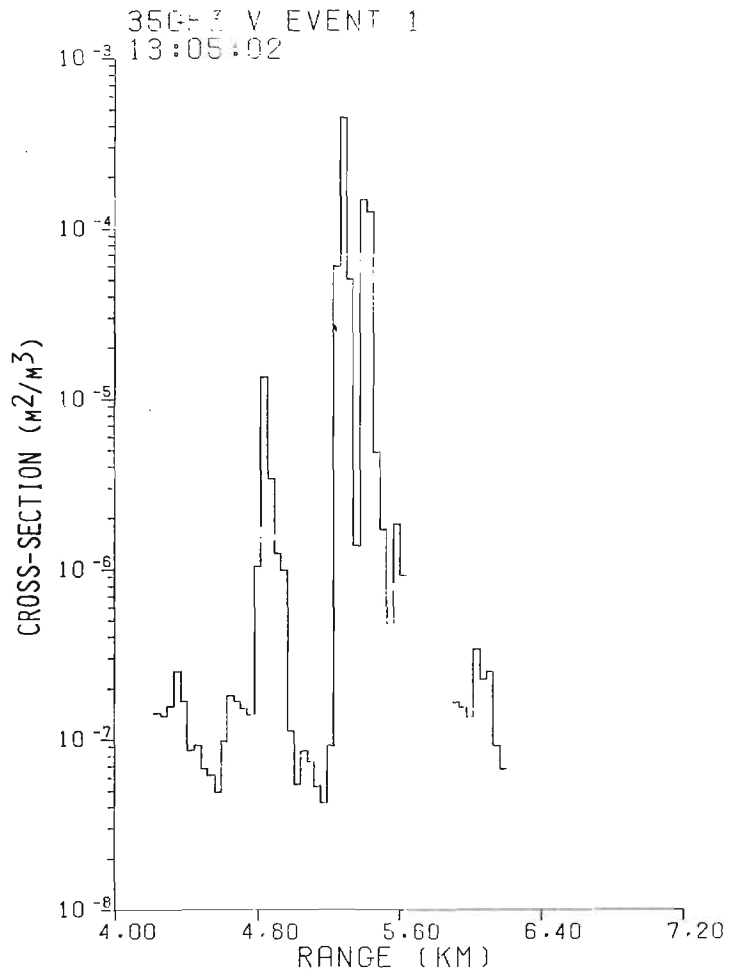


a. HV Polarization

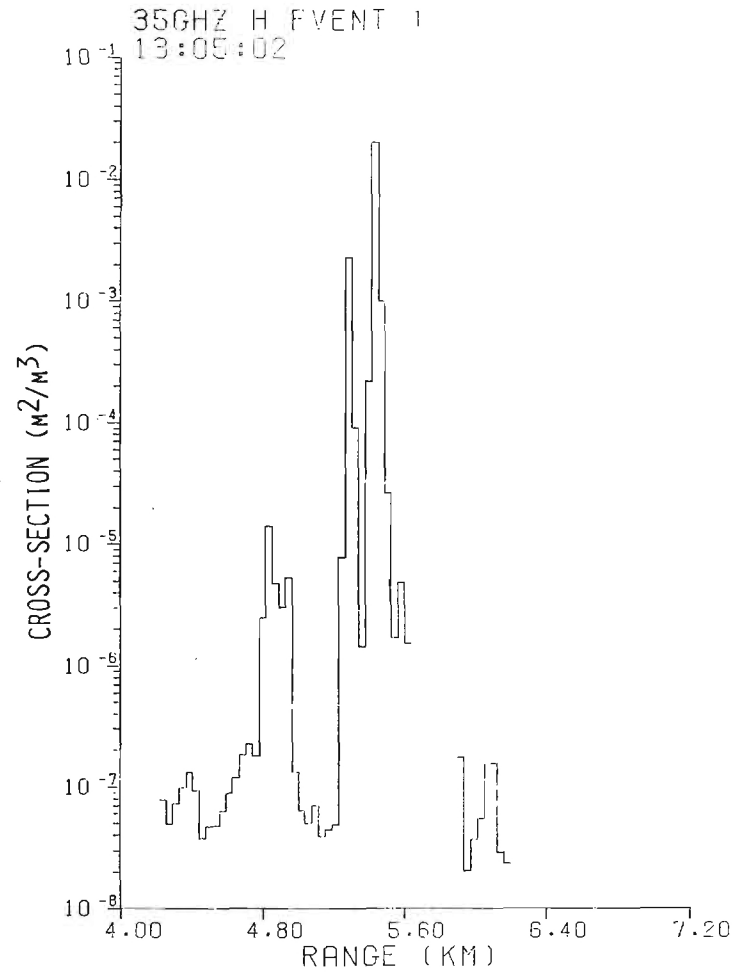


b. HH Polarization

Figure A-1. 9.4 GHz radar cross section vs. range; Event 1, $T_0 + 2$ seconds.

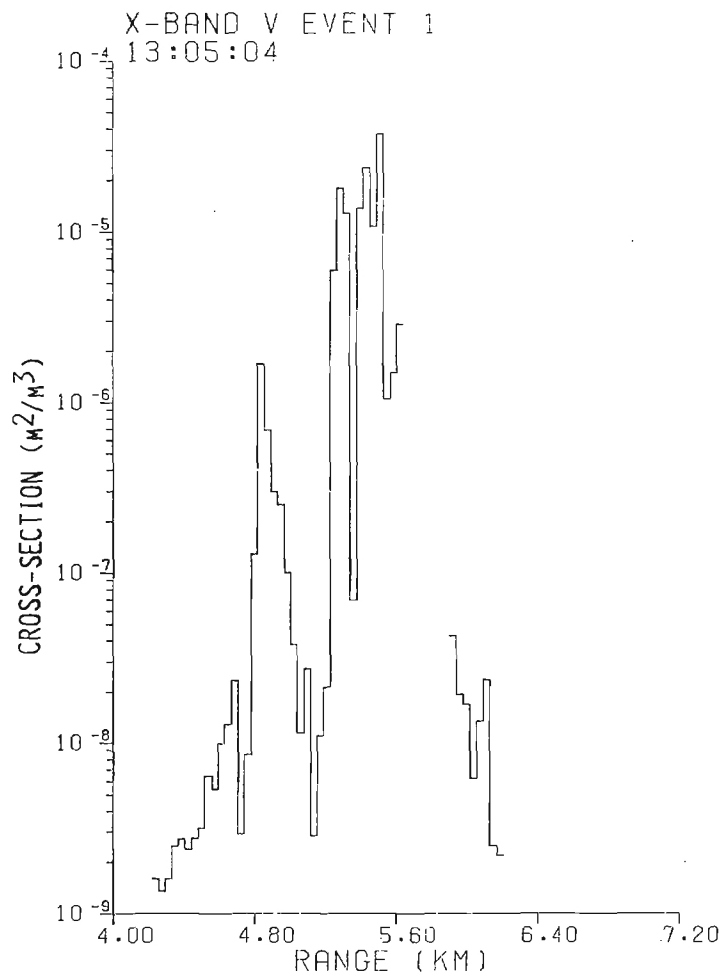


a. HV Polarization

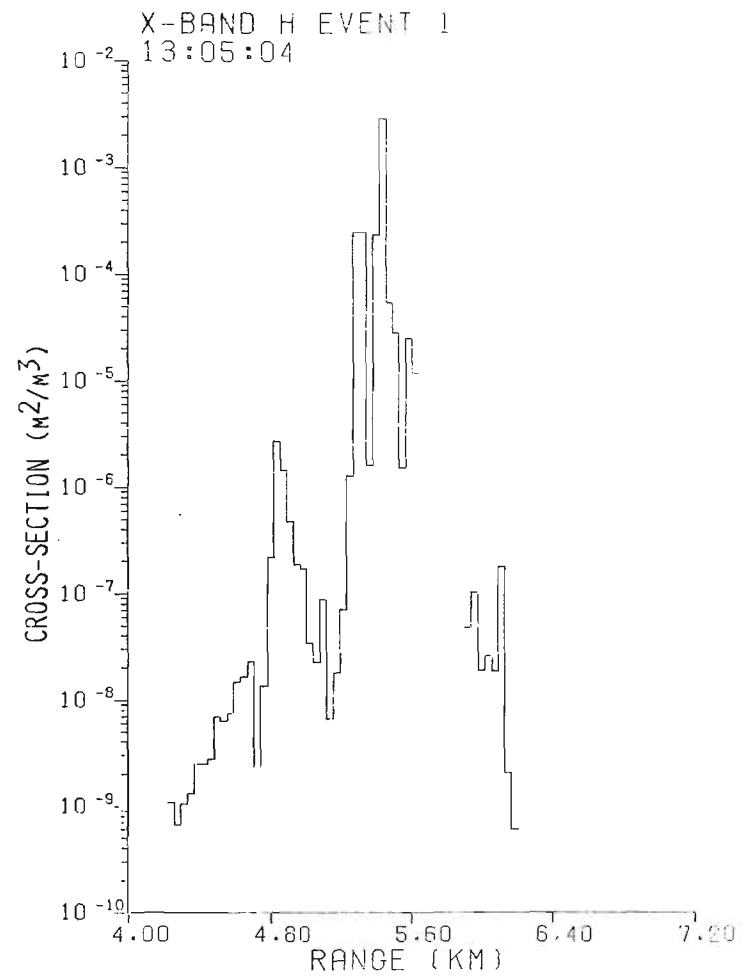


b. HH Polarization

Figure A-2. 35 GHz radar cross section vs. range; Event 1, $T_0 + 2$ seconds.

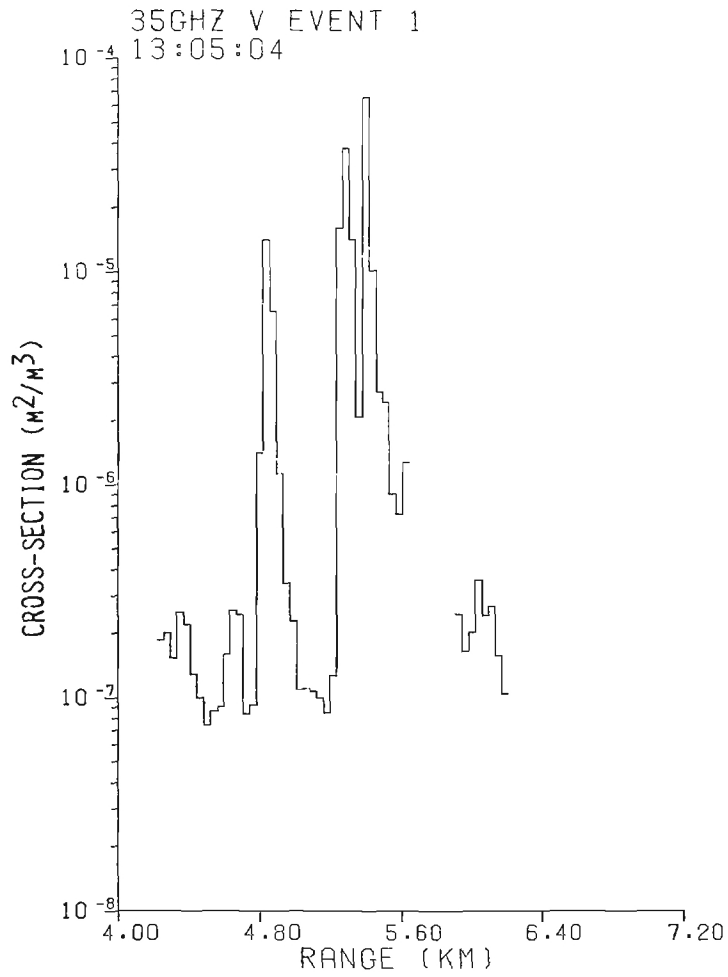


a. HV Polarization

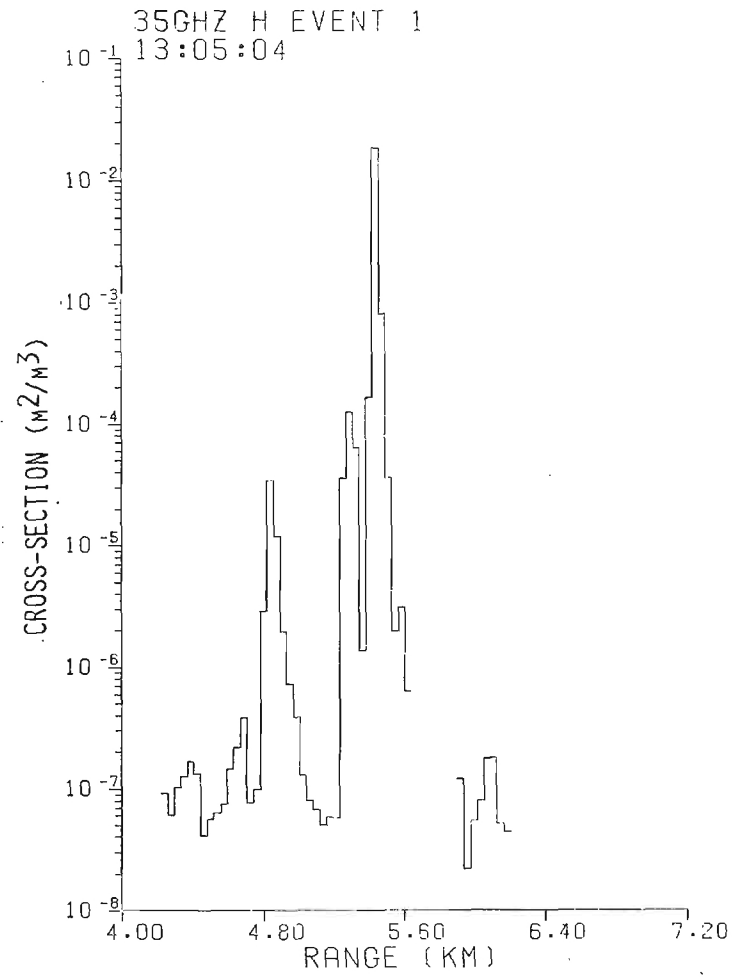


b. HH Polarization

Figure A-3. 9.4 GHz radar cross section vs. range; Event 1, $T_0 + 4$ seconds.

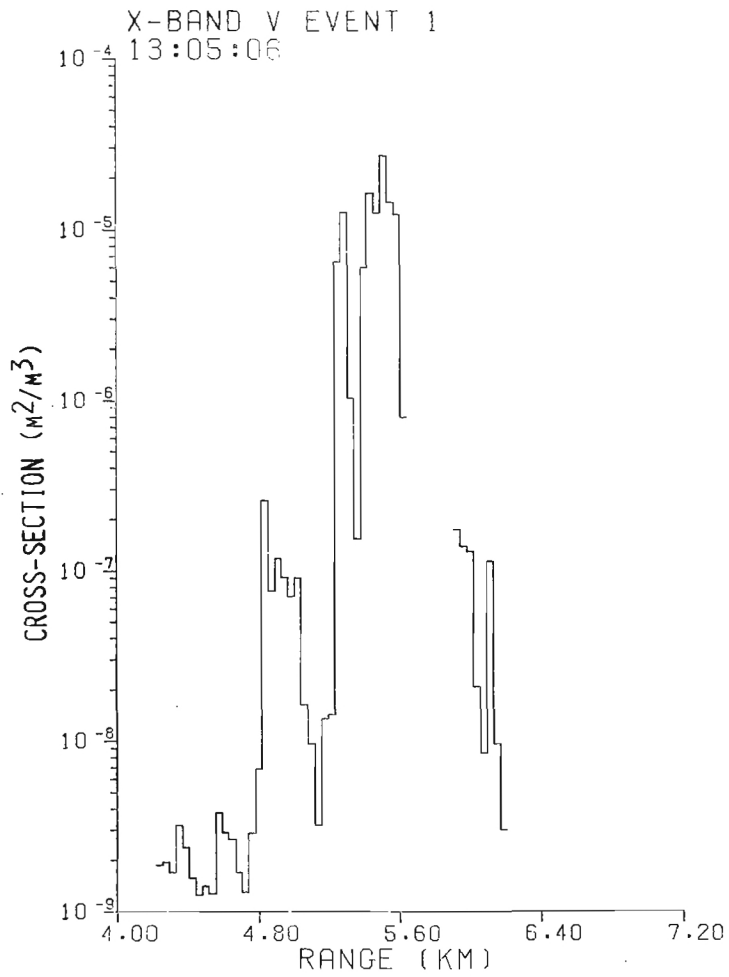


a. HV Polarization

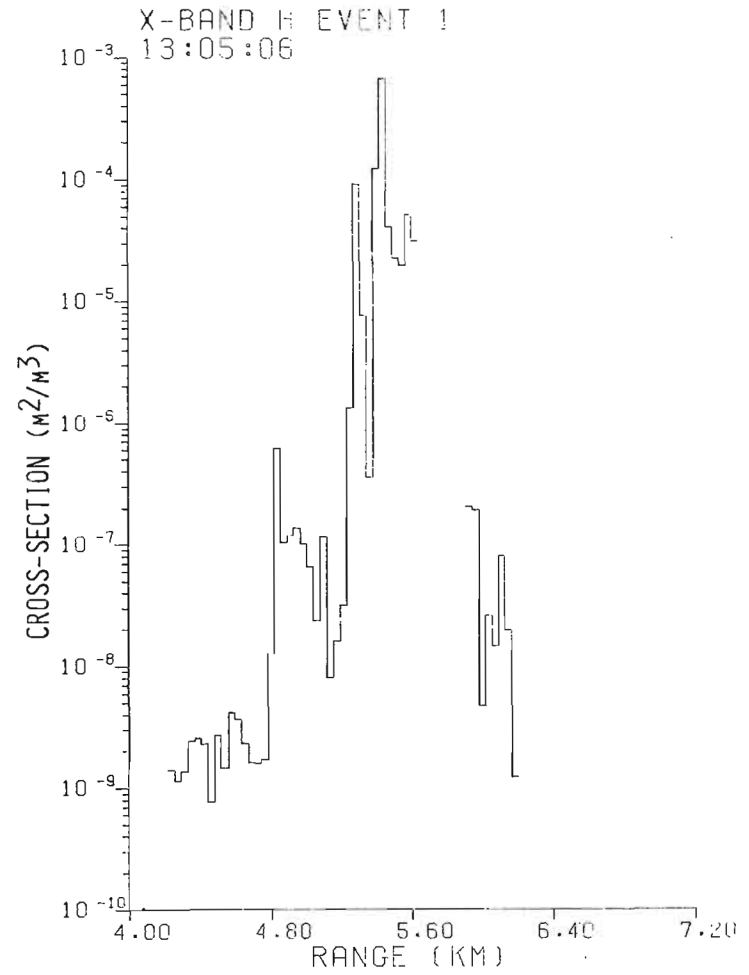


b. HH Polarization

Figure A-4. 35 GHz radar cross section vs. range; Event 1, $T_0 + 4$ seconds.

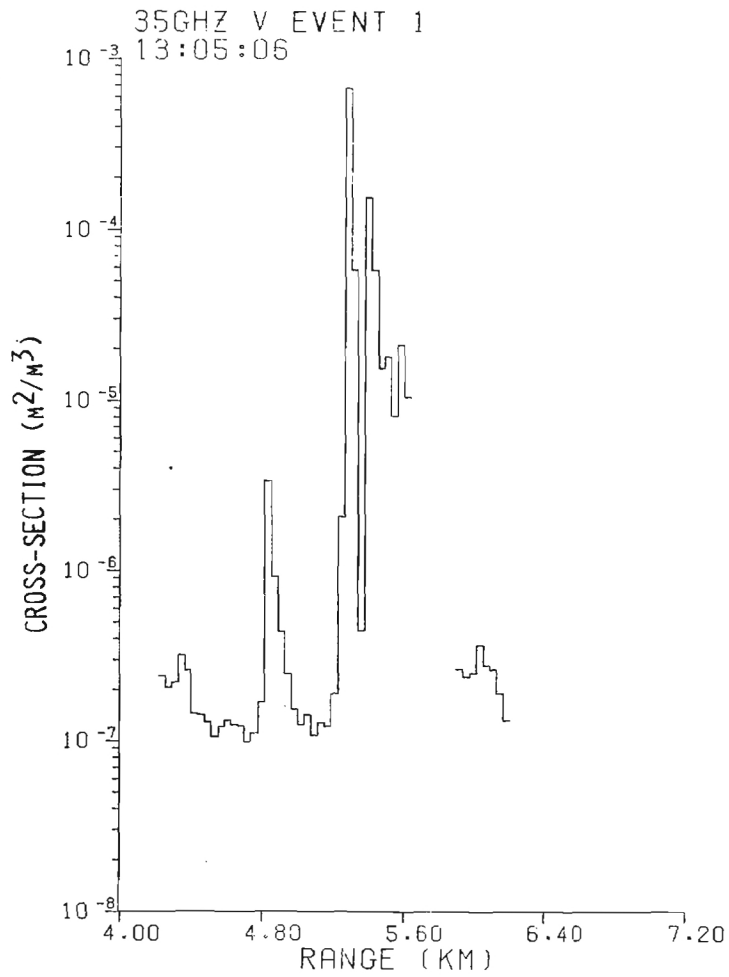


a. HV Polarization

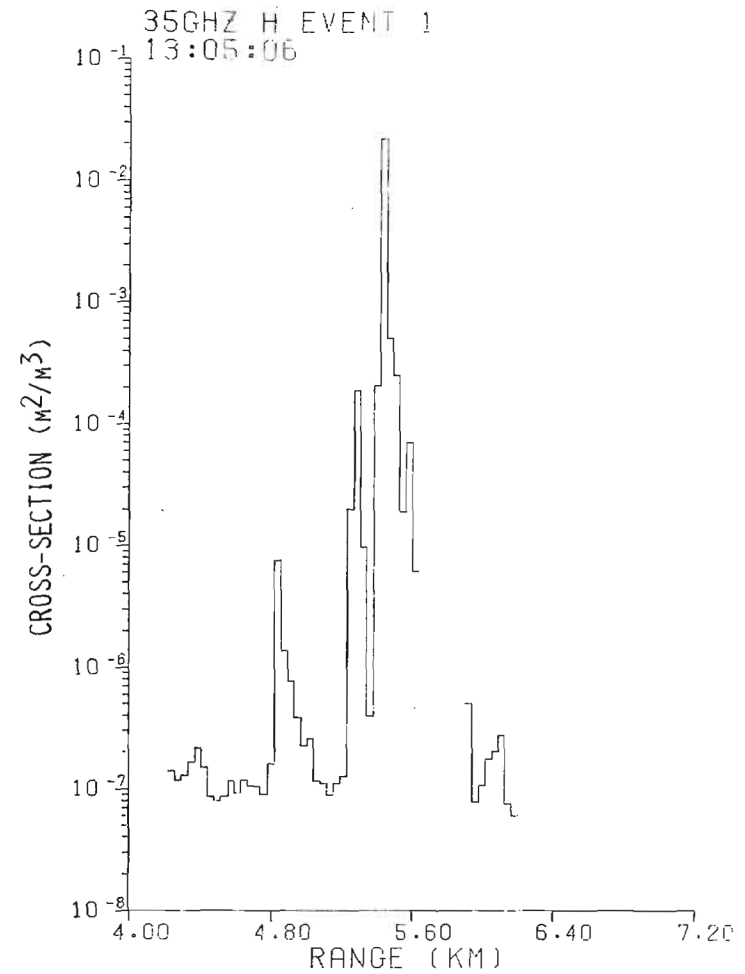


b. HH Polarization

Figure A-5. 9.4 GHz radar cross section vs. range; Event 1, $T_0 + 6$ seconds.

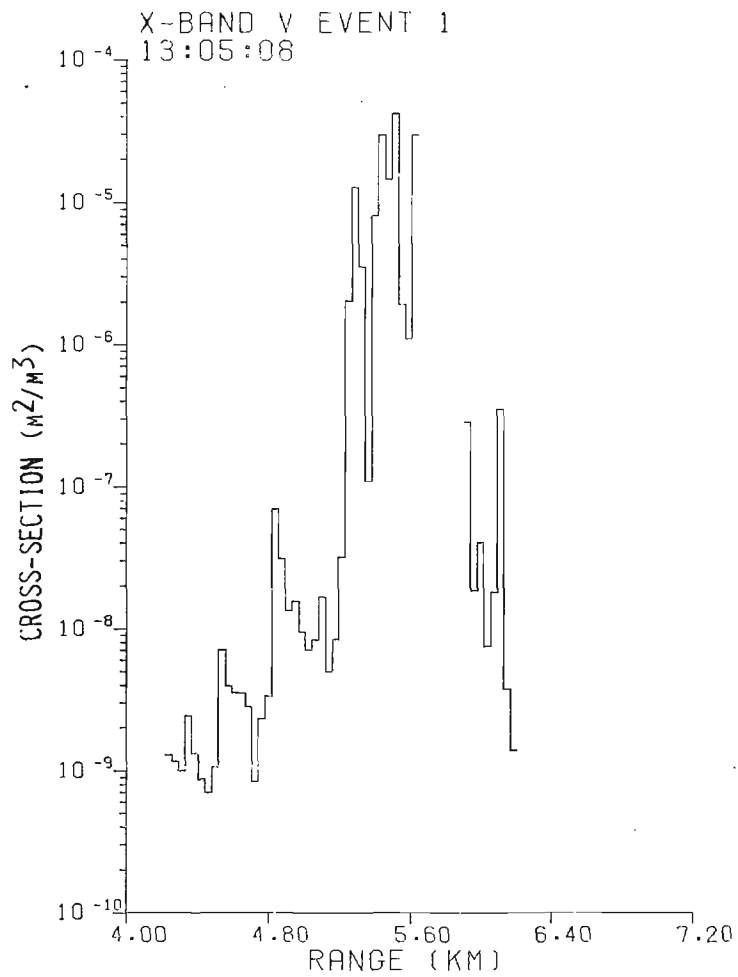


a. HV Polarization

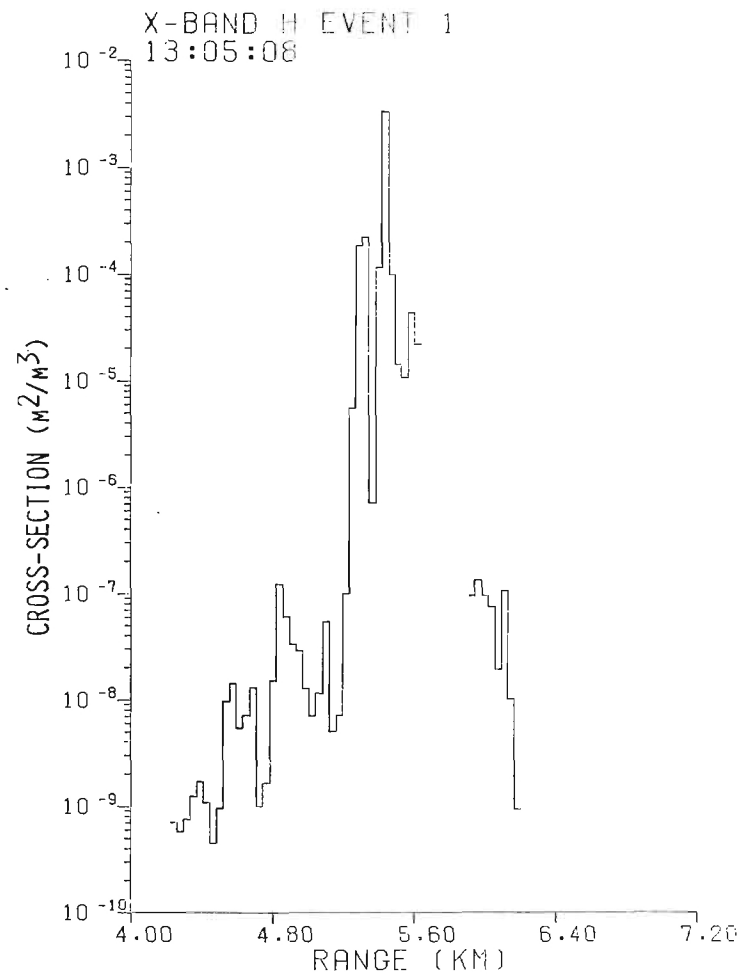


b. HH Polarization

Figure A-6. 35 GHz radar cross section vs. range; Event 1, $T_0 + 6$ seconds.

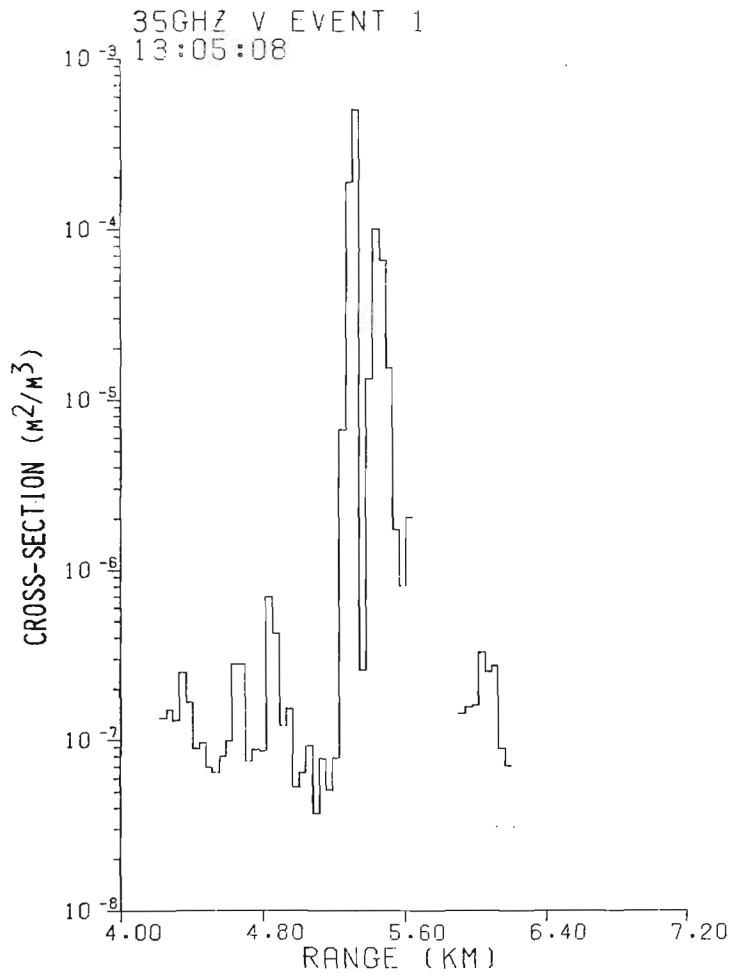


a. HV Polarization

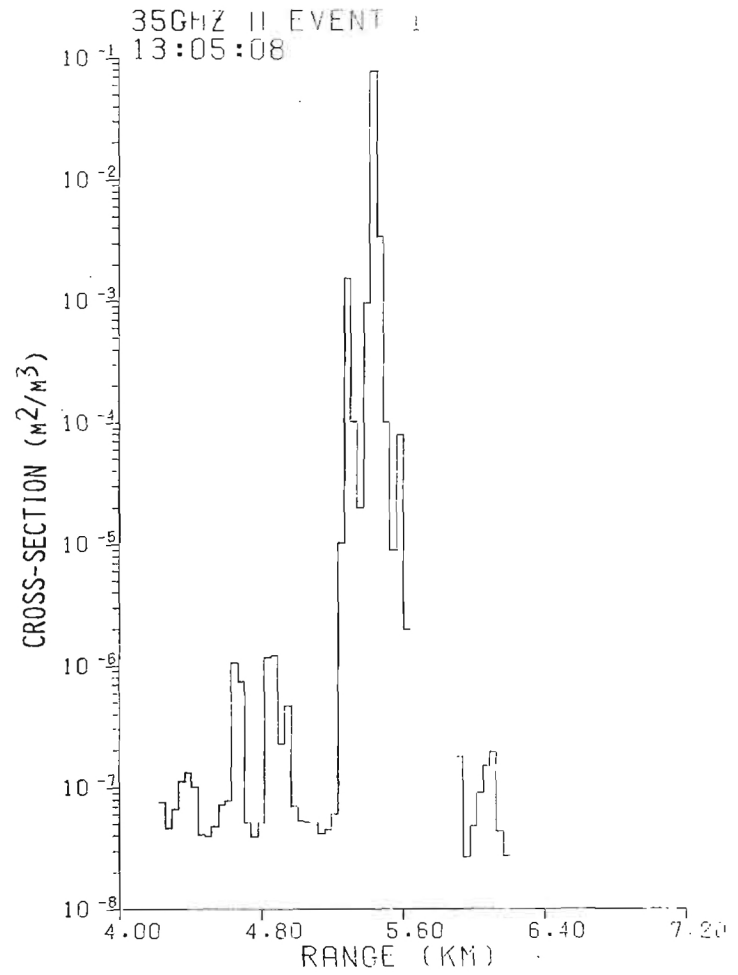


b. HH Polarization

Figure A-7. 9.4 GHz radar cross section vs. range; Event 1, $T_0 + 8$ seconds.

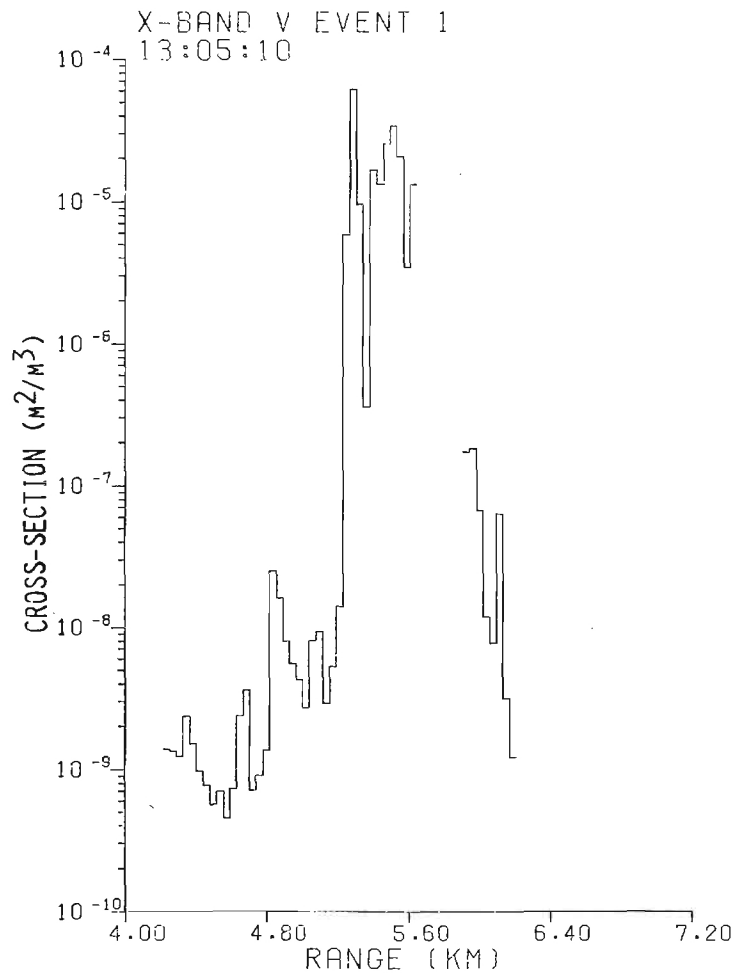


a. HV Polarization

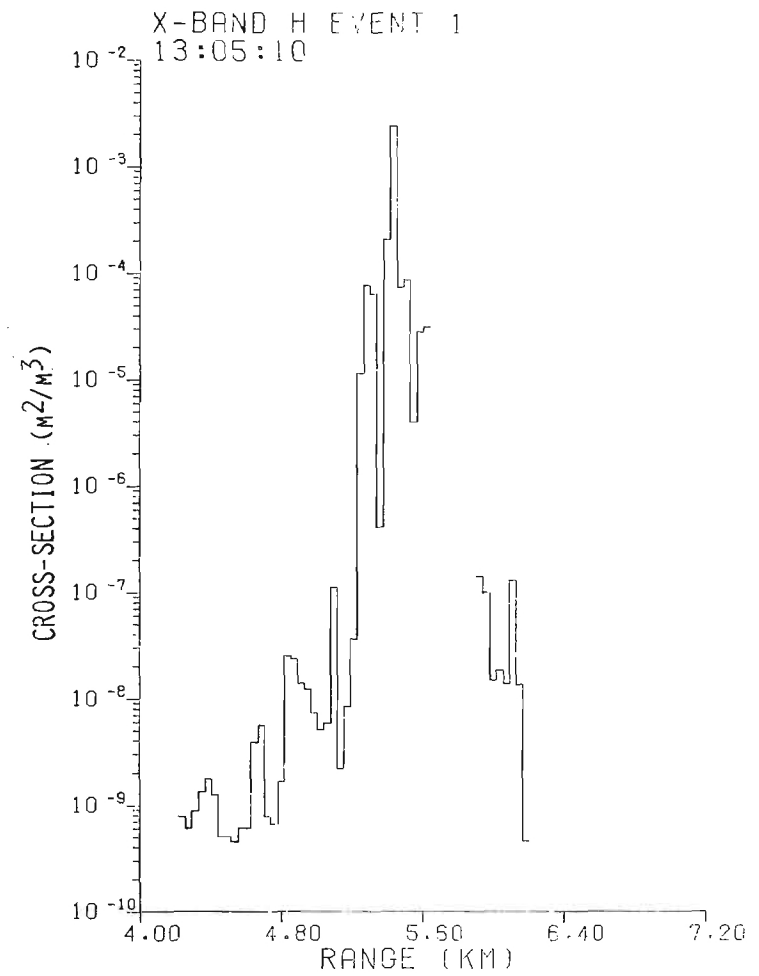


b. HH Polarization

Figure A-8. 35 GHz radar cross section vs. range; Event 1, $T_0 + 8$ seconds.

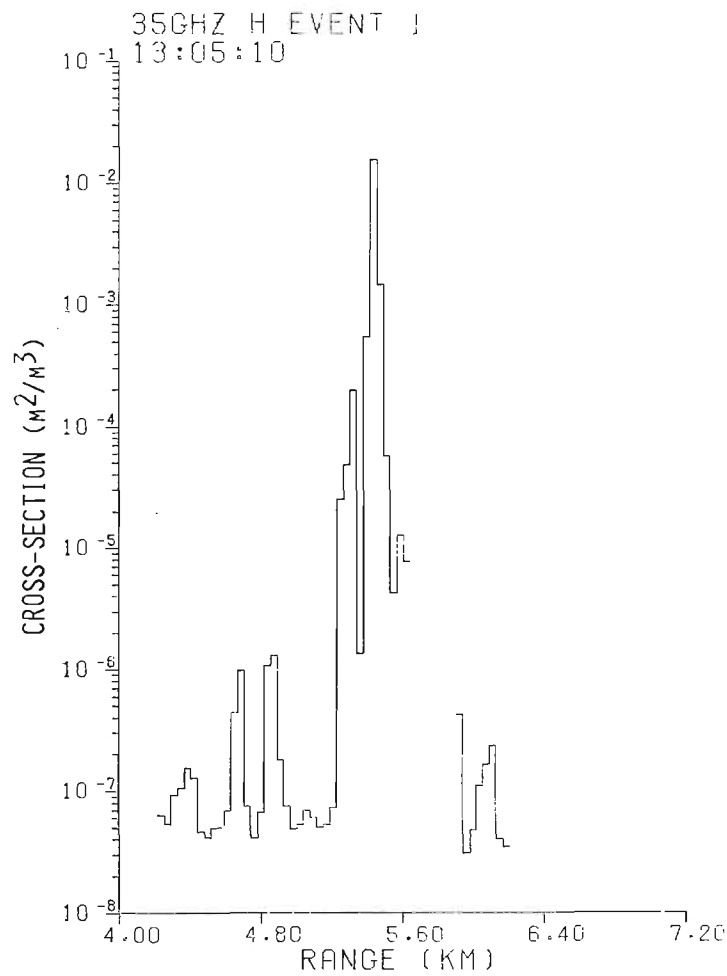
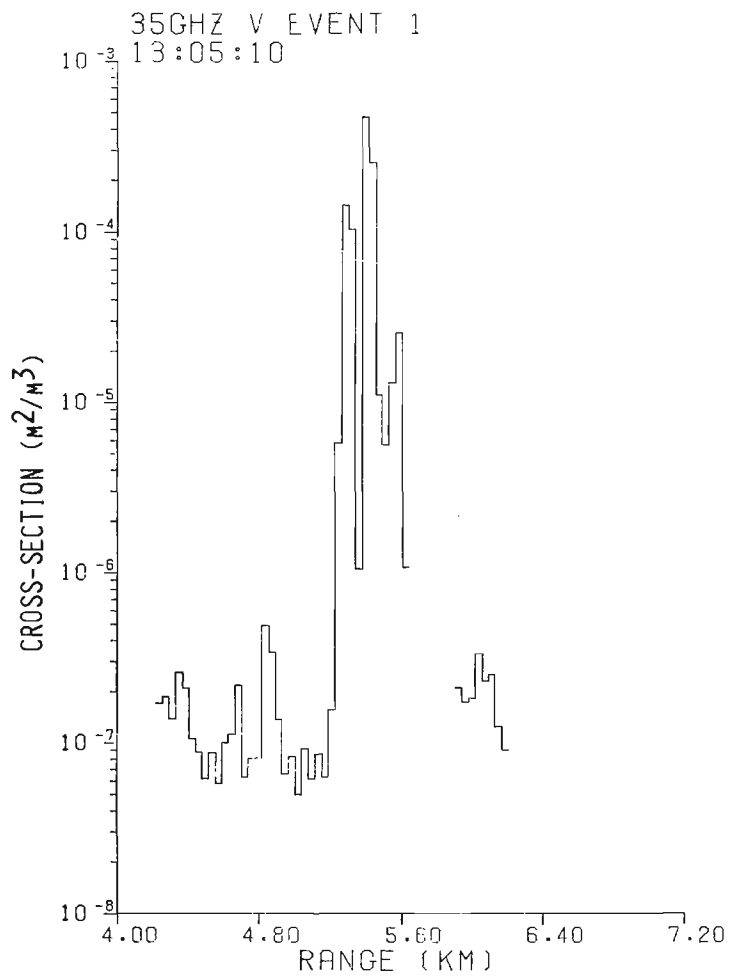


a. HV Polarization



b. HH Polarization

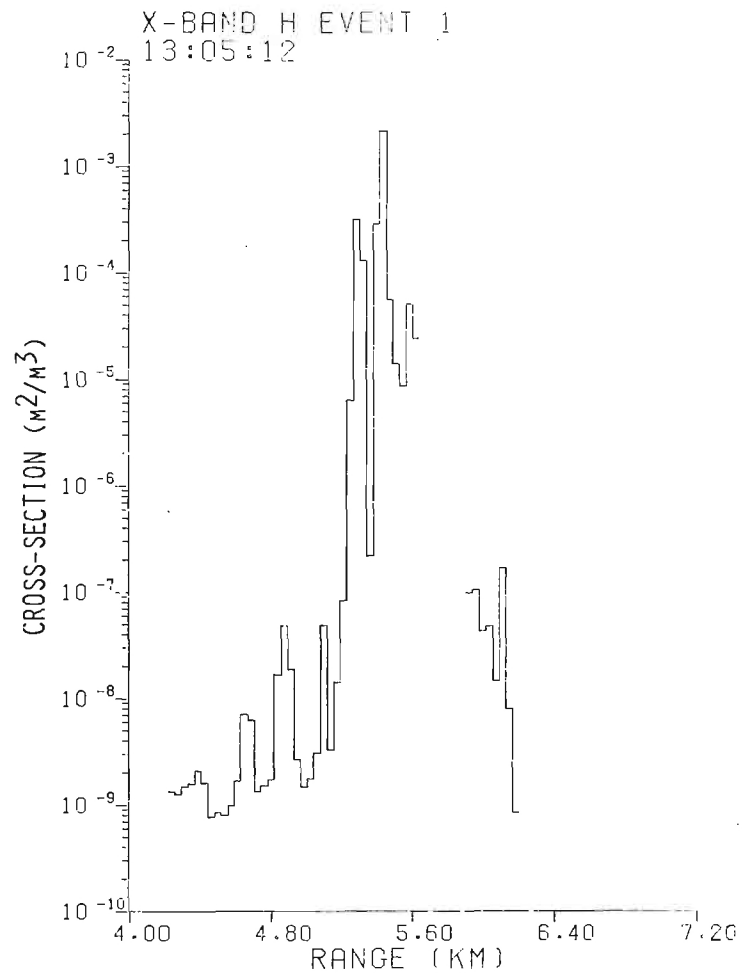
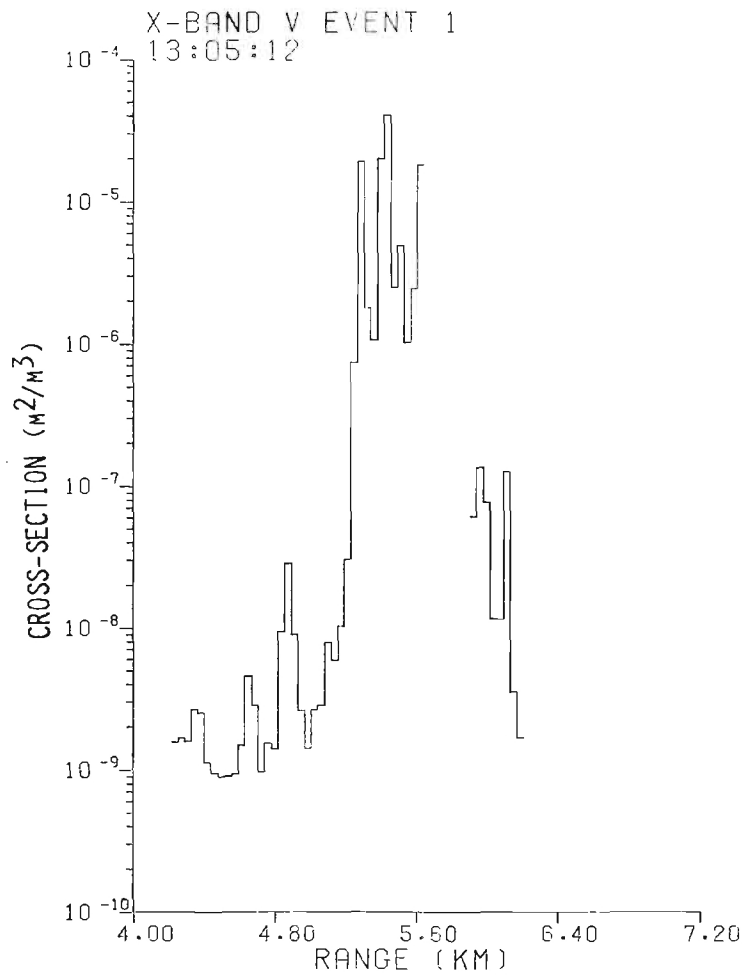
Figure A-9. 9.4 GHz radar cross section vs. range; Event 1, $T_0 + 10$ seconds.



a. HV Polarization

b. HH Polarization

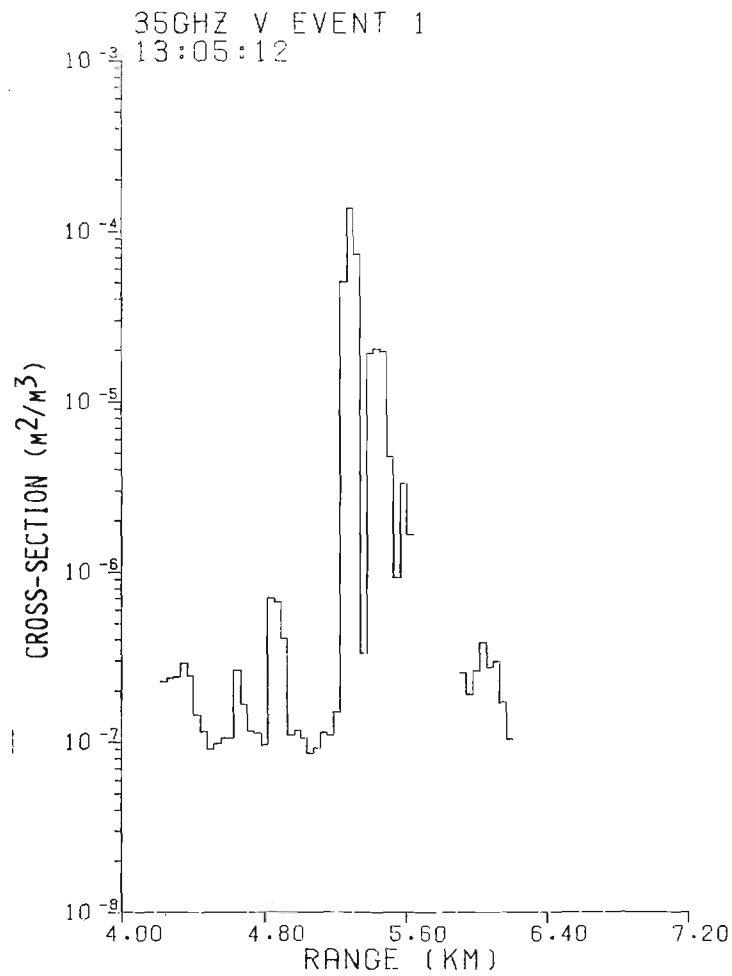
Figure A-10. 35 GHz radar cross section vs. range; Event 1, $T_0 + 10$ seconds.



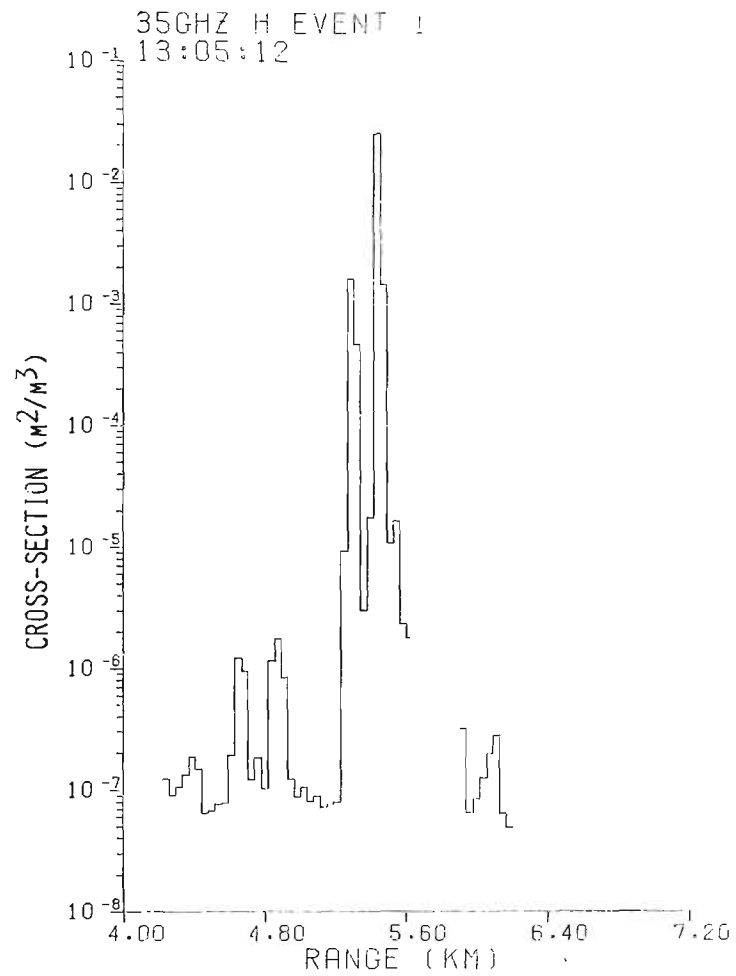
a. HV Polarization

b. HH Polarization

Figure A-II. 9.4 GHz radar cross section vs. range; Event 1, $T_0 + 12$ seconds.

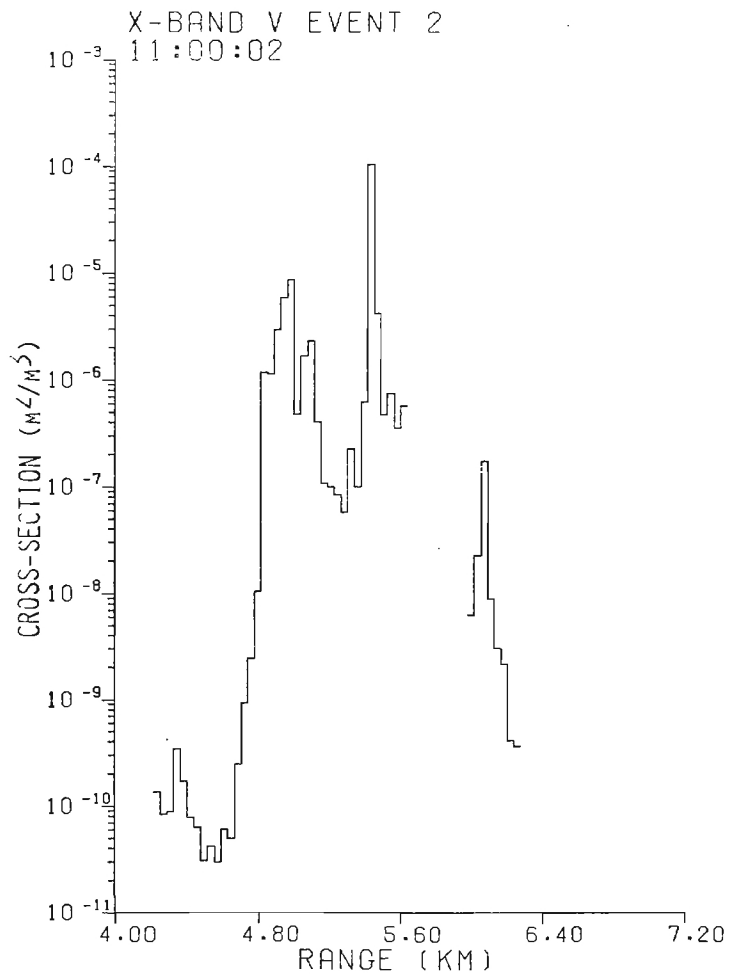


a. HV Polarization

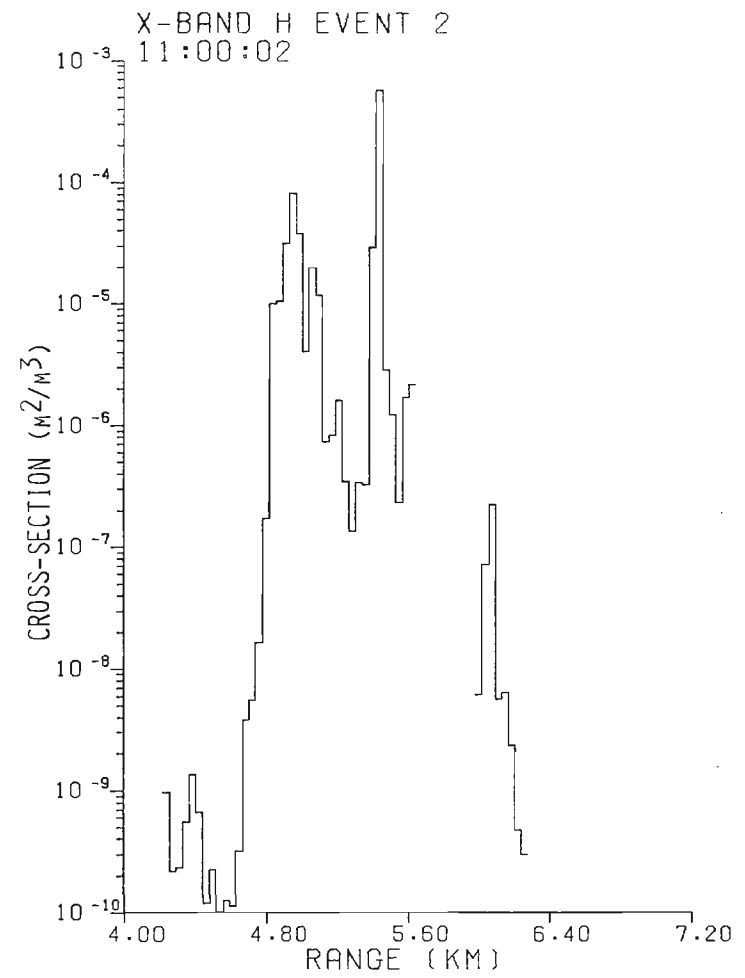


b. HH Polarization

Figure A-12. 35 GHz radar cross section vs. range; Event 1, $T_0 + 12$ seconds.

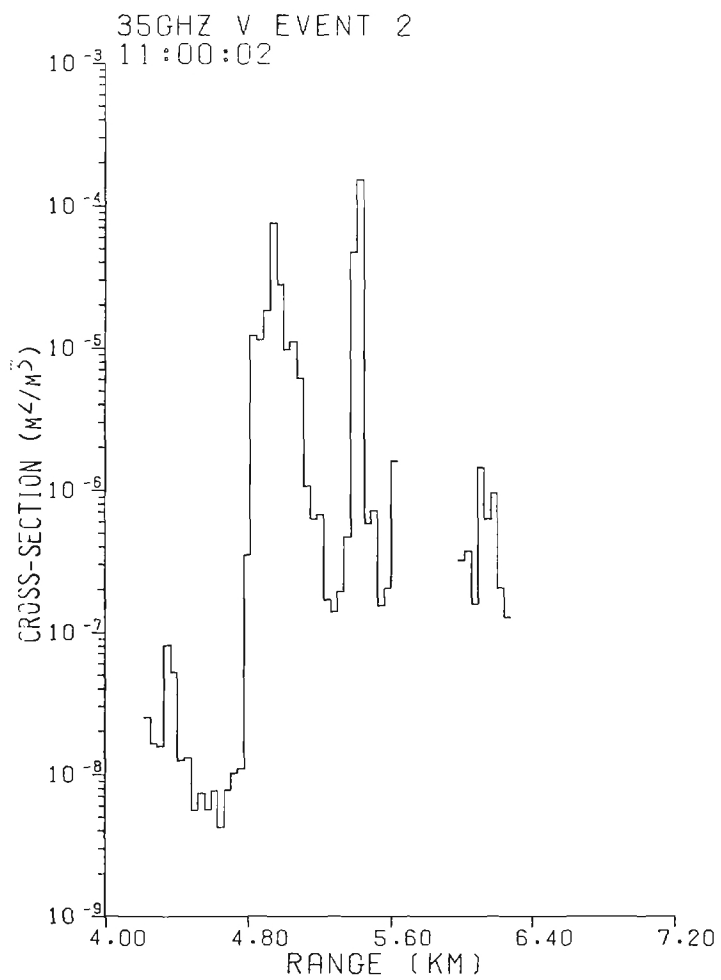


a. HV Polarization

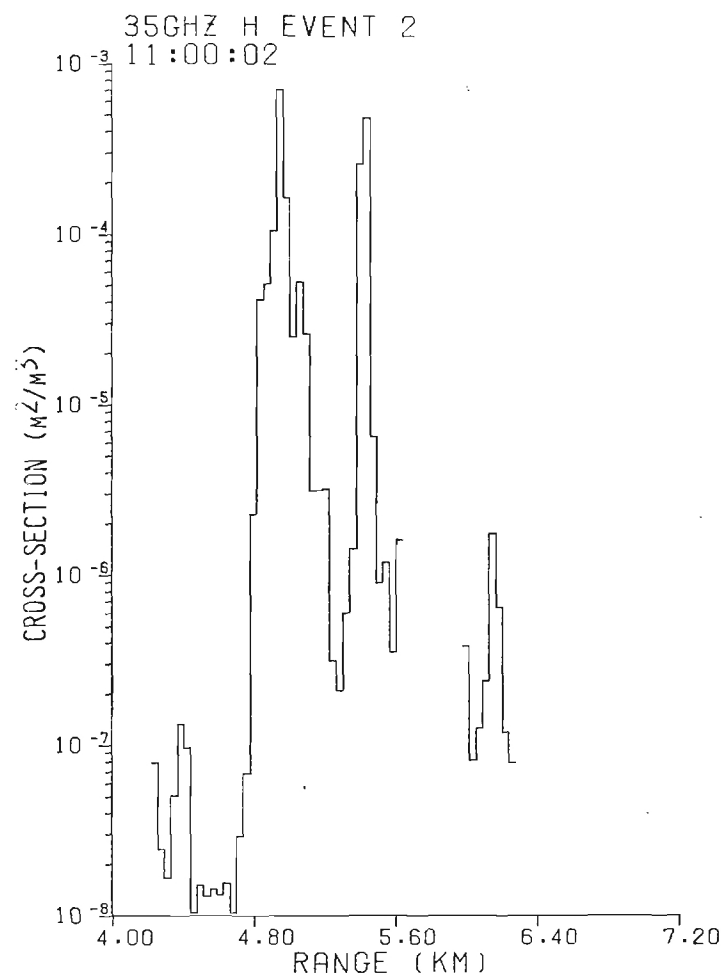


b. HH Polarization

Figure A-13. 9.4 GHz radar cross section vs. range; Event 2, $T_0 + 2$ seconds.

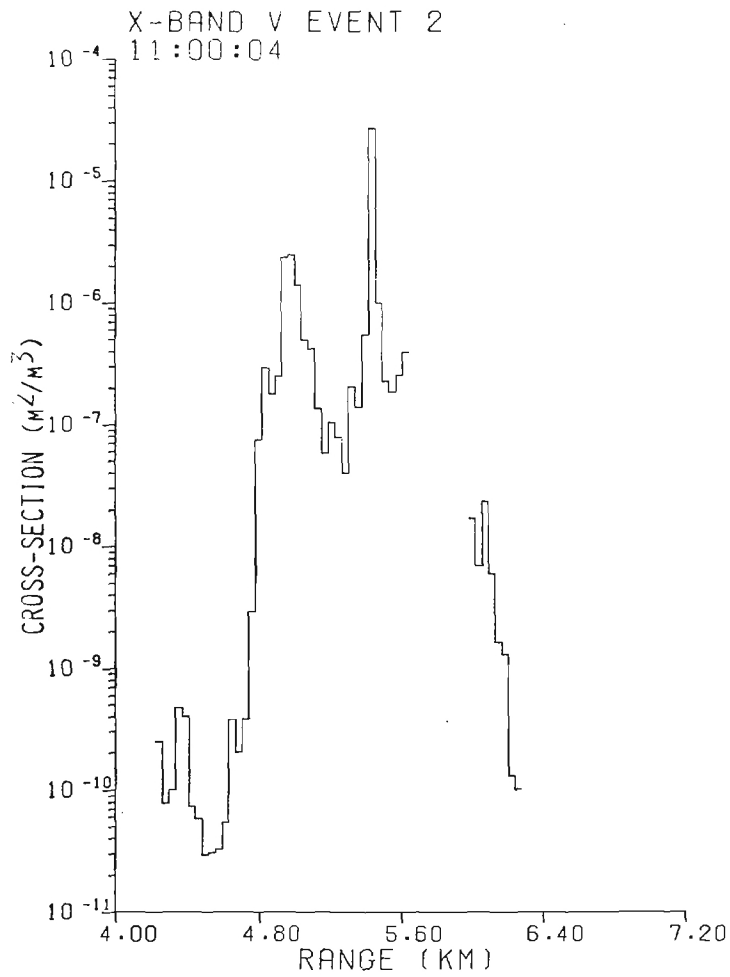


a. HV Polarization

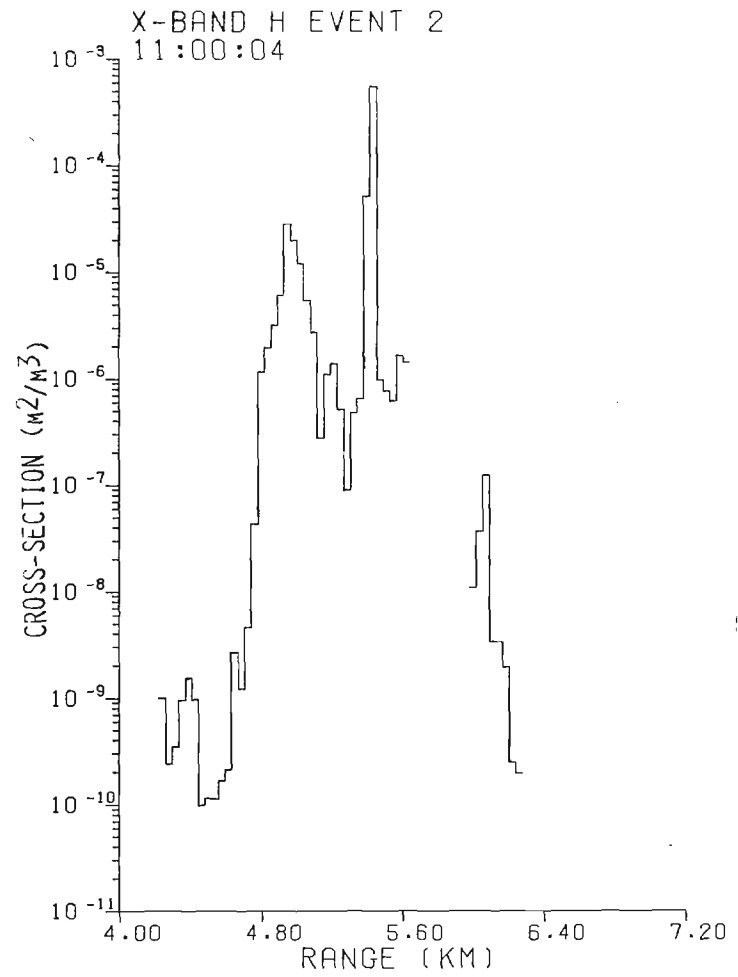


b. HH Polarization

Figure A-14. 35 GHz radar cross section vs. range; Event 2, $T_0 + 2$ seconds.

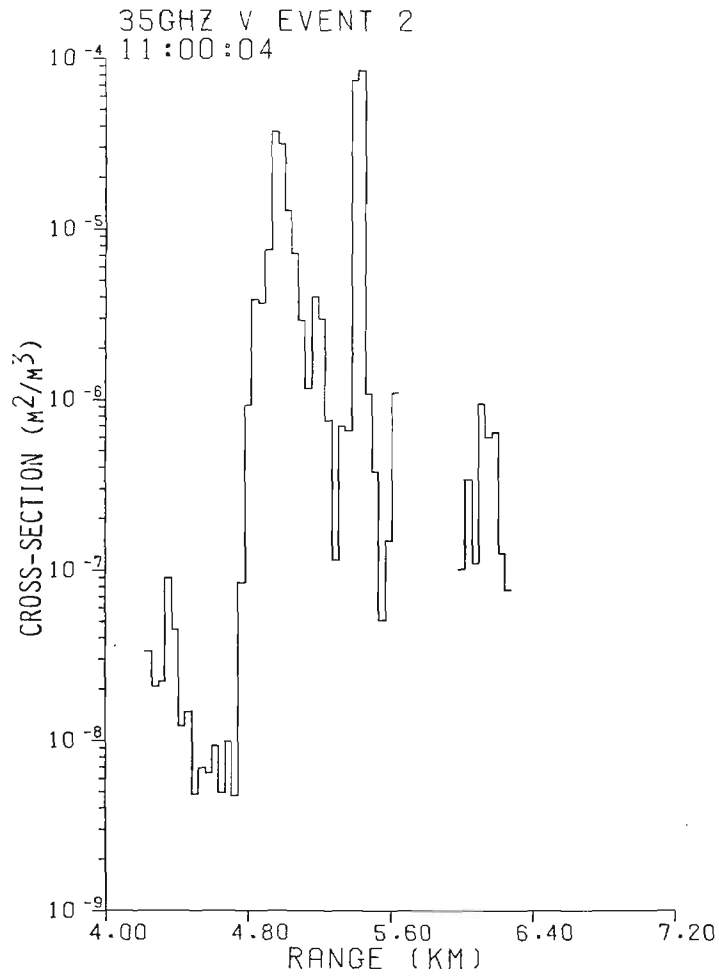


a. HV Polarization

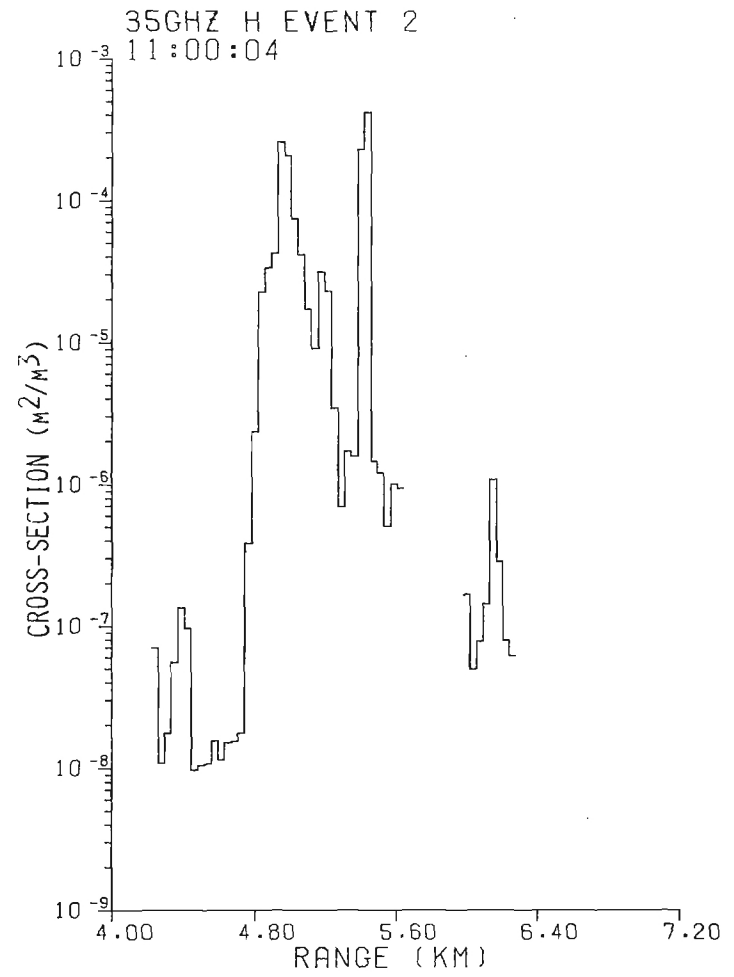


b. HH Polarization

Figure A-15. 9.4 GHz radar cross section vs. range; Event 2, $T_0 + 4$ seconds.

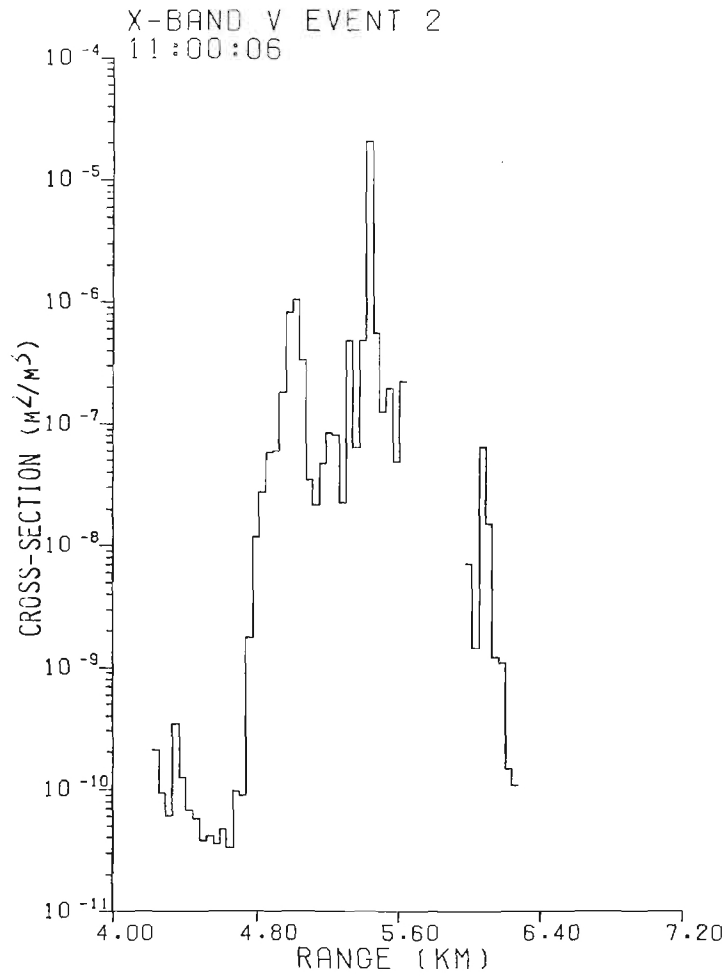


a. HV Polarization

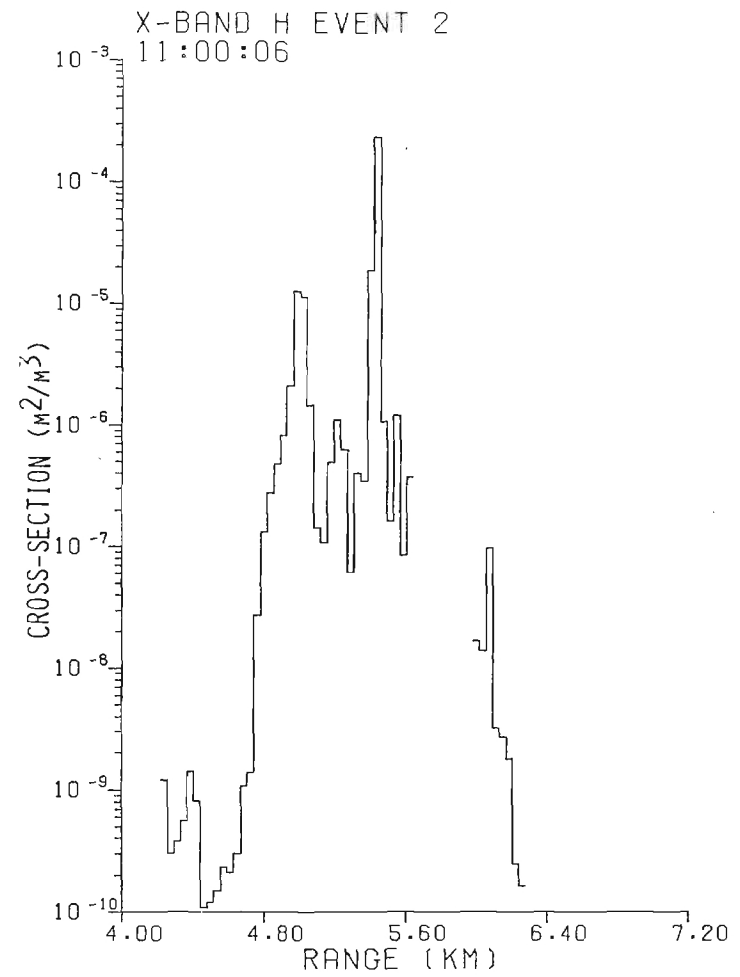


b. HH Polarization

Figure A-16. 35 GHz radar cross section vs. range; Event 2, $T_0 + 4$ seconds.

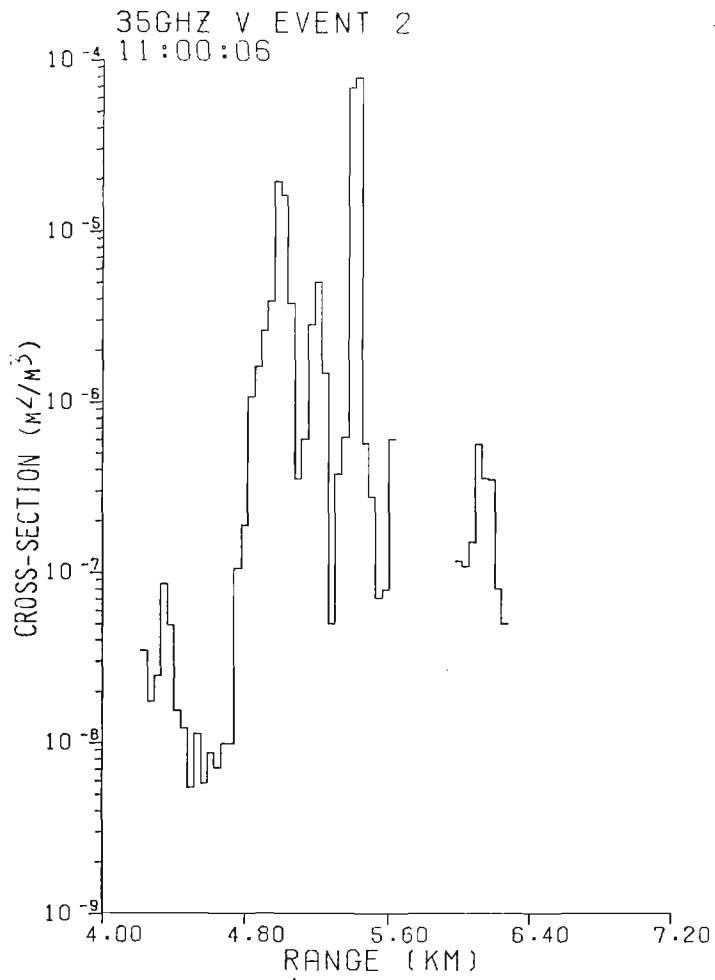


a. HV Polarization

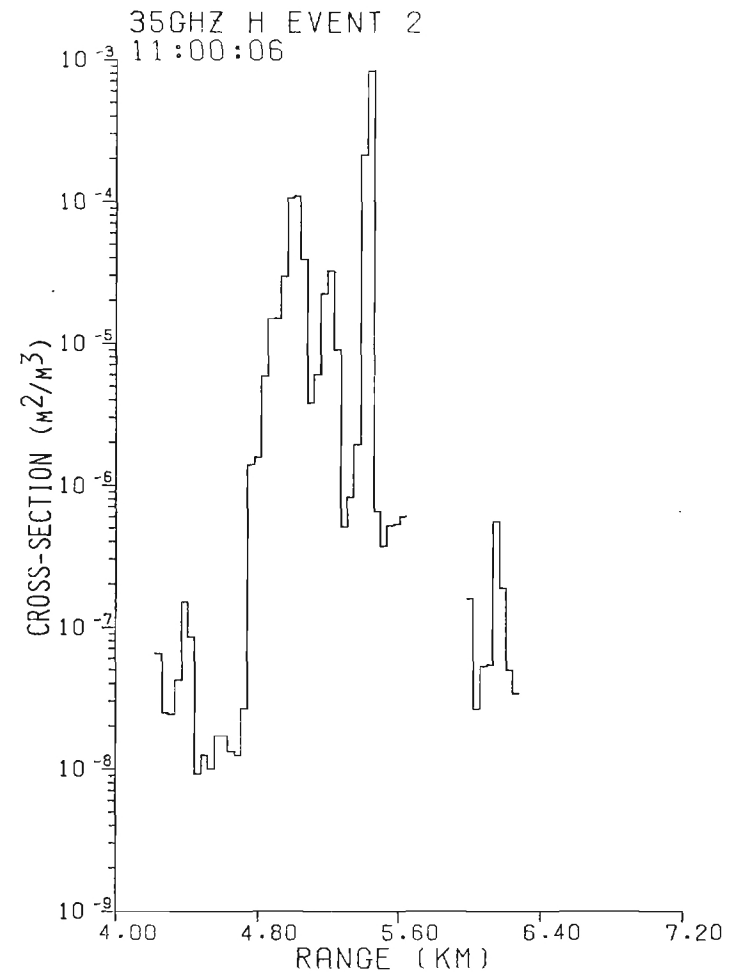


b. HH Polarization

Figure A-17. 9.4 GHz radar cross section vs. range; Event 2, $T_0 + 6$ seconds.

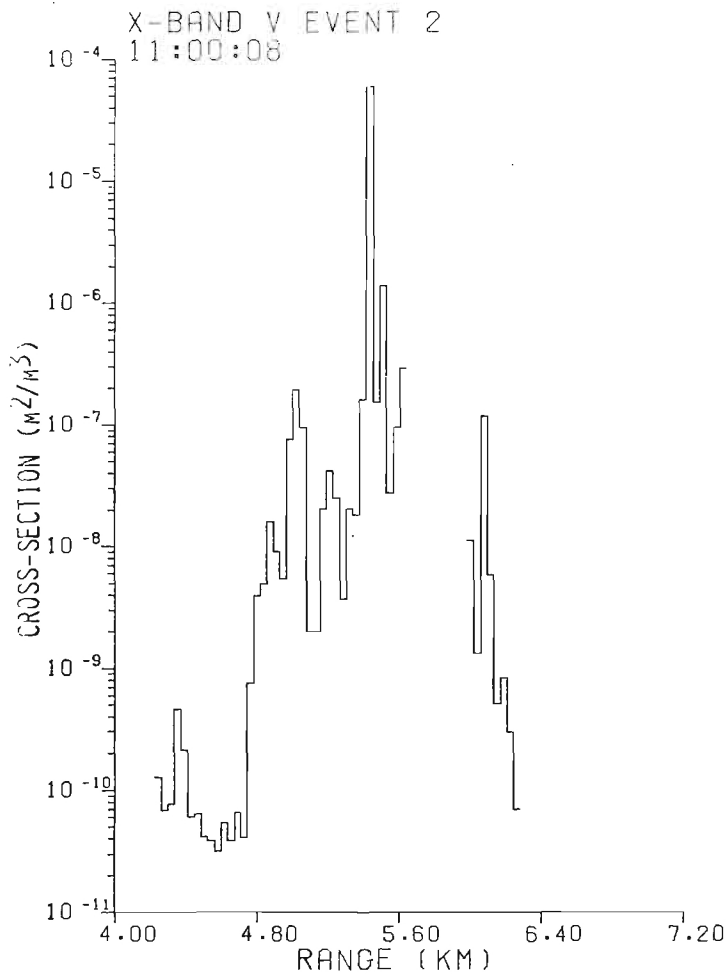


a. HV Polarization

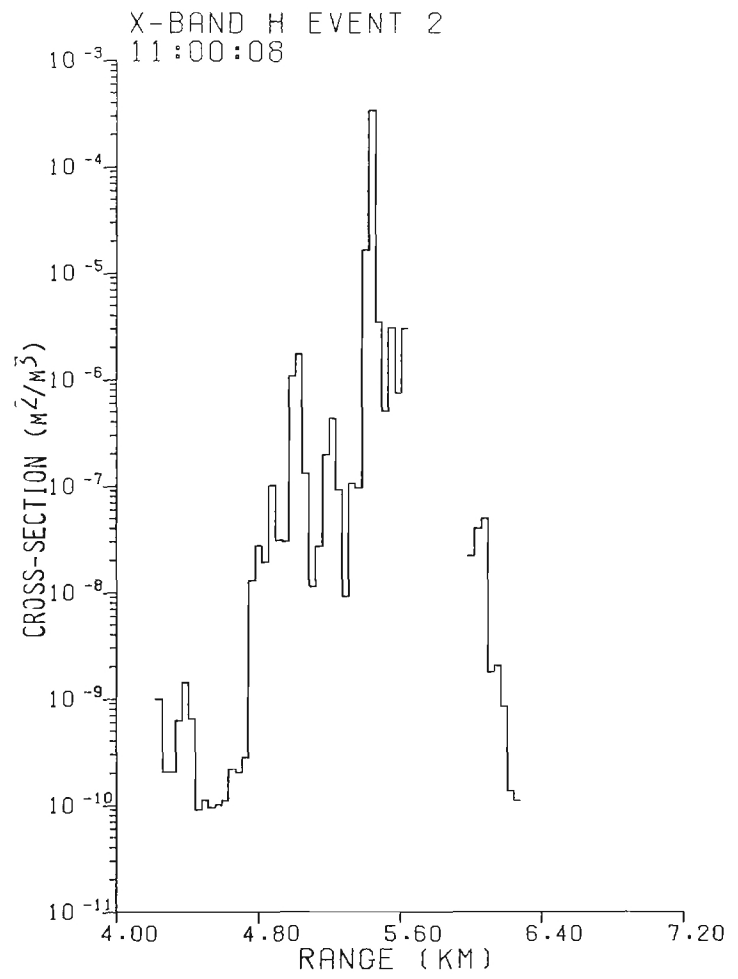


b. HH Polarization

Figure A-18. 35 GHz radar cross section vs. range; Event 2, $T_0 + 6$ seconds.

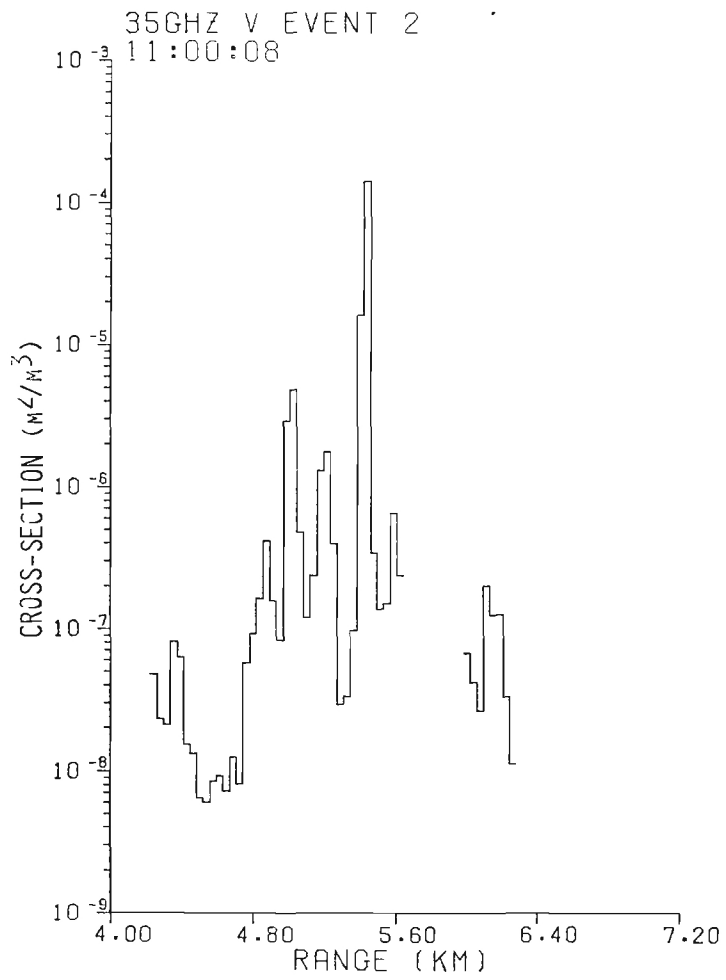


a. HV Polarization

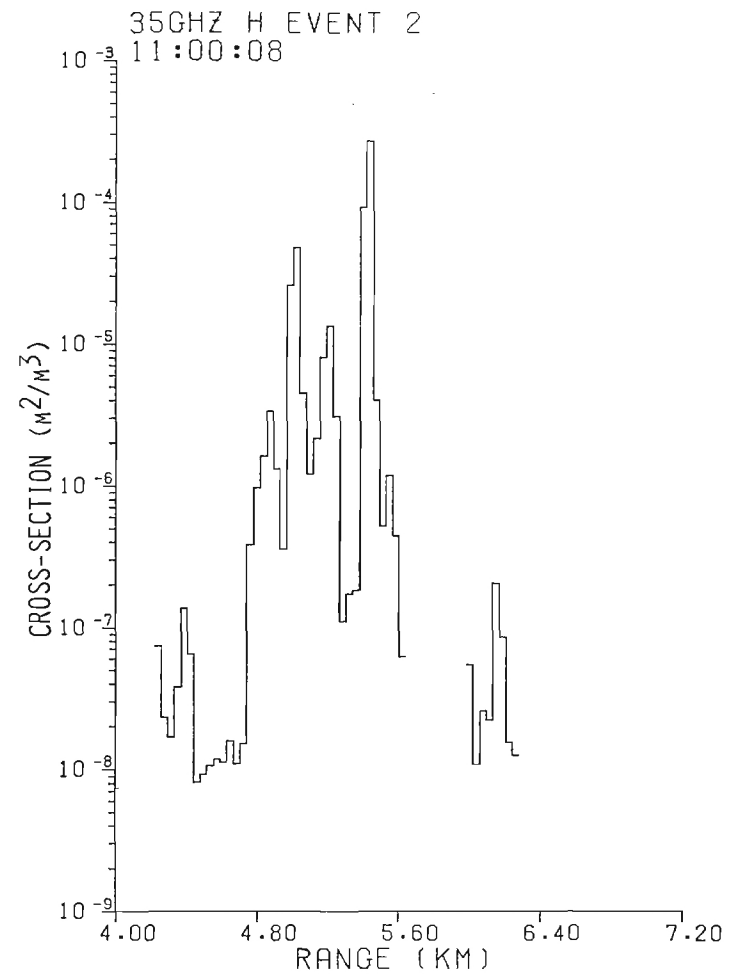


b. HH Polarization

Figure A-19. 9.4 GHz radar cross section vs. range; Event 2, $T_0 + 8$ seconds.

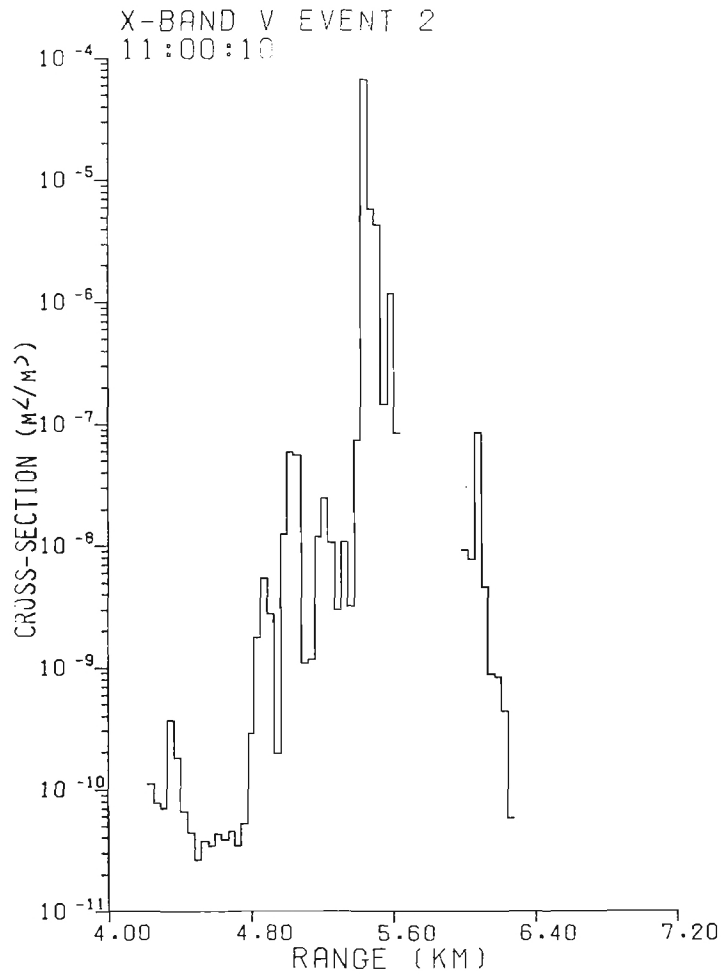


a. HV Polarization

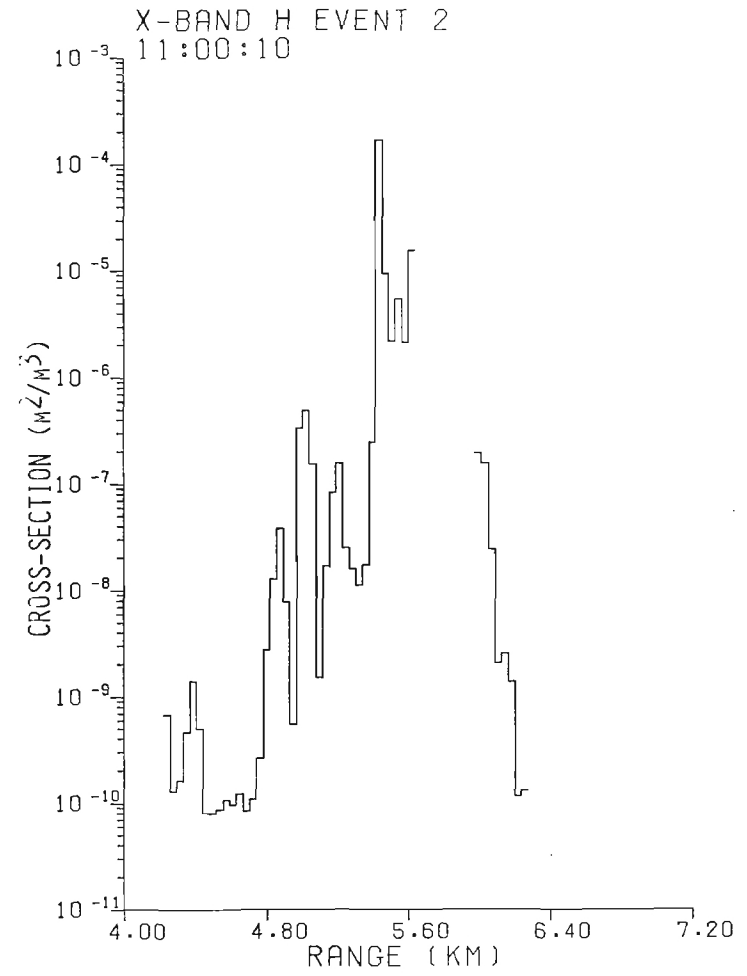


b. HH Polarization

Figure A-20. 35 GHz radar cross section vs. range; Event 2, $T_0 + 8$ seconds.

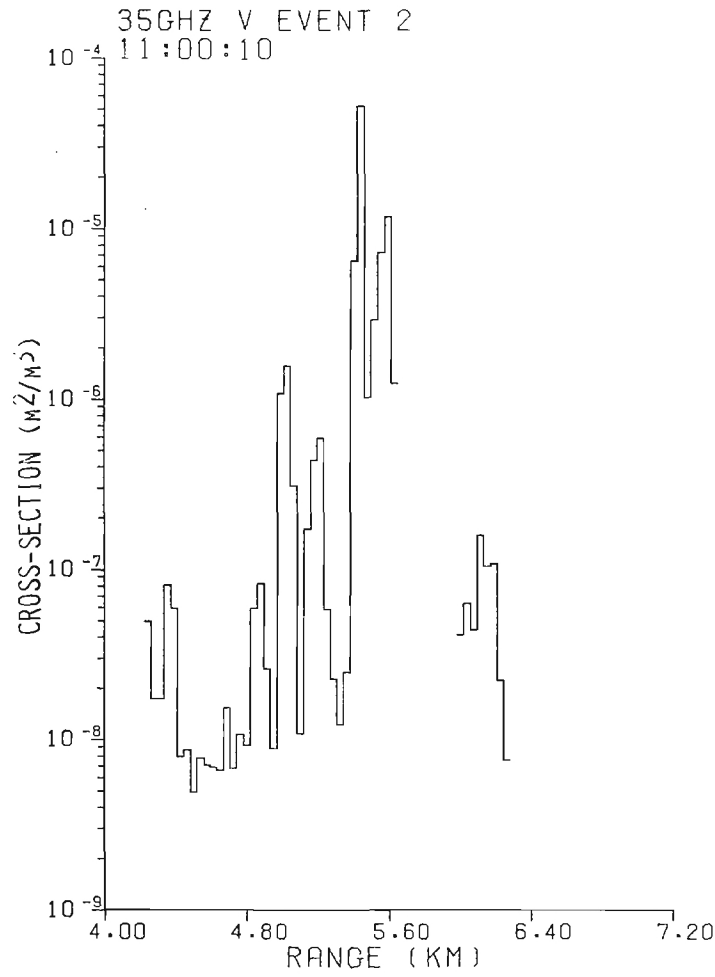


a. HV Polarization

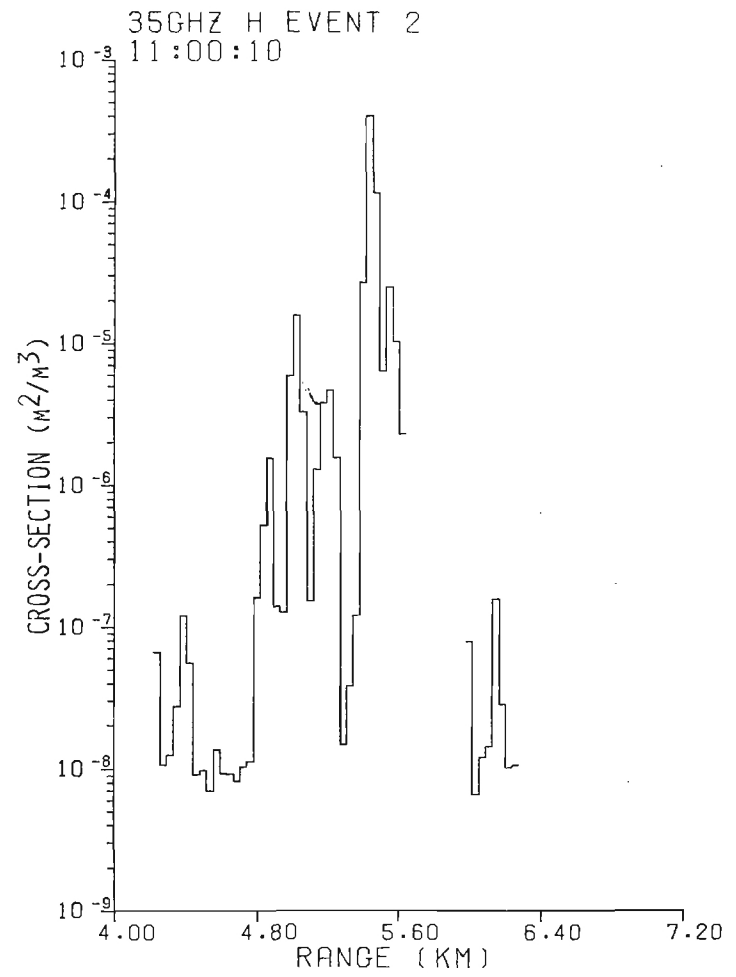


b. HH Polarization

Figure A-21. 9.4 GHz radar cross section vs. range; Event 2, $T_0 + 10$ seconds.

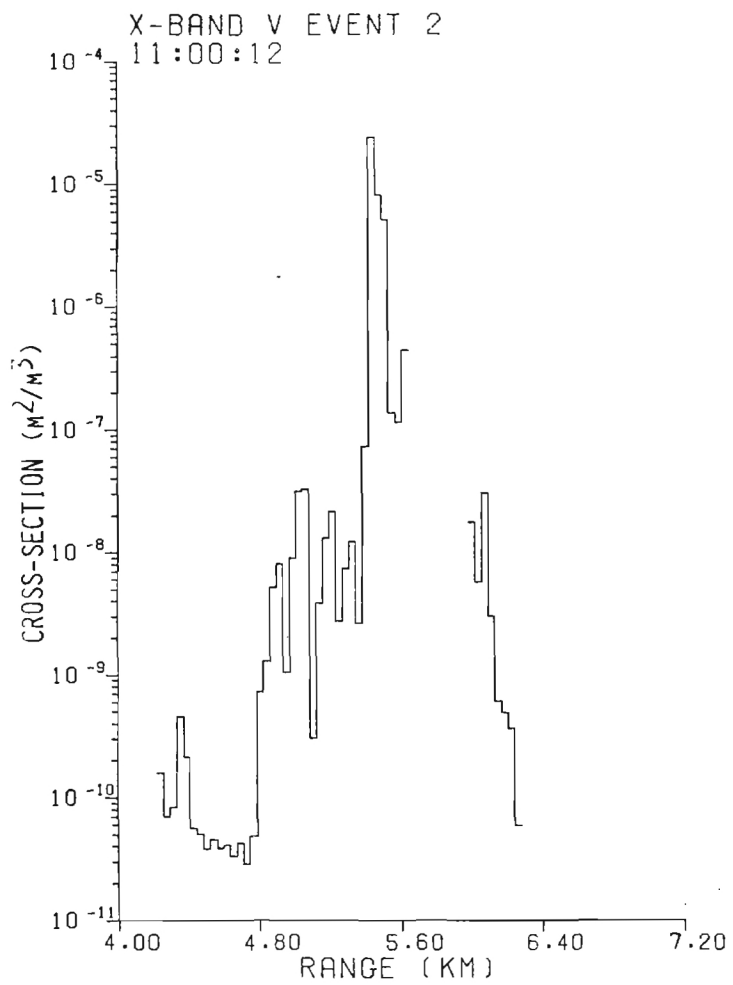


a. HV Polarization

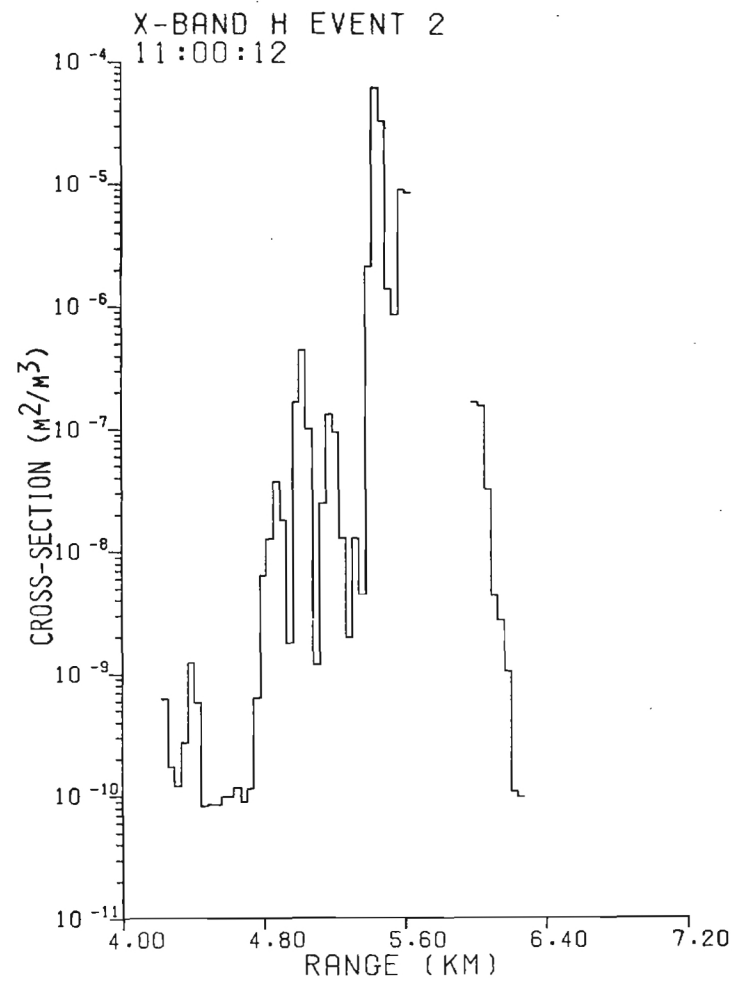


b. HH Polarization

Figure A-22. 35 GHz radar cross section vs. range; Event 2, $T_0 + 10$ seconds.

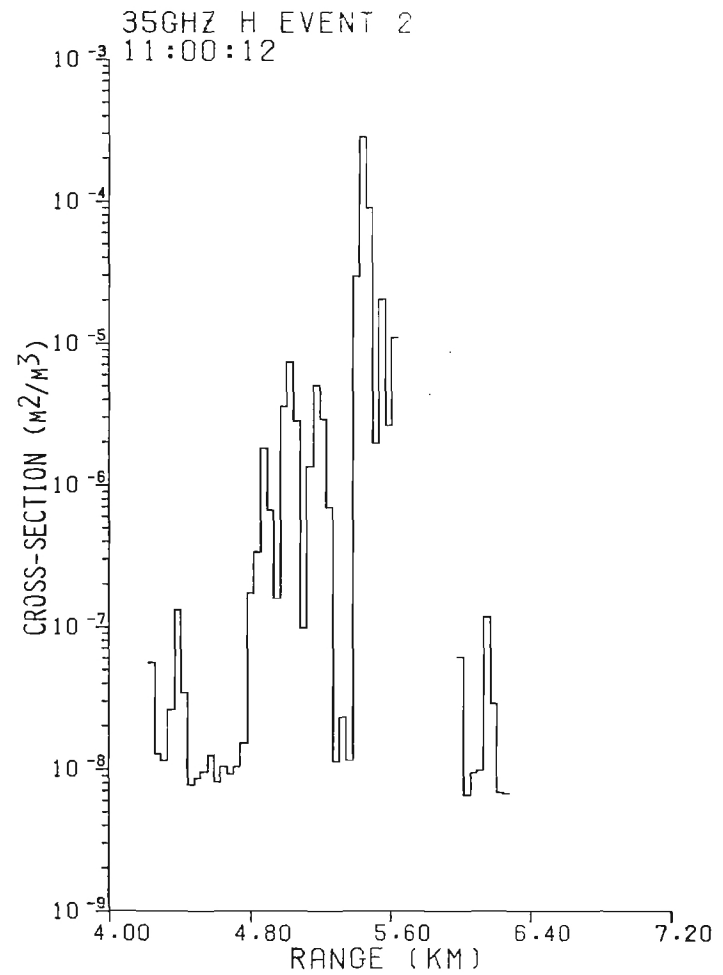
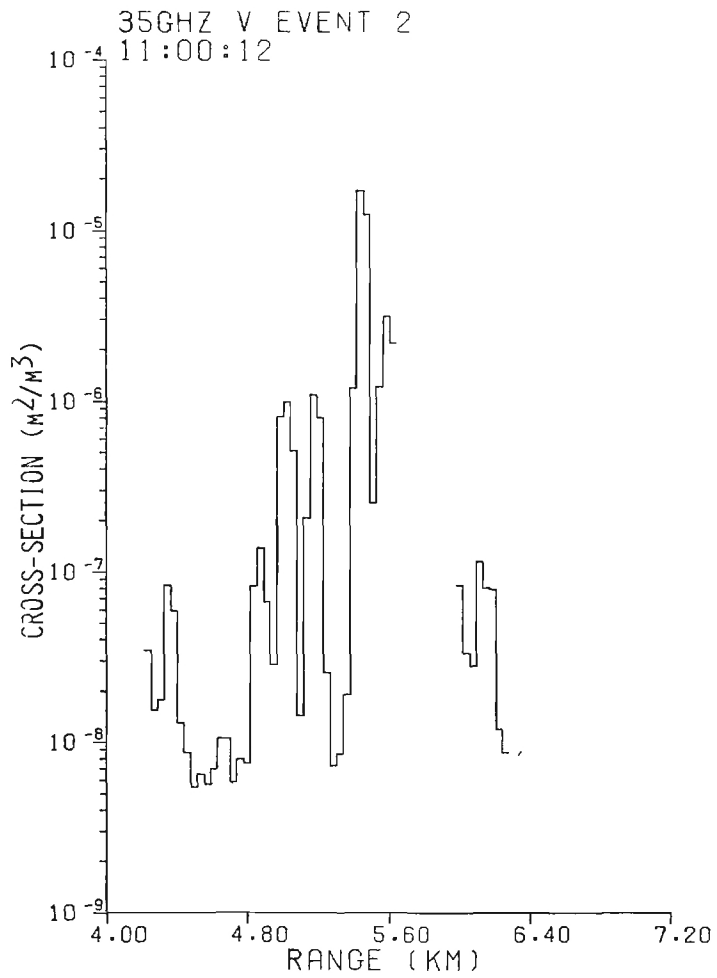


a. HV Polarization



b. HH Polarization

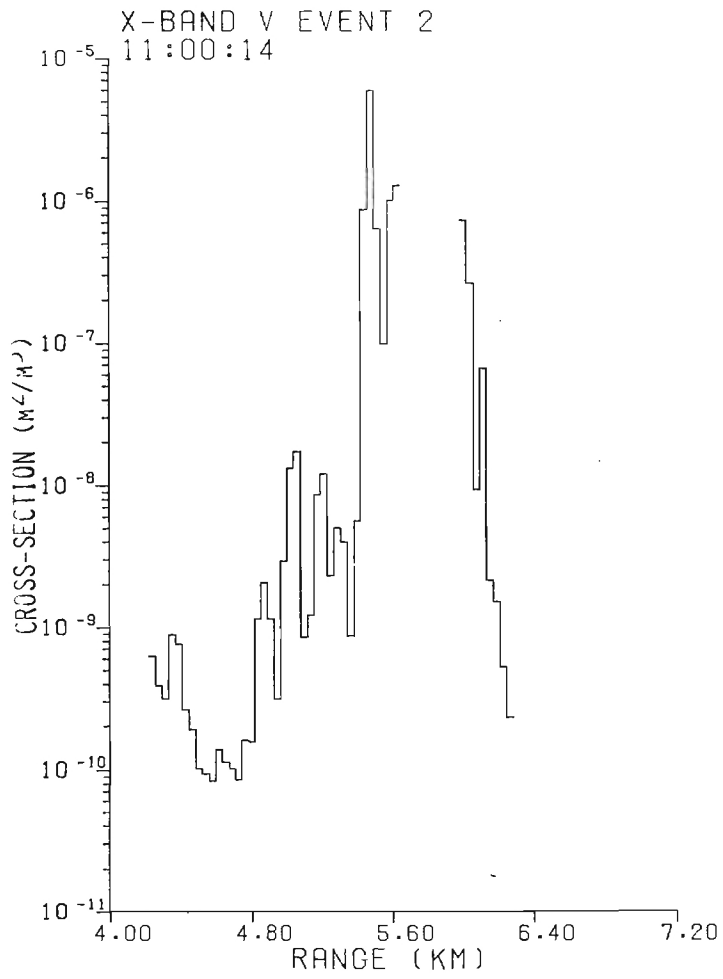
Figure A-23. 9.4 GHz radar cross section vs. range; Event 2, $T_0 + 12$ seconds.



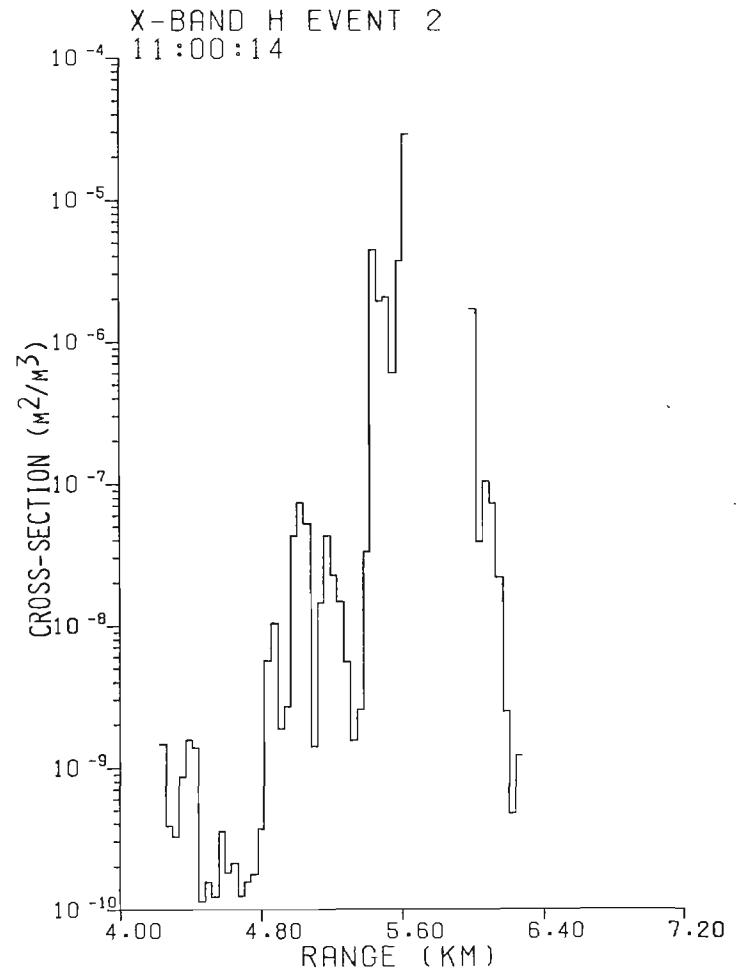
a. HV Polarization

b. HH Polarization

Figure A-24. 35 GHz radar cross section vs. range; Event 2, $T_0 + 12$ seconds.

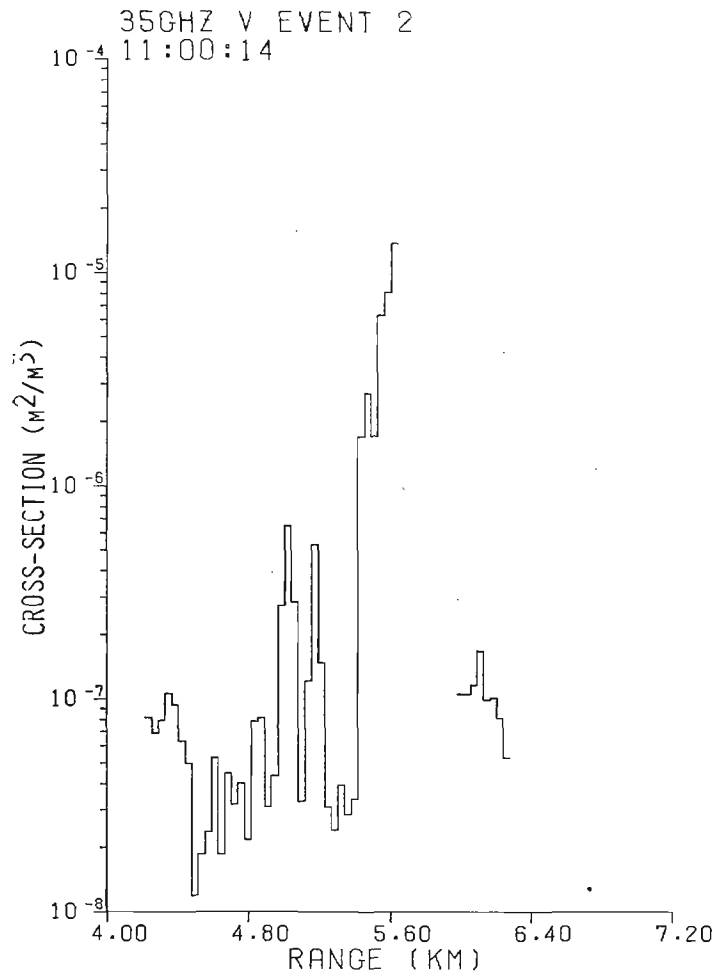


a. HV Polarization

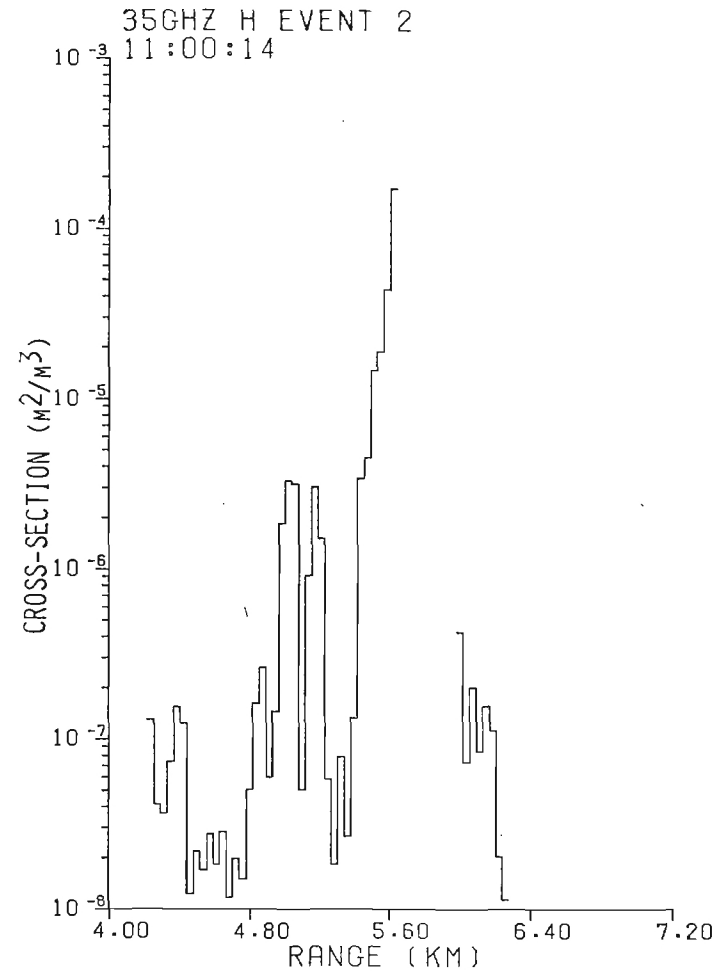


b. HH Polarization

Figure A-25. 9.4 GHz radar cross section vs. range; Event 2, $T_0 + 14$ seconds.

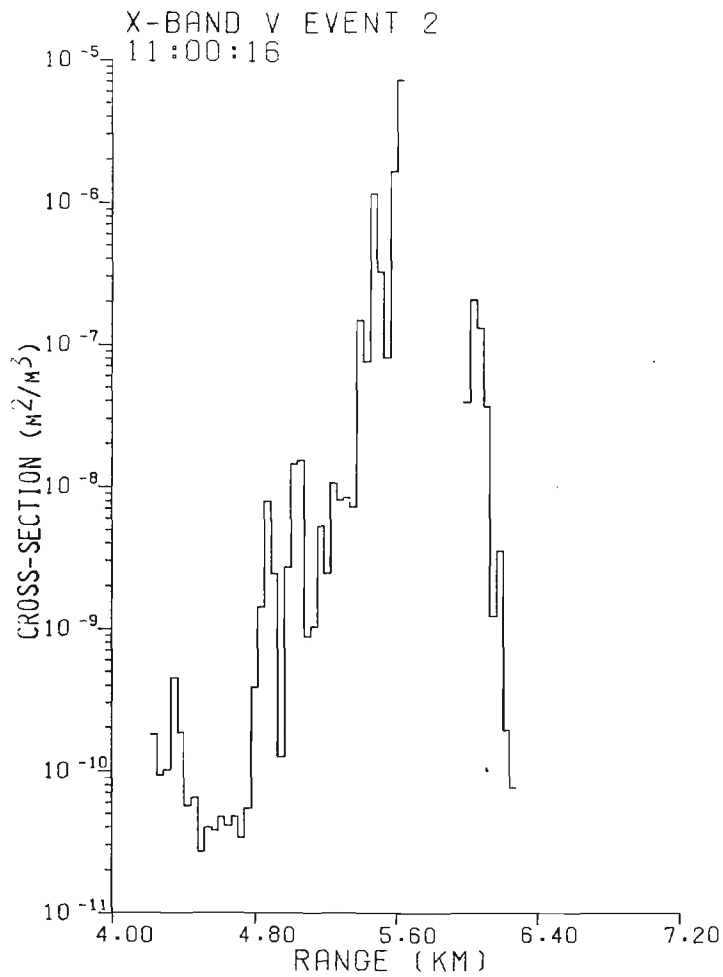


a. HV Polarization

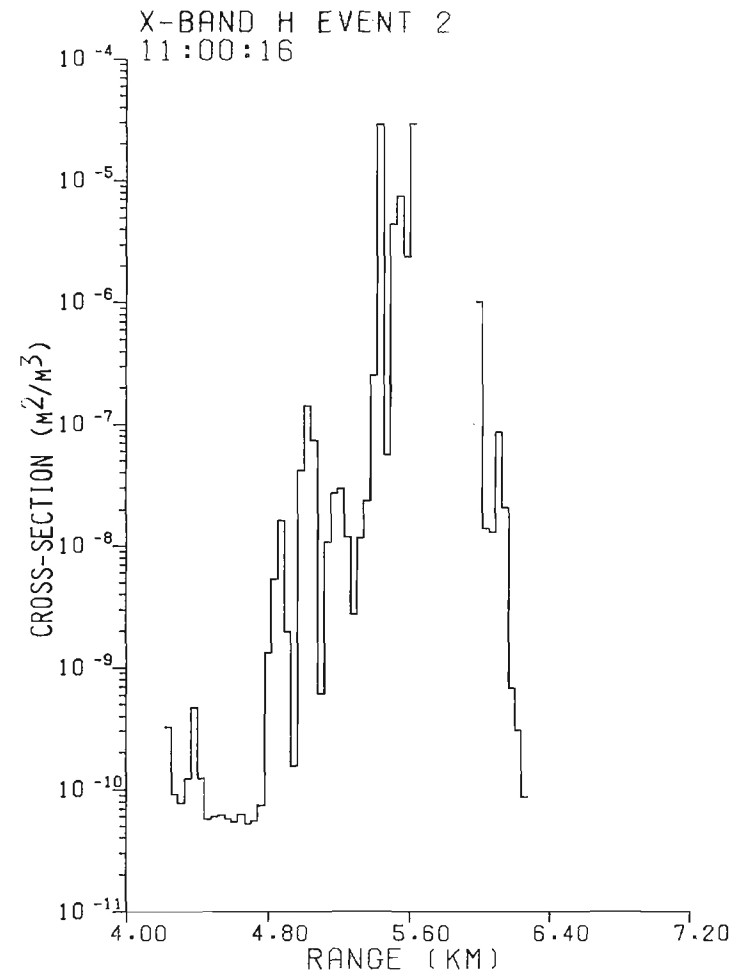


b. HH Polarization

Figure A-26. 35 GHz radar cross section vs. range; Event 2, $T_0 + 14$ seconds.

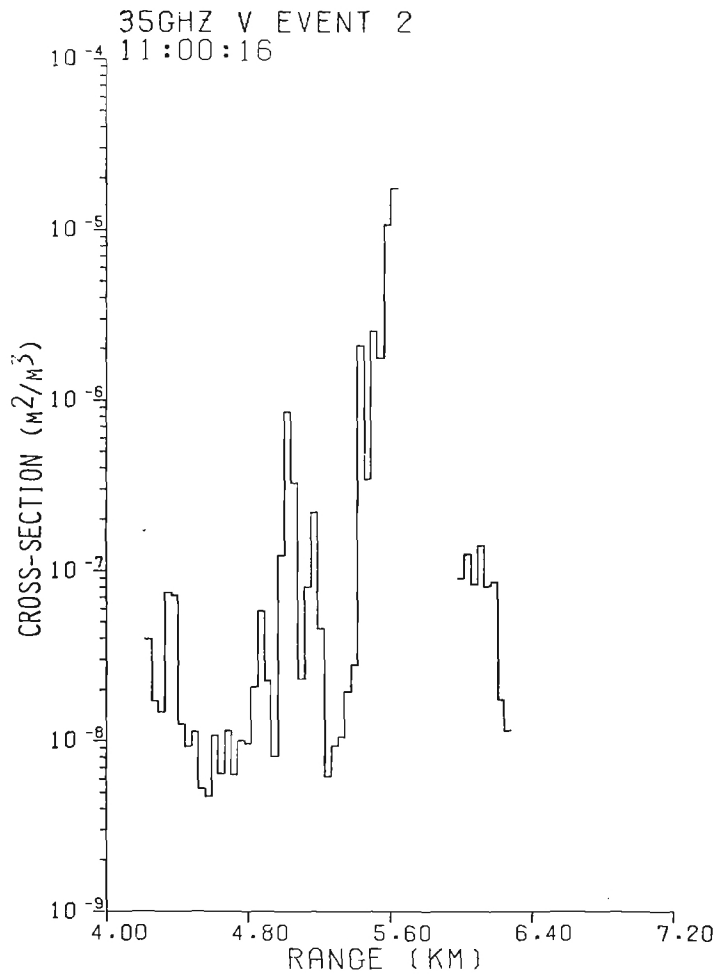


a. HV Polarization

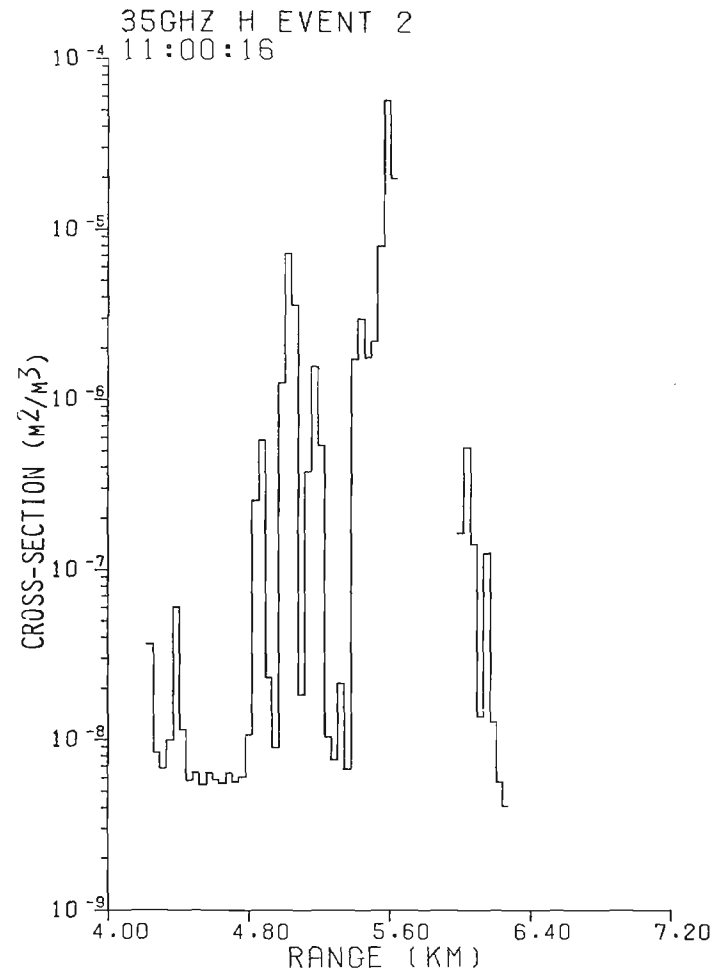


b. HH Polarization

Figure A-27. 9.4 GHz radar cross section vs. range; Event 2, $T_0 + 16$ seconds.

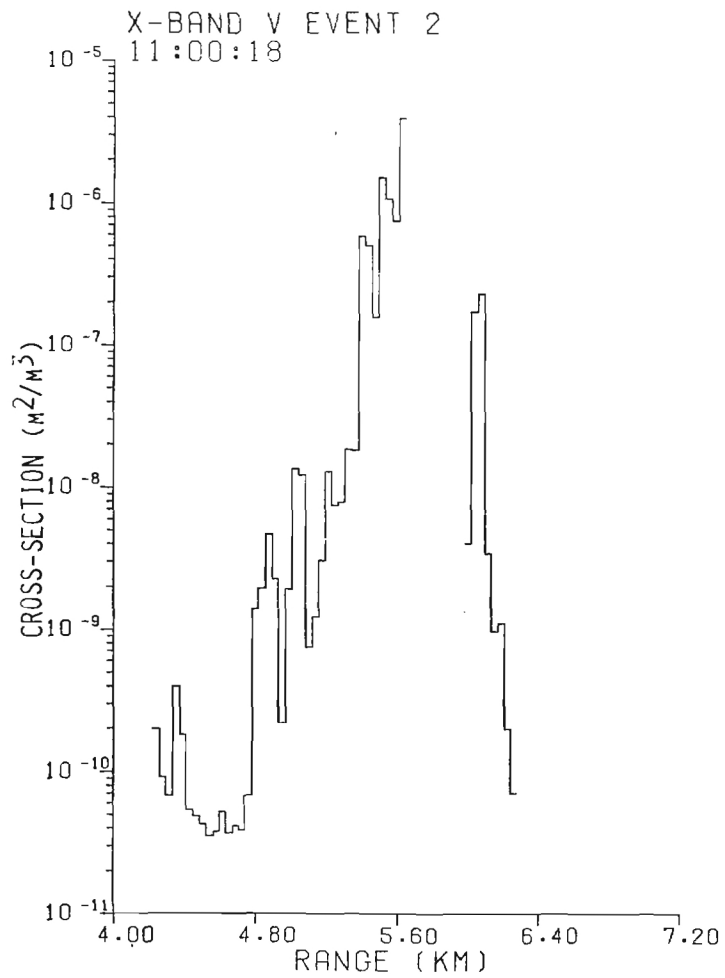


a. HV Polarization

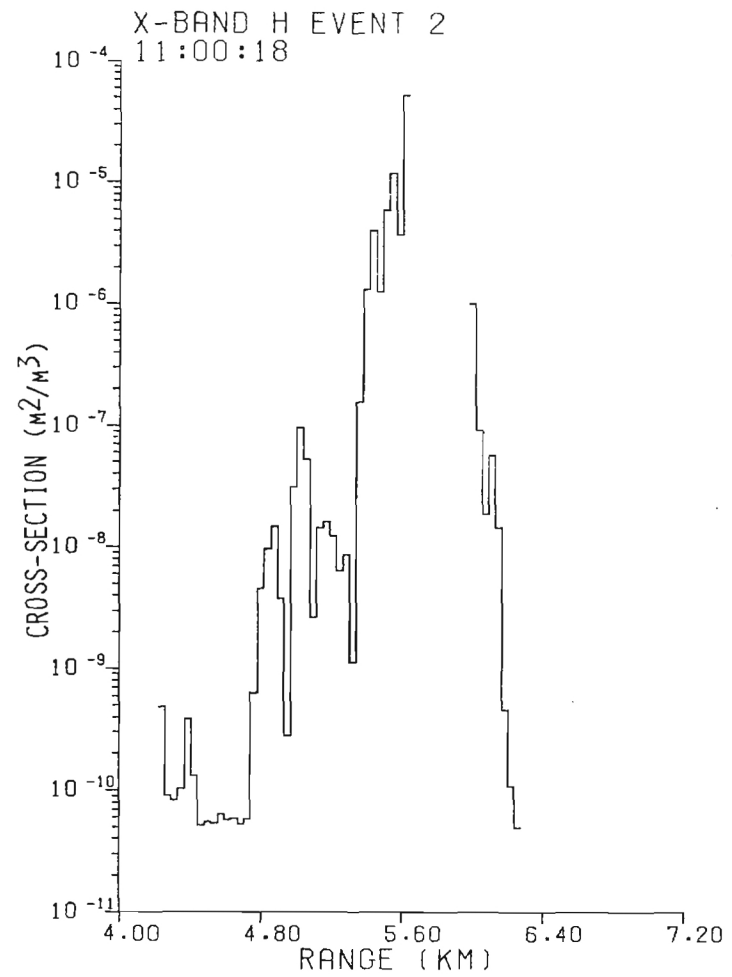


b. HH Polarization

Figure A-28. 35 GHz radar cross section vs. range; Event 2, $T_0 + 16$ seconds.

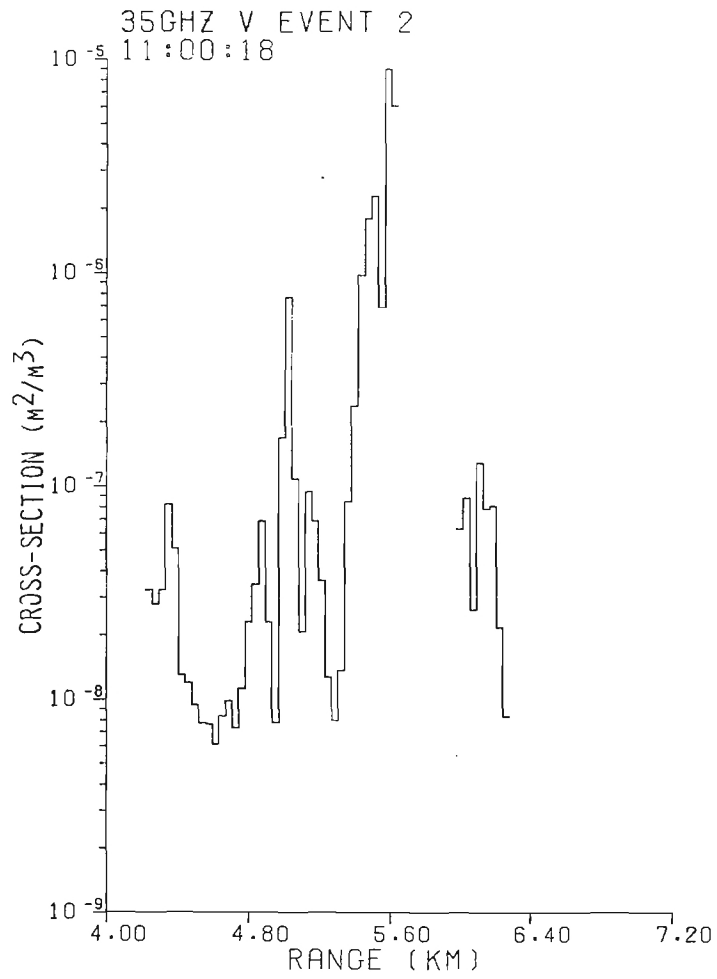


a. HV Polarization

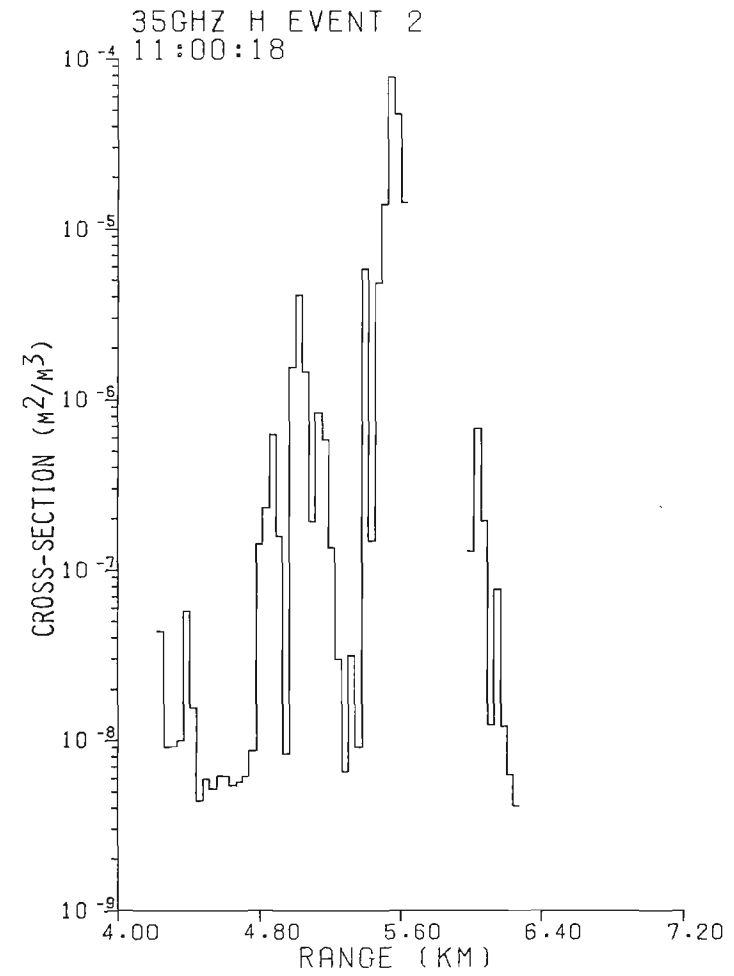


b. HH Polarization

Figure A-29. 9.4 GHz radar cross section vs. range; Event 2, $T_0 + 18$ seconds.

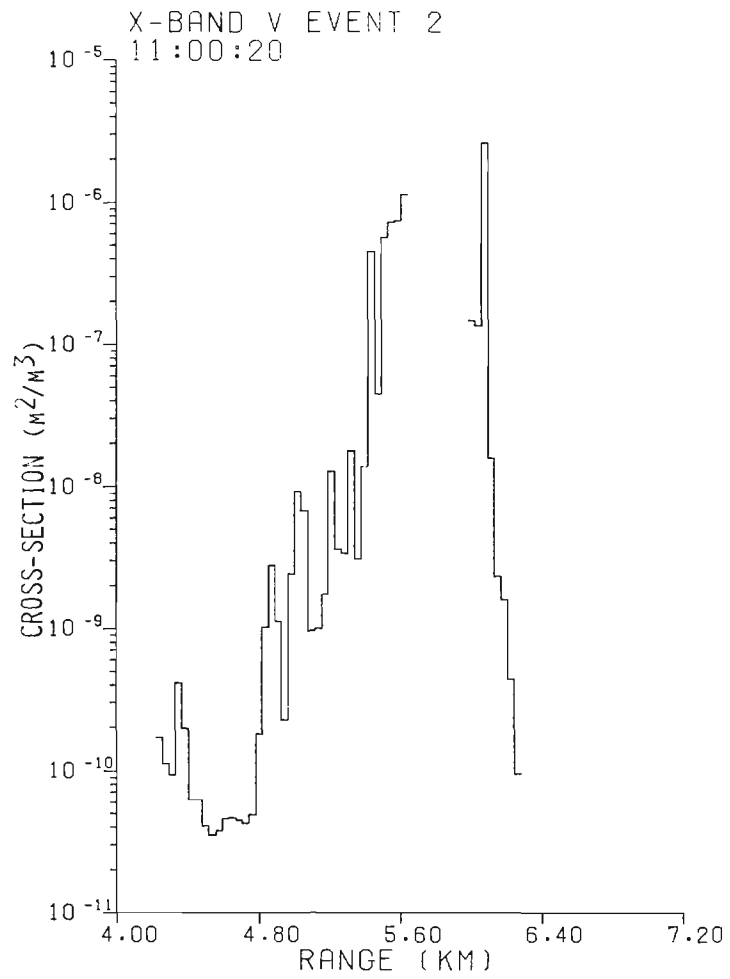


a. HV Polarization

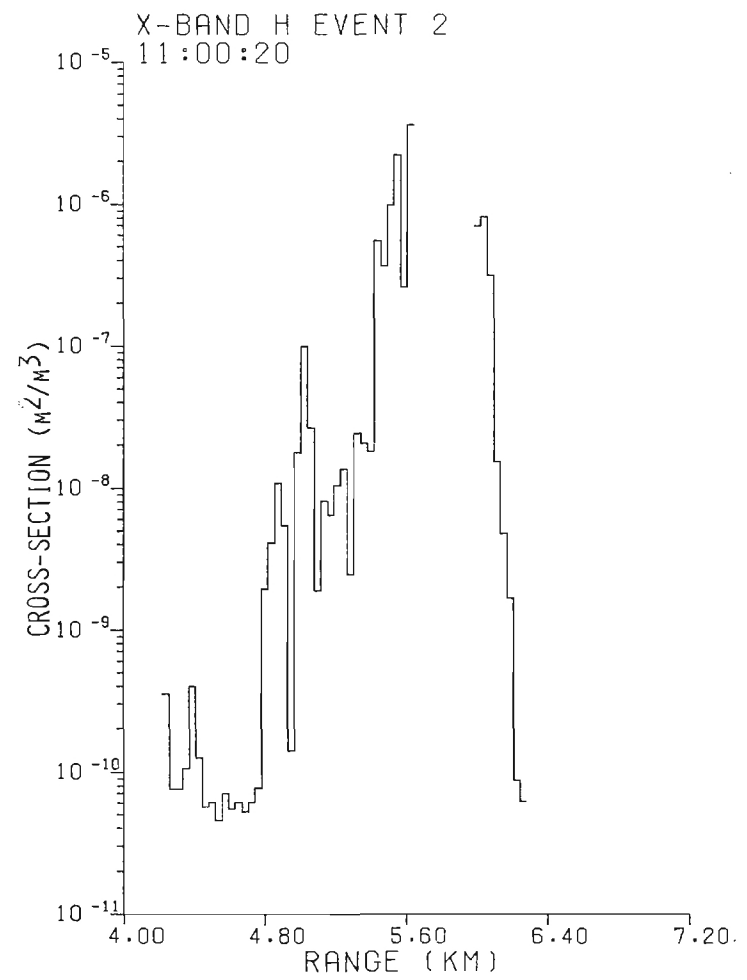


b. HH Polarization

Figure A-30. 35 GHz radar cross section vs. range; Event 2, $T_0 + 18$ seconds.

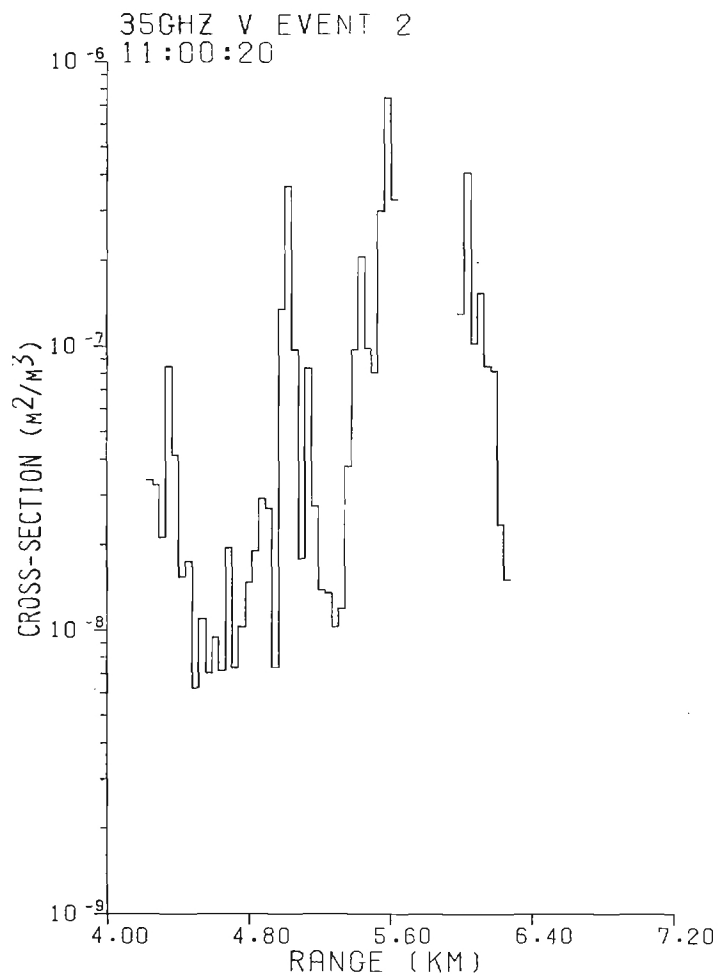


a. HV Polarization

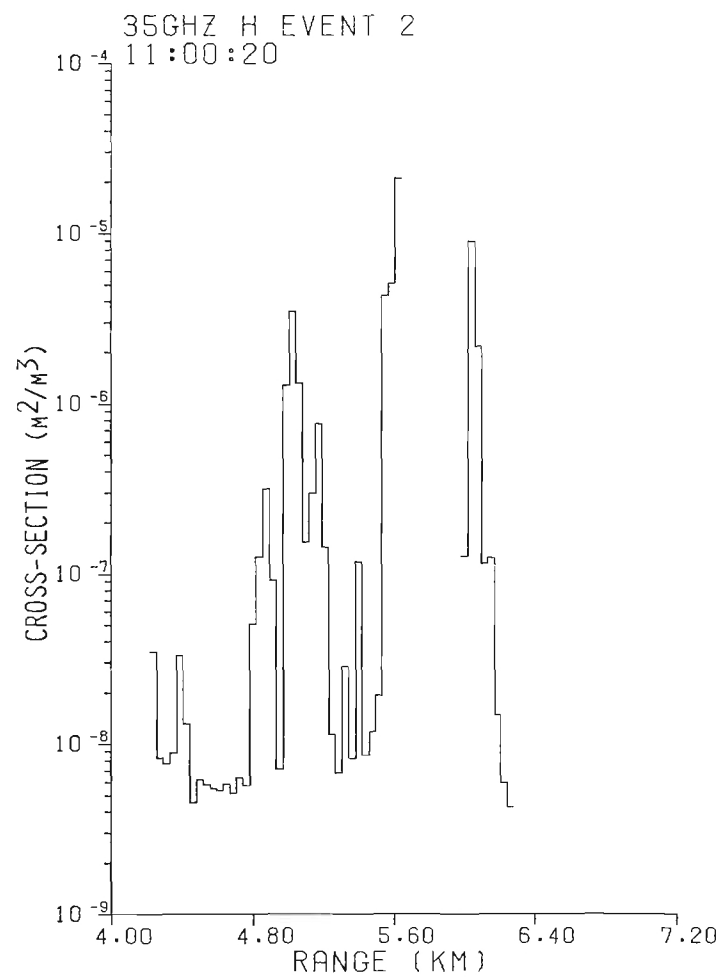


b. HH Polarization

Figure A-31. 9.4 GHz radar cross section vs. range; Event 2, $T_0 + 20$ seconds.



a. HV Polarization



b. HH Polarization

Figure A-32. 35 GHz radar cross section vs. range; Event 2, $T_0 + 20$ seconds.